# 國 立 交 通 大 學

## 電子物理學系


## 博 士 論 文

Ginzburg-Landau 理論對於 Type-II 超導體的傳輸性質與漲落之研究

Ginzburg-Landau theory of transport properties and fluctuations in Type-II superconductors


博 究 生：卜德廷

指導教授：儒森斯坦 教授



中 華 民 國 九十九 年 十二 月

# Ginzburg-Landau 理論對於 type-II 超導體的傳輸性質與漲落之研究
# Ginzburg-Landau theory of transport properties and fluctuations in type-II superconductors


博 究 生：卜德廷　　Student：Bui Duc Tinh

指導教授：儒森斯坦　　Advisor：Baruch Rosenstein


國 立 交 通 大 學

電子物理 學 系

博 士 論 文

A Thesis

Submitted to Department of Electrophysics

College of Science

National Chiao Tung University

in partial Fulfilment of the Requirements

for the Degree of

Doctor of Philosophy

in

Electrophysics

November 2010

Hsinchu, Taiwan, Republic of China

中華民國 九十九 年 十二 月

# Acknowledgements

I wish to express my deepest gratitude to Professor Baruch Rosenstein for his guidance and support throughout my research. I appreciate the scientific collaboration with him.

My special thanks to Professor Dingping Li for his help on some parts of my work.

# Ginzburg-Landau 理論對於 Type-II 超導體的傳輸性質與漲落之研究

學生: 卜德廷　　指導教授: 儒森斯坦

國立交通大學
電子物理系

## 摘要

高溫超導的發現有趣地修改了超導體熱擾動性質,尤其是熱力學性質和傳輸性質(尤其是熱流傳輸)。我們在這工作理考慮在磁場下的超導體的擾動效應。在高溫擾動的影響下,特別是對一些非傳統超導體中很強的各向非均勻性的磁特性,系統的熱力學性質和傳輸特性會影響渦流的運動。

高溫超導的 Ginzburg-Landau (GL)現象描述顯著成功地描述各種熱力學和傳輸特性。在平均場近似下,擾動可以忽略的情況下它變得相當容易。然而當擾動不可被忽略時,即使是等效描述也會變的相當複雜。當增加需要的假設時,有些進展已經被達成。額外的假設通常用於解析的計算,只有最低的 Landau 能階顯著的貢獻到我們關注的物理量上。對最近實驗研究的大範疇外來的參數(磁場,溫度),這種近似是無效的,因此必須推廣理論到包含所有的 Landau 能階。

過去只有電性傳輸的理論被發展,然而最近實驗已經能夠觀察到磁熱效應和熱流傳輸現象,像是 Nernst 和熱電功率,我們需要延伸擾動理論去包含這些現象。當只考慮高斯擾動時,熱電阻率和電阻率在平均場的轉換溫度下是被預測會發散,這個理論與實驗結果矛盾。其中一個重要的結論是要符合實驗結果必須要考慮擾動間的交互作用。之前的工作是 S. Ullah 和 A. T. Dorsey 在 GL 方程式中,在最低的 Landau 能階中應用 Hartree-Fock 近似去處理四次方項計算熱流傳輸問題。

在這個論文中,我的工作使用更有系統的高斯近似法去推廣包含所有 Landau 能階,並且計算有趣的物理量,像是橫向熱電阻率和 Nernst 訊號去描述 Nernst 效應,也算了在線性響應下的第二類超導體的渦流範疇中之交流電阻率。我們使用包含雜訊的時變 GL(TDGL)方程式。我們的理論數值結果可以吻合數個高溫超導中的實驗數據。

我也使用線性響應研究在外加磁場下層狀第二類超導體中的傳輸特性。使用 TDGL 方程式以及熱雜訊可以得到電阻率和霍爾電阻率。我們的理論結果定量上吻合在強電場下高溫導體的實驗數據。

# GINZBURG-LANDAU OF TRANSPORT PROPERTIES AND FLUCTUATIONS IN TYPE-II SUPERCONDUCTORS

Student: Bui Duc Tinh Advisor: Baruch Rosenstein

Department of Electrophysics

National Chiao-Tung University

## Abstract

The discovery of high-temperature superconductors (HTSC) has revived interest in thermal fluctuation effects in superconductors, both in thermodynamic properties and in transport properties, with emphasis on the heat transport. In this work we shall be concerned with the effect of fluctuations on the transport properties of a superconductor in a magnetic field. Under the influence of fluctuations at high temperature, the motions of vortices are responsible for the thermodynamic properties and transport properties of systems especially for those unconventional superconductors due to it's strong anisotropic magnetic properties.

The Ginzburg-Landau (GL) phenomenological description of high superconductors has been remarkably successful in describing various thermodynamic and transport properties. In the mean field approximation, when the fluctuations are neglected, it is relatively simple. However when fluctuations are not negligible, even this effective description becomes very complicated. Some progress can be achieved when certain additional assumptions are added. An additional assumption, often made in analytical calculations, is that only the lowest Landau level significantly contributes to physical quantities of interest. However, in a large domain of external parameters (magnetic field, temperature) currently under experimental investigation, this approximation is not valid and now there is a need to generalize the theory to include all Landau levels.

In the past only electric transport has been thoroughly developed theoretically. However recent experimental advance in observing various magnetocaloric coefficient and heat

transport phenomena like the Nernst and thermoelectric power necessitate extension of the fluctuations theory to include these phenomena. When only the Gaussian fluctuations are considered, then the thermoelectric conductivity and the electrical conductivity were predicted to diverge at the mean-field transition temperature, in conflict with the experimental results. One of important conclusions is that interactions between the fluctuations must be considered in order to obtain even qualitative agreement with the experimental results. An early work on this subject was application of the Hartree-Fock approximation to treat the quartic term within the lowest Landau level approximation in the GL Hamiltonian for heat transport current by S. Ullah and A. T. Dorsey.

In this thesis I have extended the work to include all Landau level, use more systematic Gaussian approximation and calculate physical quantities of current interest like the transverse thermoelectric conductivity and the Nernst signal , describing the Nernst effect, as well as ac conductivity in linear response in Type-II superconductor in the vortex-liquid regime. The time-dependent Ginzburg-Landau (TDGL) equation with thermal noise is used. Our results show a good agreement with several experiment and numerical simulation on HTSC.

I also studied the transport properties in a layered Type-II superconductor under magnetic field beyond the linear response. By using TDGL equation with thermal noise is to obtain electrical conductivity and Hall conductivity. Our results are in good qualitative and even qualitative agreement with experimental data on HTSC in strong electric fields.

# Contents

# List of Figures

# Chapter 1

# Introduction

## 1.1 Superconductivity

Superconductivity was first discovered in 1911 by Heike Kamerlingh Onnes while he was studying the resistance of mercury. At the temperature of 4.2 K, he observed that the resistance suddenly disappeared and became unmeasurable in a small temperature regime. For some decades later there was no theoretical understanding of the superconducting mechanism except the classical interpretation of London's equations of the Meissner effect [1], which was able to describe the basic electromagnetic properties of a homogeneous superconductor. The London theory and its future generalizations introduced two important scales: the concepts of correlation length $\xi$ and penetration depth $\lambda$. Those two parameter characterize many physical properties of a system. Only in 1950, the first phenomenological theory of superconductivity was proposed by GL [2]. This theory, which is called GL theory of superconductivity had great success in explaining the macroscopic properties of superconductors. In particular, Abrikosov [3] showed that the GL theory predicts the division of superconductors into the two categories now referred to as Type-I and Type-II. Seven years later, the complete microscopic theory of superconductivity was finally proposed by Bardeen-Cooper-Schrieffer (BCS) [4]. The BCS theory explained the superconducting current as a superfluid density of Cooper pairs, i.e., pairs of electrons

interacting through the exchange of phonons. This theory is successfully applied to most superconducting elements which are now called conventional superconductors.

As was shown by Abrikosov [3], two types of superconductors exist, differing by the value of $\kappa = \lambda/\xi$ called the GL parameter and behaving differently in the presence of a magnetic field. Superconductors with $\kappa < 1/\sqrt{2}$ are called Type-I, and those with $\kappa > 1/\sqrt{2}$ are called Type-II. The values $1/\sqrt{2}$ is an exact solution where the interface energy( between superconductivity and normal state) vanished. Type-I superconductors

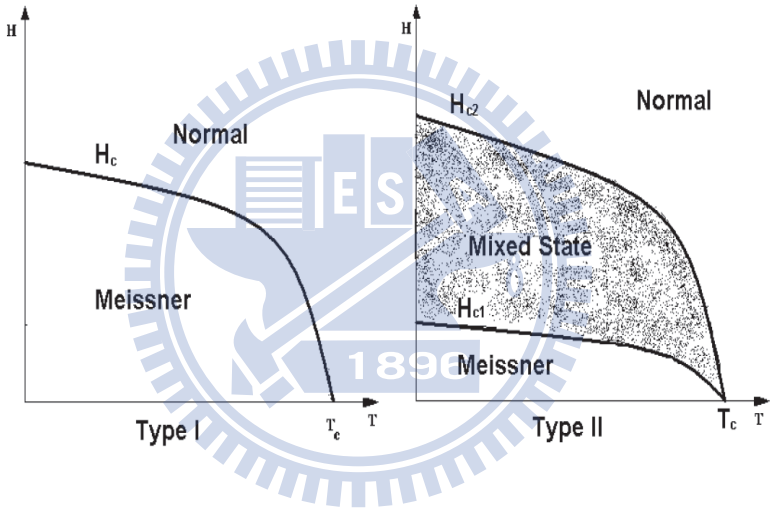


Figure 1.1: The H-T phase diagram of Type-I and Type-II superconductors.

can exist in one of two thermodynamically stable states - either in the normal, or in the superconducting state. The superconducting state is energetically favorable at $T < T_c$ and $H < H_c$. $H_c$ and $T_c$ are mutually dependent, see Fig. 1.1. Applying an external magnetic field to the system turns on the surface supercurrents, which screen the field from the interior of the superconductor. It does not allow external magnetic field to penetrate deeper than $\lambda$. This phenomenon is called the Meissner effect, and the whole state is sometimes called the Meissner state. In this state the material has perfect diamagnetism The magnetization defined as $4\pi M = B(r) - H($ where $B = 0$ in Meissner state) is negative and proportional to up to $H_c$. In idea sample, it has a reversible hysteresis curve.

Unlike Type-I, Type-II superconductors have an extra thermodynamically stable state -

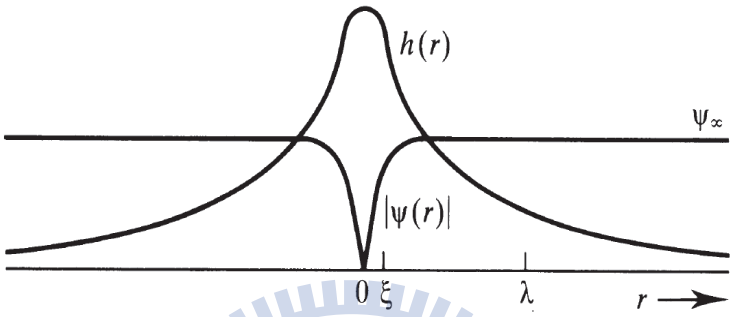


Figure 1.2: The order parameter and the magnetic field profiles of a single Abrikosov vortex.

the mixed state [3], in which the external magnetic field partially penetrates the bulk of the superconductor, locally destroying superconductivity. In this case two critical magnetic fields exist, $H_{c1}$ and $H_{c2}$ (see Fig. 1.1). $H_{c1}$ is the lower critical magnetic field, at which the magnetic field starts penetrating into the bulk of the superconductor and superconductivity begins to decline, and $H_{c2}$ is the upper critical field, at which the magnetic field fills the whole sample, i.e. superconductivity is destroyed while the normal metallic state is recovered . The $H_{c1}$ is mainly determined by the London penetration depth $\lambda$, which is the length scale determining the electromagnetic response of the superconductor. From the London equation set, one got $H_{c1} = (\Phi_0/4\pi\lambda^2)log(\kappa)$. The upper critical field $H_{c2}$ is determined by the coherence length $\xi$ of superconductor, which determines the spatial response of the macroscopic field. The relation between $H_{c2}$ and $\xi$ are given by $H_{c2} = \Phi_0/4\pi\xi^2$, where $\Phi_0$ is a fluxon. The transition to normal state is of second order.

The differences in the behavior of Type-I and Type-II superconductors can be explained if one examines the transitional energy between the normal and the superconducting domains, which is positive in Type-I and negative in Type-II superconductors.

In this study, we have interest on physics of the mixed state. In the mixed state, the penetration of the magnetic flux into the superconductor takes place in the form of long thin flux lines, called *Abrikosov vortices or fluxons* (see Fig. 1.2). At the center of each vortex a normal core exists, bearing the created by supercurrents moving around the core. The characteristic radius of the core, i.e., the radius at which the order parameter decay from its maximal value to zero is $\xi$, while the magnetic field and the supercurrents, which surround the core, spread as far as $\lambda$ from it. The amount of magnetic flux $\Phi$ carried by each vortex is quantized and equal to an integer number of unit quanta $\Phi_0 = hc/2e = 2.07 \times 10^{-7}$ (Gcm$^2$) magnetic flux

## 1.2 Fluctuation phenomena in superconductor

The fluctuation phenomena in clean bulk superconductors become important only in a very narrow ( $10^{-12}$ K) region in the vicinity of the transition temperature [5]. Aslamazov and Larkin [6] demonstrated that the fluctuation region in dirty superconducting films is determined by the resistance per film unit square and could be much wider than in bulk samples. Even more importantly they demonstrated the presence of fluctuation effects beyond the critical region, and not only in thermodynamic but in kinetic characteristics of superconductors too. They have discovered the phenomenon which is called paraconductivity today: the decrease of the resistance of superconductor in the normal phase, still at $T > T_c$. Simultaneously this phenomenon was experimentally observed by Glover [7] and his results were found in perfect agreement with the Aslamazov-Larkin (AL) theory. Since this time the variety of fluctuation effects have been discovered. Their manifestation have been investigated also today, especially in new superconducting systems.

The characteristic feature of superconducting fluctuations is their strong dependence on temperature and magnetic fields in the vicinity of phase transition. This allows us to definitely separate the fluctuation effects from other contributions and to use them as the source of information about the microscopic parameters of a material. Accounting

for fluctuation effects is necessary in the design of superconducting devices. Many ideas of the theory of superconducting fluctuations have been used in other fields of condensed matter theory, e.g. in developing of the theory of quantum fluctuations.

In the fluctuation theory, as in modern statistical physics on the whole, two methods have been mainly used: they are the diagrammatic technique and the method of functional (continual) integration over the order parameter. Each of them has its own advantages and disadvantages [8]. The years of the fluctuation boom coincided with the greatest development of the diagrammatic methods of many body theory in condensed matter physics. These methods turned out to be extremely powerful: any physical problem, after its clear formulation and the writing down of the Hamiltonian, can be reduced to the summation of some classes of diagrams. The diagrammatic technique allows us in a unique way to describe the quantum and classical fluctuations, the thermodynamical, and transport effects. The diagrammatic technique is especially suited to problems containing a small parameter: in this case it is possible to restrict their summation to the ladder approximation only. In the theory of superconducting fluctuations one such small parameter exists: as we will show below, it is the so-called Ginzburg-Levanyuk number $Gi_{(D)}$ which is expressed as some power of the small parameters $T_c/E_F$. In the vicinity of transition, superconducting fluctuations in influence different physical properties of metal and lead to the appearance of small corrections to corresponding physical characteristics in a wide range of temperatures. Due to the above mentioned smallness of $Gi_{(D)}$ these corrections can be evaluated quantitatively in the wide enough temperature region. On the other hand, their specific dependence on the nearness to the critical temperature $T - T_c$ allows us to separate them in experiments from other effects.

In the description of the effect of fluctuations on thermodynamic properties of the system the method of functional integration turned out to be simpler. The ladder approximation in the diagrammatic approach is equivalent to the Gaussian approximation in functional integration. The method of functional integration turns out to be more effective in the case of strong fluctuations, for instance, in the immediate vicinity of the

phase transition. The final equations of the renormalization group carried out by means of functional integrations turn out to be equivalent to the result of the summation of the parquet diagrams series. Nevertheless, the former derivation is much simpler.

## 1.3 Phenomenology of fluctuation thermodynamics and transport

The problem of fluctuation smearing of the superconducting transition was not even considered during the first half of the century after the discovery of superconductivity. In bulk samples of traditional superconductors the critical temperature $T_c$ sharply divides the superconducting and the normal phases. It is worth mentioning that such behavior of the physical characteristics of superconductors is in perfect agreement with both the GL phenomenological theory (1950) [2] and the BCS microscopic theory of superconductivity (1957) [4].

The characteristics of high temperature and organic superconductors, low-dimensional and amorphous superconducting systems studied today strongly differ from those of the traditional superconductors discussed in textbooks. The transitions turn out to be much more smeared out. The appearance of superconducting fluctuations above the critical temperature leads to precursor effects of the superconducting phase occurring while the system is still in the normal phase, sometimes far from $T_c$. The conductivity, the heat capacity, the diamagnetic susceptibility, the sound attenuation, etc. may increase considerably in the vicinity of the transition temperature.

The first numerical estimation of the fluctuation contribution to the heat capacity of a superconductor in the vicinity of $T_c$ was done by Ginzburg in 1960 [5]. In that paper he showed that superconducting fluctuations increase the heat capacity even above $T_c$. In this way fluctuations change the temperature dependence of the specific heat in the vicinity of the critical temperature where, according to the phenomenological Landau theory of second-order phase transitions, a jump should take place. The range of temper-

atures where the fluctuation correction to the heat capacity of a bulk, clean, conventional superconductor is relevant was estimated by Ginzburg to be

$$Gi \sim 10^{-12} \div 10^{-14}, \tag{1.1}$$

The correction occurs in a temperature range $\delta T$ many orders of magnitude smaller than that accessible in real experiments.

In the 1950s and 1960s the formulation of the microscopic theory of superconductivity, the theory of Type-II superconductors, and the search for HTSC attracted the attention of researchers to dirty systems, superconducting films and filaments. In 1968, in papers by Aslamazov and Larkin [6], and Maki [9], and a little later in a paper by Thompson [10], the fundament of the microscopic theory of fluctuations in the normal phase of a superconductor in the vicinity of the critical temperature were formulated. This microscopic approach confirmed Ginzburg's evaluation [5] for the width of the fluctuation region in a bulk clean superconductor. Moreover, it was found that the fluctuation effects increase drastically in thin dirty superconducting films and whiskers. In the cited papers it was demonstrated that fluctuations affect not only the thermodynamical properties of a superconductor but its dynamics too. Simultaneously the fluctuation smearing of the resistive transition in bismuth amorphous films was found experimentally by Glover [7], and it was perfectly fitted by the microscopic theory.

In the BCS theory [4] only the Cooper pairs forming a Bose-condensate are considered. Fluctuation theory deals with the Cooper pairs out of the condensate. In some phenomena these fluctuation Cooper pairs behave similarly to quasiparticles but with one important difference. While for the well defined quasiparticle the energy has to be much larger than its inverse life time, for the fluctuation Cooper pairs the "binding energy" $E_0$ turns out to be of the same order. The Cooper pair life time $\tau_{GL}$ is determined by its decay into two free electrons. Evidently, at the transition temperature the Cooper pairs start to condense and $\tau_{GL} = \infty$. Therefore it is natural to suppose from dimensional analysis that

$\tau_{GL} \sim \hbar/k_B(T-T_c)$. The microscopic theory confirms this hypothesis and gives the exact coefficient:

$$\tau_{GL} = \frac{\pi\hbar}{8k_B(T-T_c)}. \tag{1.2}$$

Another important difference of the fluctuation Cooper pairs from quasiparticles lies in their large size $\xi(T)$. This size is determined by the distance by which the electrons forming the fluctuation Cooper pair move apart during the pair lifetime $\tau_{GL}$. In the case of an impure superconductor the electron motion is diffusive with the diffusion coefficient $D_{diff} \sim v_F^2\tau_{scatt}$ ($\tau_{scatt}$ is the electron scattering time), and $\xi_{dir}(T) = \sqrt{D_{diff}\tau_{GL}} \sim v_F\sqrt{\tau_{scatt}\tau_{GL}}$. In the case of a clean superconductor, where $k_BT\tau_{scatt} \gg \hbar$ , impurity scattering no longer affects the electron correlations. In this case the time of electron ballistic motion turns out to be less than the electron-impurity scattering time $\tau_{scatt}$ and is determined by the uncertainty principle: $\tau_{bal} \sim \hbar/k_BT$. Then this time has to be used in this case for the determination of the effective size instead of $\tau_{scatt}$: $\xi_{cl}(T) \sim v_F\sqrt{\hbar\tau_{GL}/k_BT}$. In both cases the coherence length grows with the approach to the critical temperature as $\epsilon^{-1/2}$, where

$$\epsilon = \ln\frac{T}{T_c} \approx \frac{T-T_c}{T_c}, \tag{1.3}$$

is the reduced temperature. The coherence length can be written in the unique way ($\xi = \xi_{cl,dir}$):

$$\xi(T) = \frac{\xi}{\sqrt{\epsilon}}. \tag{1.4}$$

Finally it is necessary to recognize that fluctuation Cooper pairs can really be treated as classical objects, but that these objects instead of Boltzmann particles appear as classical fields in the sense of Rayleigh–Jeans. That is why the more appropriate tool to study fluctuation phenomena is not the Boltzmann transport equation but the GL equation for

classical fields. Nevertheless, at the qualitative level the treatment of fluctuation Cooper pairs as particles. it was demonstrated [8], in the framework of both the phenomenological GL theory and the microscopic BCS theory, that in the vicinity of the transition.

The complete description of its thermodynamic properties can be done through the calculation of the partition function [8]:

$$Z = tr\left\{\exp\left(-\frac{\widehat{H}}{T}\right)\right\}. \tag{1.5}$$

In the vicinity of the superconducting transition, side by side with the fermionic electron excitations, fluctuation Cooper pairs of a bosonic nature appear in the system. As already mentioned, they can be described by means of classical bosonic complex fields $\Psi(\mathbf{r})$ which can be treated as "Cooper pair wave functions". Therefore the calculation of the trace in (1.5) can be separated into a summation over the "fast" electron degrees of freedom and a further functional integration carried out over all possible configurations of the "steady flow" Cooper pairs wave functions:

$$Z = \int \mathfrak{D}\Psi\mathfrak{D}\Psi^*(\mathbf{r}) \exp\left(-\frac{F[\Psi(\mathbf{r})]}{T}\right), \tag{1.6}$$

where $F[\Psi(\mathbf{r})]$ is GL functional.

The appearance of fluctuating Cooper pairs above $T_c$ leads to the opening of a "new channel" for charge transfer. In the Introduction the fluctuation Cooper pairs were treated as carriers with charge $2e$ while their lifetime $\tau_{GL}$ was chosen to play the role of the scattering time in the Drude formula. The generalization of the phenomenological GL functional approach to transport phenomena was presented in [8]. Dealing with the fluctuation order parameter, it is possible to describe correctly the paraconductivity type fluctuation contributions to the normal resistance and magnetoconductivity, Nernst effect, Hall effect, thermoelectric power and thermal conductivity at the edge of the transition [8].

# Chapter 2

# Theory of Nernst effect in high-$T_C$ superconductor

## 2.1 Introduction

The electric field is induced in a metal under magnetic field by the temperature gradient $\nabla T$ perpendicular to the magnetic field $\mathbf{H}$, phenomenon known as Nernst effect [8] (direction of the electric field being perpendicular to both $\nabla T$ and $\mathbf{H}$). Recently the Nernst effect in high-$T_c$ superconductors and low-temperature superconductor attracted attention both theoretically [8, 11–15] and experimentally [16–24]. In these materials effect of thermal fluctuations is very strong leading to depinning of Abrikosov vortices created by the magnetic field in Type-II superconductor below second critical field $H_{c2}(T)$. In the mixed state the Nernst effect is large due to vortex motion, while in the normal state and in the vortex lattice or glass states it is typically smaller. The Nernst effect therefore is a probe of thermal fluctuations phenomena in the vortex matter, but in principle could shed some light on the underlying microscopic mechanism of superconductivity in cuprates. In the vortex-liquid state, a gradient $-\nabla T$ drives the vortices to the cooler end of the sample because a normal vortex core has a finite amount of entropy relative to the zero-entropy condensate Fig. 2.1 [25, 26]. Because of the $2\pi$ phase singularity at each vortex core,

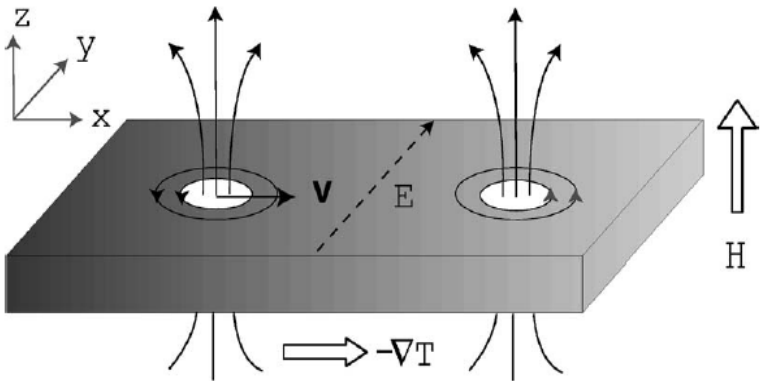


Figure 2.1: The vortex-Nernst effect in a Type-II superconductor. Concentric circles represent vortices.

vortex motion induces phase slippage [27]. By the Josephson equation $2eV_J = \hbar\dot{\theta}$, the time derivative of the phase $\dot{\theta}$ produces an electrochemical potential difference $V_J$. We have $\dot{\theta} = 2\pi\dot{N}_v$, where $\dot{N}_v$ is the number of vortices crossing a line $\|\hat{\mathbf{y}}$. per second. The Josephson voltage $V_J$ may be expressed as a transverse electric field $\mathbf{E} = \mathbf{B} \times \mathbf{v}$ which is detected as the Nernst signal.

Figure 2.2 shows the setup in the Nernst experiment [23]. One end of the crystal is glued with silver epoxy onto a sapphire substrate, which is heat-sunk to a copper cold finger. A thin-film heater, silver-epoxied to the top edge of the crystal, generates the heat current flowing in the ab plane of the crystal. The temperature difference $\Delta T$ is measured by a pair of fine-gauge Chromel-Alumel thermocouples. A pair of Ohmic contacts are prepared on the edge of the sample by annealing different kinds of conductive materials. After the bath temperature is stabilized, the gradient is turned on. The Nernst voltage is preamplified and measured by a nanovoltmeter as the magnetic field is slowly ramped up. To remove stray longitudinal signals due to misalignment of the contacts, the magnetic field is swept in both directions. Only the field-asymmetric part of the raw data is taken as the Nernst signal.

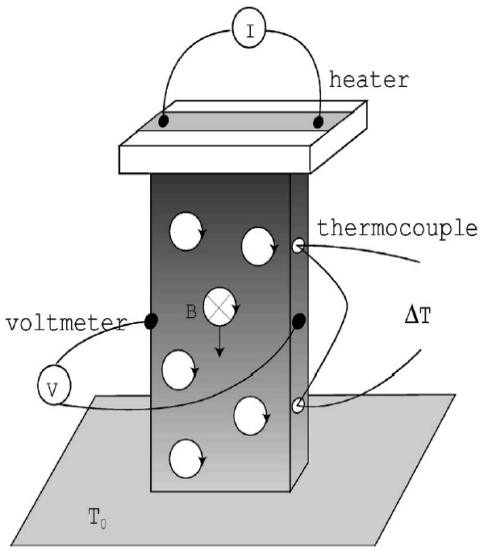


Figure 2.2: Crystal mounting geometry in the Nernst experiment.

Measurements of $e_N$ in fields $H$ up to 45 T [23] reveal that the vortex Nernst signal $e_N$ has a characteristic "tilted-hill" profile, which is qualitatively distinct from that of quasiparticles. The hill profile, which is observed above and below $T_c$, underscores the continuity between the vortex-liquid state below $T_c$ and the Nernst region above $T_c$. Recently, the study of the Nernst effect in $NbSe_2$ reveals a large quasiparticle contribution with a magnitude comparable and a sign opposite to the vortex signal [24]. A large negative Nernst coefficient, persisting at temperatures well above $T_c$=7.2 K, was found in this metal. However, we will concentrate on the vortex-Nernst effect in Type-II superconductor of the overdoped $La_{2-x}Sr_xCuO_4$ (LaSCO) [21], underdoped and overdoped $YBa_2Cu_3O_y$ (YBCO) [21], where $e_N$ is intrinsically strongly nonlinear in $H$ and generally much larger than in nonmagnetic normal metal.

In this study we revisit the calculation in TDGL originally performed in Ref. [11] to obtain explicit expressions for the transverse thermoelectric conductivity $\alpha_{xy}$ and the Nernst signal $e_N$ in both a two dimensional $2D$) and a three dimensional ($3D$) model. Typically only the lowest Landau level (LLL) contribution was investigated [28]. We extend it to higher Landau levels necessary for exploring the experimentally accessible parameter region and find range of applicability of the results due to approximations

made, disorder and crystallization. In this theory the strength of the thermal fluctuations is described by just one dimensionless adjustable parameter $\eta$ (closely related to the Ginzburg number $Gi$). This parameter determines simultaneously the location of the melting line measured on the same samples in recent experiments on Nernst effect. The expression of Ref. [29] for the melting line is in good agreement with many experiments in very wide range of materials (as was established recently in [30]) and MC simulation. Then fitting of the transverse thermoelectric conductivity and related quantities practically has no free parameters (of course there is a certain freedom in determining mean field parameters like $H_{c2}$ and $T_c$, but the range is limited by experimental values). The value fitted from the Nernst effect turns out to be consistent with that derived from the melting line calculated in [29]. We will present the fitting of the melting line for the overdoped LaSCO [21], underdoped and overdoped YBCO [21].

## 2.2 Heat transport and Nernst effect

When a temperature gradient exists in a metal, the motion of the conduction electrons provides the of heat (in the form of kinetic energy) from hotter to cooler regions. In good conductors such as cooper and silver this transport involves the same phonon collision processes that are responsible for the transport of electric charge. Hence these metals tend to have the same thermal and electrical relaxation times at room temperature. An additional complication in the heat transport case is that the carriers of heat can be either charge carriers like electrons or electrically neutral phonons, whereas electrical current arises only from charge carrier transport. The transformation to the superconducting sate changes the nature of the carriers of the electric current, so it is to be expected that the transport of heat will be strongly affected.

The thermal current density **J** is the thermal energy per unit time crossing a unit area aligned perpendicular to the direction of heat flow. It is a vector representing the

transport of entropy density $S_\phi$ at the velocity $\mathbf{v}$,

$$\mathbf{J} = TS_\phi \mathbf{v}, \tag{2.1}$$

from the hotter to the cooler regions of the material [31]. It is proportional to the gradient of the temperature $\nabla T$ through Fourier's law,

$$\mathbf{J} = -K\nabla T, \tag{2.2}$$

where $K$ is the coefficient of thermal conductivity.

In the normal state, electrical conductors are good conductors of heat in accordance with the law of Wiedermann and Franz. In the superconducting state, in contrast, the heat conductivity can be much lower because, as Uher [32] points out, Cooper pairs carry no entropy and do not scatter phonon.

In normal state, the principal carriers of thermal energy through metals in the normal state are conduction electrons and phonons. Heat conduction via each of these two channels acts independently, so that the two channels constitute parallel paths for the passage of heat. A simple model for the conduction of heat between two points A and B in the sample is to represent the two channels by parallel resistors with conductivities $K_e$ and $K_{ph}$ for the electronic and phonon paths, respectively. The conductivities add directly, as in the electrical analogue of parallel resistors, to give the total thermal conductivity $K$,

$$K = K_e + K_{ph}, \tag{2.3}$$

In superconducting state, thermal conductivity involves the transport of entropy $S_\phi$; super electrons, however, do not carry entropy nor do they scatter phonons. Thus the thermal conductivity can be expected to decrease toward zero.

The heat current is sophisticated and has been the subject of a 30 years discussion. This is due to the fact that the notion of heat itself is not well-defined in the Hamiltonian

formalism, so in order to be consistent A. Larkin and A. Varlamov defined the heat current, the heat transport current and the magnetization current from the basic principles of thermodynamics [8].

The Nernst effect is well-known in semiconductors and turns out to be small in good metals. The problem of the fluctuation contribution to the Nernst (and also in the related Ettinghausen) effect attracted special attention after the experiments [16–18] which demonstrated the appearance of a fluctuation tail above the critical temperature in the Nernst signal of the high temperature superconductor. More recently, the Nernst effect again returned to the center of attention with the appearance of measurements showing a sizeable signal well above $T_c$, in particular in the underdoped regime [19, 20, 23, 24].

## 2.3 Nernst effect in superconductor

The appearance of a fluctuation tail above the critical temperature in the Nernst signal was observed in strongly Type-II superconductors, both low-$T_c$ like $NbSe_2$ and NbSi films [24] and several different high-temperature materials [17–20, 23]. The related Ettingshausen effect was detected as well [16]. In particular, the Nernst effect was observed well above $T_{c2}(H)$ and even above $T_c$ in $Bi_2Sr_2CaCu_2O_{8+\delta}$ (Bi2212) [23] , strongly underdoped YBCO [20, 21, 23] and LaSCO [19, 20, 22, 23]. With the overdoped regime (LaSCO with $x = 0.20$ and $T_c$=28 K) in Fig. 2.3, the signal rises steeply at each temperature $T$, attaining a prominent maximum before decreasing. The total data set defines experimentally the region in $H$ and $T$ where vorticity is strongly present. At high fields, all the curves below 14 K are observed to follow a common curve towards zero (dashed line). Hence all the low-$T$ curves vanish at the intercept of the common curve with the field axis (45-50 T), which corresponds to $H_{c2}(0)$. Going to higher $T$, we immediately encounter an anomaly we immediately encounter an anomaly. Conventionally, the $H_{c2}$ line goes linearly to zero at $T_c$. Hence, $e_y$ ought to be finite in a field interval that $\to 0$ as $T \to T_c$. In sharp contrast, we find that, close to $T_c$, but the magnitude of $e_y$ remains

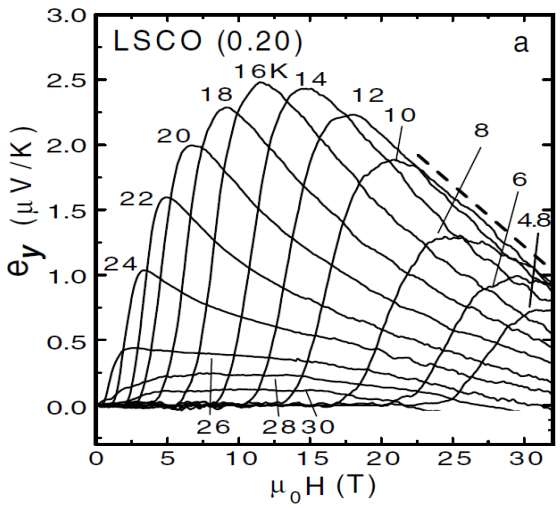


Figure 2.3: The field dependence of $e_y$ at indicated $T$ in samples LaSCO.

large and nearly unchanged up to intense fields for close to $T_c$. The anomalous features of the Nernst signal become more pronounced when we go to the underdoped regime. The results in underdoped YBCO (with $y = 6.50$ and $T_c$=50 K) are showed in Fig. 2.4. As $H$ increases above melting line, $e_y$ rises rapidly, but attains a very broad maximum that extends undiminished to 30 T. These layered materials are highly anisotropic and

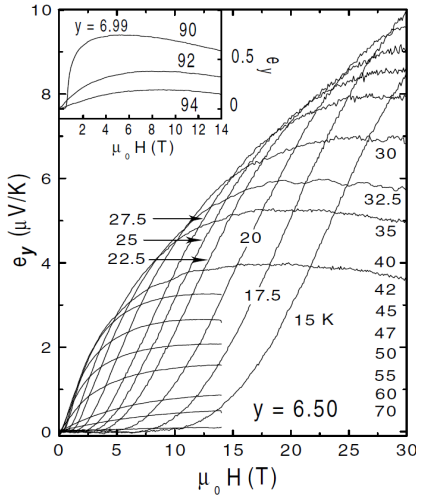


Figure 2.4: The field dependence of $e_y$ at indicated $T$ in samples YBCO.

can be described by a quasi two dimensional model. Due to reduced dimensionality the

effect of thermal fluctuations is enhanced. However in less anisotropic materials like the hole-doped cuprate $Nd_{2-x}Ce_xCuO_4$ (NCCO) [23] and weakly anisotropic and overdoped or fully oxidized $YBCO_{6.99}$ [23] the effect persists. Fluctuations in these materials cannot be described by a $2D$ model and generalization to anisotropic $3D$ model is required. The quasiparticle contribution to the Nernst signal attains a magnitude comparable to the vortex signal in the superconducting state. More recently, in experiment on amorphous thin films of the conventional low temperature superconductor $Nb_{0.15}Si_{0.85}$[24], a Nernst signal generated by short-lived Cooper pairs in the normal state in Fig. 2.5. In these

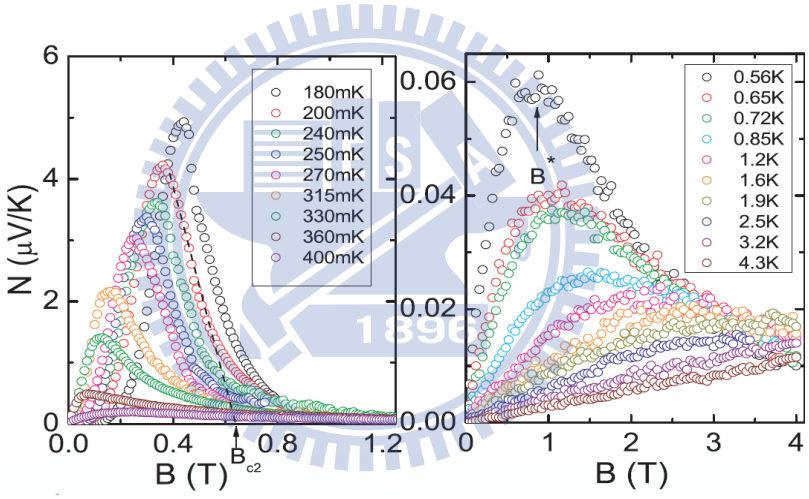


Figure 2.5: (Color) Nernst signal ($N$) as a function of magnetic field for temperatures ranging from 0.180 K to 0.360 K (upper left panel) and from 0.56 to 4.3 K (upper right panel) measured on thin films of $Nb_{0.15}Si_{0.85}$ (with $T_c$=380 mK and thicknesses 35 nm).

amorphous films, the contribution of free electrons to the Nernst signal is negligible. Indeed, the Nernst coefficient of a metal scales with electron mobility. The extremely short mean free path of electrons in amorphous $Nb_{0.15}Si_{0.85}$ damps the normal-state Nernst effect and allows a direct comparison of the data with theory. In the zero-field limit and close to $T_c$, the magnitude of the Nernst coefficient was found to be in quantitative agreement with a theoretical prediction [12] by Ussishkin *et al*, invoking the superconducting correlation length as its single parameter. At high temperature and finite magnetic field,

the data were found to deviate from the theoretical expression. In electron-doped cuprate NCCO the quasiparticle contribution to the Nernst signal is large [23]. The quasiparticle contribution actually dominates the Nernst signal far below $T_c$. Nevertheless, the vortex signal retains its characteristic tilted-hill profile which is easily distinguished from the monotonic quasiparticle contribution.

The observation of the Nernst effect above $T_c$ along with other strong fluctuation effects was interpreted as a support for the preformed pairs scenario for the mechanism of the transition to the superconducting state. At the same time thermal fluctuations in high-$T_c$ materials lead to many other remarkable phenomena, most notably vortex lattice melting and thermal depinning well studied both experimentally and theoretically over the last two decades, so that the theory of the Nernst effect should be consistent with the theory of these phenomena. Most importantly, the material parameters determining the fluctuation strengths can be determined from these better studied effects since in many recent experiments at least the melting line was measured on the same samples.

Theory of the electronic and the heat transport (including the Nernst effect) based on the phenomenological TDGL equations with thermal noise describing strongly fluctuating superconductors was developed long time ago [8, 11]. More recently within the same framework I. Ussishkin *et al.* [12] calculated perturbatively the low-field Nernst effect for $T > T_c$ due to contribution of Gaussian fluctuations and obtained results in agreement with a microscopic Aslamazov-Larkin [8] calculation. They obtained the result for $\alpha_{xy}^{SC}$, which diverges as the conductivity, and in reasonable agreement with experimental data on LaSCO in Fig. 2.6.

$$\alpha_{xy}^{SC} \propto \sigma_{xy}^{SC} \propto \frac{1}{(T-T_c)^{(d-4)/2}}. \tag{2.4}$$

If only Gaussian fluctuations are considered then, $\alpha_{xy}$, diverges at the mean-field transition, in conflict with the experimental results. One of important conclusions that interactions between the fluctuations must be considered in order to obtain even qualitative

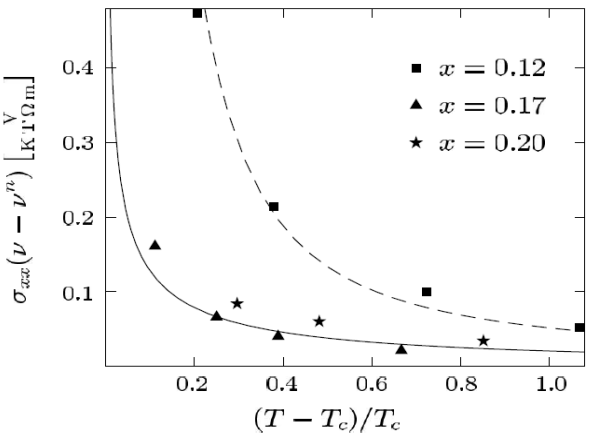


Figure 2.6: Points are $\sigma_{xx}(\nu-\nu^n)$ for different samples of LaSCO, with $x=0.12$ (underdoped, $T_c$=29 K), $x=0.17$ (near optimal doping, $T_c$=36 K), and $x=0.2$ (overdoped, $T_c$=27 K). The solid line is the theoretical value of $\alpha_{xy}/B$, using $\xi$=30 Å and an anisotropy of $\gamma=20$. The dashed line is obtained using a Hartree approximation.

agreement with the experimental results. S. Ullah and A. T. Dorsey [11] applied the Hartree approximation to treat the quartic term in the GL Hamiltonian within LLL. In the limit of high magnetic fields, they found a smooth crosser from a regime dominated by two-dimensional Gaussian fluctuation for $T > T_{c2}(H)$, to mean-field results for $T < T_{c2}(H)$, with no intervening divergence, in agreement with the experimental results. The absence of such a divergence is due to the one-dimensional character of the fluctuations-fluctuations transverse to the applied magnetic fields.

S. Mukerjee *et al.* [14] numerically simulated the two dimensional TDGL equation with Langevin thermal noise for $T < T_c$ and obtained results in reasonable agreement with experimental data on LaSCO [21] at lower temperature, but the transverse thermoelectric conductivity became independent of magnetic field at higher temperatures in contrast to experiment. The simulation of this system, even in $2D$, is difficult and it was one of our goals to supplement it with a reliable analytical expression in the region of the vortex liquid, namely in the region above the melting line (see Fig. 2.7) at which the vortex matter becomes homogeneous on a scale of several lattice spacings and the crystalline symmetry is lost. In this phase the pinning is ineffective and, unlike in the vortex glass

phase, vortices actively promote the Nernst effect. Recent understanding of the vortex matter phase diagram is summarized in Fig. 2.7. There are four phases separated by two transition lines [33]: the first order melting line (sometimes called the order-disorder line at lower temperatures, $H_m(T)$ line in Fig. 2.7) and the irreversibility (or glass) continuous transition. The melting line separates crystalline phases from a homogeneous phases,

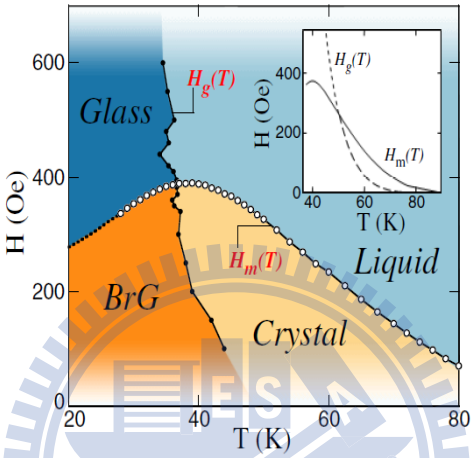


Figure 2.7: The thermodynamic phase diagram of BSCCO accommodates four distinct phases, separated by a first order melting line $H_m(T)$ (open circles), which is intersected by the second-order glass line $H_g(T)$ (solid dots). The inset plots an equivalent phase diagram, calculated based on Ref. [29], consisting of a second-order replica symmetry breaking lines $H_g(T)$ both above (dotted line) and below (dashed line) the first-order transition $H_m(T)$ (solid line).

while the glass line ($H_g(T)$ line in Fig. 2.7) separates pinned phases from the unpinned ones. The mean field $H_{c2}(T)$ line in strongly fluctuating superconductors becomes a crossover. Both pinning and crystalline order lead to a strong reduction of the Nernst signal and therefore these phases will not be considered here. We concentrate on the vortex liquid phase (see Fig. 2.7) and discuss the melting line and disorder only as limits of applicability of the theory and for determining the material parameters. The quantitative GL theory of the vortex liquid have been developed recently and it was established that the Hartree-Fock approach for the thermodynamic is close to the convergent Borel-Pade one in the wide region of the vortex liquid phase [29].

## 2.4 The Ginzburg-Landau Model in $2D$

### 2.4.1 Free energy

To describe fluctuation of order parameter in thin films or layered superconductors one can start with the GL free energy:

$$F = s' \int d\mathbf{r} \frac{\hbar^2}{2m^*} |\mathbf{D}\Psi|^2 + a|\Psi|^2 + \frac{b'}{2}|\Psi|^4, \tag{2.5}$$

where $\mathbf{A} = (-By, 0)$ describes a constant and practically homogeneous magnetic field (we generally neglect small fluctuations of the magnetic field due to magnetization which are of order $1/\kappa^2 << 1$ in the region of interest) in Landau gauge and the covariant derivative is defined by $\mathbf{D} \equiv \nabla + i(2\pi/\Phi_0)\mathbf{A}$, with $\Phi_0 = hc/e^*$ being the flux quantum, $e^* = 2|e|$. For simplicity we assume linear dependence $a(T) = \alpha T_c^{mf}(\bar{t}_{mf} - 1)$, $\bar{t}_{mf} = T/T_c^{mf}$, although the temperature dependence can be easily modified to better describe the experimental coherence length. The "mean field" critical temperature $T_c^{mf}$ depends on the ultraviolet (UV) cutoff, $\Lambda$, specified later. It is higher than measured critical temperature $T_c$ due to strong thermal fluctuations on the mesoscopic scale. The order parameter effective "thickness" of a layer, $s'$, is assumed to be small enough, so that order parameter does not vary considerably inside the layer (namely does not exceed the coherence length $\xi_z(T)$ along the field direction) and layers are nearly independent. We apply this model to describe experiments not just in BiSCCO and other highly anisotropic materials, but also in overdoped LaSCO [21] and strongly underdoped YBCO [21]. For more isotropic optimally doped or fully doped YBCO [21] an anisotropic $3D$ GL model (neglecting the layered structure) would be more appropriate. For materials between the two extremes, a more complicated model like the Lawrence-Doniach one should be used.

### 2.4.2 Relaxation dynamics and thermal fluctuations

Since we are interested in transport phenomena, it is necessary to introduce some kind of dynamics for the order parameter. The simplest is a gauge-invariant version of the "Type A" relaxational dynamics [8, 34]. In the presence of thermal fluctuations, which on the mesoscopic scale are represented by a complex white noise [8, 35], it reads:

$$\frac{\hbar^2\gamma'}{2m^*}D_t\Psi = -\frac{\delta F}{\delta\Psi^*} + \zeta, \tag{2.6}$$

called in the present context TDGL equation. Explicitly the TDGL equation for the superconducting order parameter is

$$\frac{\hbar^2\gamma'}{2m^*}D_t\Psi = \frac{\hbar^2}{2m^*}\mathbf{D}^2\Psi - a\Psi - b'|\Psi|^2\Psi + \zeta, \tag{2.7}$$

where $D_t \equiv \partial/\partial t - i(e^*/\hbar)\Phi$ is the covariant time derivative with $\phi(\mathbf{r}) = -Ey$ being the scalar potential describing electric field. To incorporate the thermal fluctuations via Langevin method, the noise term $\zeta(\mathbf{r}, t)$, having Gaussian correlations

$$\langle\zeta^*(\mathbf{r}, t)\zeta(\mathbf{r}', t')\rangle = \frac{\hbar^2\gamma'}{m^*s'}T\delta(\mathbf{r} - \mathbf{r}')\delta(t - t'), \tag{2.8}$$

is introduced. Here $\delta(\mathbf{r}-\mathbf{r}')$ is the two dimensional $\delta$ function of the in-plane coordinates, and the inverse diffusion constant $\gamma'/2$, controlling the time scale of dynamical processes via dissipation, is real, although a small imaginary (Hall) part is also generally present [36].

Throughout most of the thesis we will use the coherence length, $\xi = (\hbar^2/2m^*\alpha T_c^{mf})^{1/2}$, the zero-temperature correlation length as a unit of length, and $H_{c2}(0) = \Phi_0/2\pi\xi^2$ being the zero-temperature critical field (extrapolated by the linear formula from $T_c$, actual $H_{c2}(T)$ at $T = 0$ is lower) as a unit of magnetic field. After the order parameter field is

rescaled as $\Psi^2 \to (2\alpha T_c^{mf}/b')\psi^2$. The dimensionless Boltzmann factor in these units is:

$$\frac{F}{T} = \frac{1}{\eta_{2D}^{mf}\bar{t}_{mf}} \int d\mathbf{r} \left[ \frac{1}{2} |D\psi|^2 - (a_h + \frac{b}{2}) |\psi|^2 + \frac{1}{2} |\psi|^4 \right], \tag{2.9}$$

where the covariant derivatives in dimensionless units in Landau gauge are $D_x = \frac{\partial}{\partial x} - iby$, $D_y = \frac{\partial}{\partial y}$ with $b = B/H_{c2}(0)$, and the constant is defined as $a_h = (1 - \bar{t}_{mf} - b)/2$. The dimensionless fluctuations' strength coefficient is

$$\eta_{2D}^{mf} = \sqrt{2Gi_{2D}^{mf}}\pi, \tag{2.10}$$

where the Ginzburg number is defined by

$$Gi_{2D}^{mf} = \frac{1}{2} \left( \frac{8e^2\kappa^2\xi^2 T_c^{mf}}{c^2\hbar^2 s'} \right)^2. \tag{2.11}$$

In analogy to the coherence length and the penetration depth, one can define a characteristic time scale. In the superconducting phase a typical "relaxation" time is $t_{GL} = \gamma'\xi^2/2$. It is convenient to use the following unit of the electric field and the dimensionless field: $E_{GL} = H_{c2}\xi/ct_{GL}, \mathcal{E} = E_y/E_{GL}$. The TDGL Eq. (2.7) written in dimensionless units reads

$$\partial_t\psi - \frac{1}{2}D^2\psi - (a_h + \frac{b}{2})\psi + |\psi|^2\psi - i\mathcal{E}y\psi = \zeta, \tag{2.12}$$

In terms of dimensionless quantities the Gaussian correlations read:

$$\langle \overline{\zeta}^*(\mathbf{r}, t)\overline{\zeta}(\mathbf{r}', t') \rangle = 2\eta_{2D}^{mf}\bar{t}_{mf}\delta(\mathbf{r} - \mathbf{r}')\delta(t - t'), \tag{2.13}$$

where the thermal noise was rescaled as $\zeta = \overline{\zeta}(2\alpha T_c^{mf})^{3/2}/b'^{1/2}$.

### 2.4.3 The heat and the electric total and transport currents

The total heat current density is written by [8, 11, 37]:

$$\mathbf{J}^h = -\frac{\hbar^2}{2m^*}\left\langle\left(\frac{\partial}{\partial t} - i\frac{e^*}{\hbar}\phi\right)\Psi^*\left(\nabla - i\frac{2\pi}{\Phi_0}\mathbf{A}\right)\Psi\right\rangle + c.c., \tag{2.14}$$

while the total electric current is

$$\mathbf{J}^e = i\frac{e^*\hbar}{2m^*}\left\langle\Psi^*\left(\nabla - i\frac{2\pi}{\Phi_0}\mathbf{A}\right)\Psi\right\rangle + c.c. \tag{2.15}$$

In terms of dimensionless quantities the currents read:

$$\mathbf{J}^h = J^h_{GL}\mathbf{j}^h, \quad \mathbf{j}^h = -\left\langle\left(\frac{\partial}{\partial t} - i\mathcal{E}y\right)\psi^*\left(\nabla - iA\right)\psi\right\rangle + c.c, \tag{2.16}$$

and

$$\mathbf{J}^e = J^e_{GL}\mathbf{j}^e, \qquad \mathbf{j}^e = \frac{i}{2}\langle\psi^* D\psi\rangle + c.c. \tag{2.17}$$

with $J^h_{GL} = c\hbar H_{c2}/(4\pi\xi^3\gamma e^*\kappa^2)$ and $J^e_{GL} = cH_{c2}/(2\pi\xi\kappa^2)$ being the unit of the heat and electric current density, respectively. Consistently the conductivity will be given in units of $\sigma_{GL} = J_{GL}/E_{GL} = c^2\gamma'/(4\pi\kappa^2)$. This unit is close to the normal state conductivity $\sigma_n$ in dirty limit superconductors [38]. In general there is a factor $k$ of order one relating the two: $\sigma_n = k\sigma_{GL}$.

An important aspect of the calculation of the electrothermal conductivity, discussed in detail [39], is the need to account for bulk magnetization currents. In the presence of a magnetic field, the system has magnetization current in equilibrium. The total heat current defined by Eq. (2.14) is thus a sum of transport and magnetization parts,

$$\mathbf{J}^h = \mathbf{J}^h_{tr} + \mathbf{J}^h_{mag}. \tag{2.18}$$

The magnetization current is current that circulates in the sample and does not contribute to the net current which measured in a transport experiment. On the other hand, it does contribute to the total microscopic current, and it is thus necessary to subtract it from the total current to obtain the transport current response. In the presence of an applied electric field, it was shown in Ref. [39] that the magnetization current is given by

$$\mathbf{J}^h_{mag} = c\mathbf{M} \times \mathbf{E}, \tag{2.19}$$

where $\mathbf{M}$ is the equilibrium magnetization.

Generally, to define the transport coefficients, the electric and heat *transport* current densities are related to the applied (sufficiently weak) electric field and the temperature gradient by

$$J^{(e)i}_{tr} = \sigma^{ij}E^j - \alpha^{ij}\nabla^j T, \tag{2.20}$$

$$J^{(h)i}_{tr} = \widetilde{\alpha}^{ij}E^j - \kappa^{ij}\nabla^j T, \tag{2.21}$$

where $\sigma$, $\alpha$, $\widetilde{\alpha}$, and $\kappa$ are the electrical, the thermoelectric, the electrothermal, and the thermal conductivity components of the conductivity tensor $(i, j = x, y)$. The Onsager relation implies $\widetilde{\alpha} = T\alpha$. The Nernst coefficient $\nu_N$, under the condition $\mathbf{J}^{(e)}_{tr} = 0$ is expressed in terms of the above coefficients as

$$\nu_N = \frac{E_y}{(-\nabla T)_x B} = \frac{1}{B}\frac{\alpha_{xy}\sigma_{xx} - \alpha_{xx}\sigma_{xy}}{\sigma^2_{xx} + \sigma^2_{xy}}. \tag{2.22}$$

If the system shows no significant Hall effect (only such systems will be considered), then $\sigma_{xy} = 0$ and the expression simplifies:

$$\nu_N = \frac{\alpha_{xy}}{B\sigma_{xx}}. \tag{2.23}$$

The Nernst signal is defined

$$e_N = \frac{E_y}{(-\nabla T)_x} = B\nu_N. \tag{2.24}$$

For comparison with experiment, the fluctuation contribution, $\sigma_{xx}$ and $e_N$, should be added to the normal sate contribution, $\sigma^n$ and $e_N^n$. However, the normal state the Nernst signal $e_N^n$ is very small in these materials [12, 23] and will be largely ignored in what follows.

It then follows that the electrothermal conductivity is given by

$$\widetilde{\alpha}_{xy} \equiv \frac{J^h_{(tr)x}}{E_y} = \frac{J^h_x}{E_y} + cM_z. \tag{2.25}$$

The both terms contribute as will be shown in the following Sections.

## 2.5 The transverse thermoelectric conductivity in the vortex liquid phase

### 2.5.1 Melting of the vortex solid, vortex glass and the range of validity of the gaussian approximation

At low temperatures vortex matter organizes itself into a (usually, but not always) hexagonal vortex lattice. When disorder can be effectively neglected (either in very clean materials or when thermal depinning occurs), one can consider transport of the vortex lattice as a whole. Expressions for the electric and the thermal conductivities near $H_{c2}(T)$ neglecting thermal fluctuations were obtained in [11], and according to results the Nernst effect is generally very small compared to one in the vortex liquid. This can be qualitatively understood as a result of rigidity of the lattice. *Below* the melting line the situation in this respect does not change much. Moreover due to unavoidable presence of disorder, the vortex lattice is pinned forming a Bragg glass in most of its domain [33]. However

in high-$T_c$ superconductors thermal fluctuations are strong enough (especially for high anisotropy and high magnetic fields) to destroy the expectation value of the condensate $\langle\psi\rangle = 0$. We always assume that thermal fluctuations melted away and in addition temperature is high enough to thermally depin the vortex liquid (avoiding the "vortex glass"). As a consequence impurities in the vortex liquid are neutralized. To determine the range of validity of the above assumptions one has to estimate the location of the melting and the irreversibility lines. Within the LLL approximation (which is valid *near melting* in wide range of parameters [29]) the line separating the crystalline and the homogeneous phases is given in $2D$ by

$$a_T^{2D} \equiv -\left(2Gi_{2D}\right)^{-1/4}\left(b\bar{t}\right)^{-1/2}\left(1-\bar{t}-b\right) = -13.6, \tag{2.26}$$

where $\bar{t} = T/T_c$ and $a_T$ is the dimensionless "LLL scaled" temperature with

$$Gi_{2D} \equiv \frac{1}{2}\left(\frac{8e^2\kappa^2\xi^2 T_c}{c^2\hbar^2 s}\right)^2, \tag{2.27}$$

being a $2D$ analog of the Ginzburg parameter characterizing the strength of thermal fluctuations on the mesoscopic scale. Eq. (2.26) determines the melting line in Fig. 2.7 and in turn the melting line fixes the $Gi$ in all the fits to experimental data below. This expression was obtained from the comparison of the calculated free energies of the vortex lattice (expansion to two loop order) and of the vortex liquid within the Borel-Pade approach. The corresponding value and definition for $3D$ are

$$a_T^{3D} = -2^{1/3}\left(Gi\right)^{-1/3}\left(b\bar{t}\right)^{-2/3}(1-\bar{t}-b) = -9.5, \tag{2.28}$$

where the Ginzburg number in $3D$ is defined as

$$Gi \equiv \frac{1}{2}\left(\frac{8e^2\kappa^2\xi T_c\gamma}{c^2\hbar^2}\right)^2, \tag{2.29}$$

and $\gamma \equiv \sqrt{m_c/m^*}$ is an anisotropy parameter. Note that here we use the standard definition of the Ginzburg number different from that in Ref. [29].

In the presence of disorder, vortex matter can be pinned. It leads to several phenomena. On the one hand side the vortex lattice is destroyed effectively at large fields, but on the other hand side vortices are pinned and cannot take advantage of thermal fluctuations. The irreversibility or the vortex glass line determining the region in which thermal fluctuations overpower the quench by disorder is given in $2D$ by [33]

$$a_T^g \equiv 4\frac{2r-1}{\sqrt{2r}}, \tag{2.30}$$

where

$$r = \frac{Gi_{2D}^{-1/2}}{4t}(1-t)^2 n, \tag{2.31}$$

and dimensionless parameter $n$ characterizes the disorder strength (similar formulas exist in $3D$) [29]. This determines the dotted line $H_g(T)$ in Fig. 2.7.

### 2.5.2 Magnetization in the vortex liquid within the Gaussian approximation

In order to calculate magnetization, it is simpler to use the statistical mechanics rather than the time dependent approach.

$$f = \frac{F}{T} = \frac{1}{\eta_{2D}^{mf}\bar{t}_{mf}} \int d\mathbf{r} \left[ \frac{1}{2} |D|^2 \psi - (a_h + \frac{b}{2}) |\psi|^2 + \frac{1}{2} |\psi|^4 \right], \tag{2.32}$$

In the framework of this approximation, free energy, Eq. (2.32), is divided into an optimized quadratic part $K$, and a "small" part $V$. Then $K$ is chosen in such a way that the energy of a Gaussian state is minimal [29]. In liquid phase with an arbitrary homogeneous

$U(1)$ symmetric state, one variational parameter $\varepsilon$ is sufficient

$$K = \frac{1}{\eta_{2D}^{mf}\bar{t}_{mf}} \int d\mathbf{r} \left[ \psi^* \left( -\frac{1}{2}D^2 - \frac{b}{2} + \varepsilon \right) \psi \right]. \tag{2.33}$$

The small perturbation is therefore

$$V = \frac{1}{\eta_{2D}^{mf}\bar{t}_{mf}} \int d\mathbf{r} \left[ (-a_h - \varepsilon) |\psi|^2 + \frac{1}{2} |\psi|^4 \right]. \tag{2.34}$$

The eigenvalue of $n^{th}$ level is $-\frac{1}{2}\mathbf{D}^2\varphi = (n + \frac{1}{2})\varphi$. For simplified in writing, we introduce $g_{gauss}(\varepsilon) = g_{trlog}(\varepsilon) + \langle V(\varepsilon) \rangle_K$ which is relative to the free energy density as $f_{eff} = -\eta_{2D}^{mf}\bar{t}_{mf} g_{gauss}$, where

$$g_{trlog} \equiv -\log \left[ \int \mathfrak{D}\psi \mathfrak{D}\psi^* \exp(-K) \right] = \frac{b}{2\pi} \sum_{n=0}^{\infty} \log(nb + \varepsilon), \tag{2.35}$$

$$\langle V \rangle_K = -(a_h + \varepsilon) \frac{b}{2\pi} \sum_{n=0}^{\infty} \frac{1}{nb + \varepsilon} + \eta_{2D}^{mf}\bar{t}_{mf} \left( \frac{b}{2\pi} \sum_{n=0}^{\infty} \frac{1}{nb + \varepsilon} \right)^2, \tag{2.36}$$

( Magnetic field independent term appear in the free energy density is dropped because it is irrelevant to our study on magnetization.) Both terms has ultraviolet divergency, namely at large $n$ the sums diverge. An UV cutoff $N_f + 1 = \frac{\Lambda}{b}$ are introduced for regularization. To extract the divergent part, one can interpolate the $g_{trlog}$ to two terms:

$$\begin{aligned} g_{trlog} &= \frac{b}{2\pi} \left\{ \sum_{n=1}^{N_f} \left[ \log(nb + \varepsilon) - \int_{n-1/2}^{n+1/2} \log(xb + \varepsilon)\, dx \right] \right. \\ &+ \left. \log\varepsilon + \sum_{n=1}^{N_f} \int_{n-1/2}^{n+1/2} \log(xb + \varepsilon)\, dx \right\}. \end{aligned} \tag{2.37}$$

The last term is divergent and for large $n$, it can be approximated by $log(1 + x) \sim x$:

$$\begin{aligned} & b \sum_{n=1}^{N_f} \int_{n-1/2}^{n+1/2} \log(xb + \varepsilon)\, dx \\ & \simeq \Lambda(\log\Lambda - 1) + (\varepsilon - b/2)\log\Lambda + (\varepsilon + b/2) - (\varepsilon + b/2)\log(\varepsilon + b/2). \end{aligned} \tag{2.38}$$

Therefore one can divided $g_{trlog}$ to an infinite part with $\Lambda$ and a finite part, $u$:

$$g_{trlog} = \frac{1}{2}\left[\Lambda(\log\Lambda - 1) + (\varepsilon - \frac{b}{2})\log\Lambda\right] + u(\varepsilon, b). \tag{2.39}$$

The finite part $u$ can be simplified as

$$u(\varepsilon, b) = \frac{b}{2\pi} f_s(\varepsilon/b) + \frac{b}{2\pi}(1/2 - \varepsilon/b)\log b, \tag{2.40}$$

where the function $f_s$ is defined as

$$f_s(x) = \log x - (x+1/2)(\log(x+1/2) - 1) + \sum_{n=1}^{\infty}\left[\log(n+x) - \int_{n-1/2}^{n+1/2}\log(y+x)dy\right], \tag{2.41}$$

which is basically $-\ln\Gamma(x)$ plus a constant.

Turning to the interactions part, we perform the "bubble" integral which diverges logarithmically:

$$\frac{b}{2\pi}\sum_{n=0}^{\infty}\frac{1}{nb+\varepsilon} = \frac{1}{2\pi}\log\Lambda + u', \tag{2.42}$$

where $u' \equiv \frac{\partial}{\partial\varepsilon}u(\varepsilon, b) = \frac{1}{2\pi}[\, f_s'(\varepsilon/b) - \log b]$, and the derivative of $f_s$ is a polygamma function, $\psi_p$, i.e.

$$f_s' = \sum_{n=1}^{\infty}\left[\frac{1}{n+x} - \int_{n-1/2}^{n+1/2}\frac{1}{(y+x)}dy\right] + \left[\frac{1}{x} - \log(x+1/2)\right] = -\psi_p(x). \tag{2.43}$$

The total free energy in Gaussian variational approximation for all Landau levels is obtained,

$$\begin{aligned} g_{gauss}(\varepsilon) &= \frac{1}{2\pi}\Lambda(\log\Lambda - 1) - \eta_{2D}\bar{t}\left(\frac{1}{2\pi}\log\Lambda\right)^2 - (a_h^r + \varepsilon)\left(\frac{1}{2\pi}\log\Lambda\right) \\ &\quad -(a_h^r + \varepsilon)u' + u(\varepsilon, b) + \eta_{2D}\bar{t}(u')^2. \end{aligned} \tag{2.44}$$

where note that $\eta_{2D}^{mf}\bar{t}_{mf} = \eta_{2D}\bar{t}$. Thus, the the temperature $T_c$ will be renormalized: $a_h^r \equiv$

$a_h - \frac{\eta_{2D}\bar{t}}{\pi}\log\Lambda = (1-\bar{t}-b)/2$. The first three terms are divergent, however, they will not contribute to physical quantities such as magnetization, specific hear ...etc. Minimizing the energy, we get the gap equation

$$\varepsilon = -a_h^r + 2\eta_{2D}\bar{t}u'(\varepsilon, b). \tag{2.45}$$

Substitute the solution $\varepsilon_s$ to $g_{gauss}$ one get the minimized free energy density $f_{eff} = -\eta_{2D}\bar{t}g$:

$$\begin{aligned} g &= \frac{1}{2\pi}\Lambda(\log\Lambda - 1) - \eta_{2D}\bar{t}\left(\frac{1}{2\pi}\log\Lambda\right)^2 - (a_h^r + \varepsilon)\left(\frac{1}{2\pi}\log\Lambda\right) \\ &\quad + u(\varepsilon, b)|_{\varepsilon_s} - \eta_{2D}\bar{t}(u')^2|_{\varepsilon_s}. \end{aligned} \tag{2.46}$$

Magnetization $2D$ can be obtained by taking the first derivative of Gibbs energy with respect to magnetic field $b$.

$$M_{2D} = -\frac{H_{c2}}{4\pi\kappa^2}\eta_{2D}\bar{t}\partial_b g = -\frac{T}{2H_{c2}\xi^2 s'}(\partial_b u - 2\eta_{2D}\bar{t}u'\partial_b u'). \tag{2.47}$$

Similar calculation, magnetization $3D$ takes a form

$$M_{3D} = -\frac{H_{c2}}{4\pi\kappa^2}\eta\bar{t}\partial_b g = -\frac{T}{2H_{c2}\xi^2\xi_z}(\partial_b u_{3D} - 2\eta\bar{t}u'_{3D}\partial_b u'_{3D}). \tag{2.48}$$

The function $u(\varepsilon, b)$ can be written in the following form

$$u_{3D}(\varepsilon, b) = \frac{1}{\sqrt{2}\pi}b^{3/2}v\left(\frac{\varepsilon}{b}\right), \tag{2.49}$$

where

$$v(x) = \sum_{n=0}^{\infty}\left[\sqrt{n+x} - \frac{2}{3}(x+n+\frac{1}{2})^{\frac{3}{2}} + \frac{2}{3}(x+n-\frac{1}{2})^{\frac{3}{2}}\right] - \frac{2}{3}(x-\frac{1}{2})^{\frac{3}{2}}. \tag{2.50}$$

### 2.5.3 Vortex liquid within the Gaussian approximation

Due to thermal fluctuations the expectation value of the order parameter in vortex liquid is zero $\langle\psi(\mathbf{r},t)\rangle = 0$. Therefore contribution to the expectation values of physical quantities like the electric and the heat current come exclusively from the correlations. The most important is the quadratic one

$$C(\mathbf{r},t;\mathbf{r}',t') = \langle\psi(\mathbf{r},t)\psi^*(\mathbf{r}',t')\rangle\,, \tag{2.51}$$

called the correlation function of the order parameter. In particular the superfluid density is

$$\langle|\psi(\mathbf{r},t)|^2\rangle = C(\mathbf{r},t;\mathbf{r},t). \tag{2.52}$$

A simple approximation which captures the most interesting fluctuations effects in the Gaussian approximation (see Refs. [35, 40] and Appendix B for details), in which the cubic term in the GL equation Eq. (2.12) $|\psi|^2\psi$ is replaced by a linear one $2\langle|\psi|^2\rangle\psi$

$$\left[\partial_t - \frac{1}{2}D^2 + \varepsilon - \frac{b}{2}\right]\psi = \zeta, \tag{2.53}$$

leading the "renormalized" value of the coefficient:

$$\varepsilon = -a_h + 2\langle|\psi|^2\rangle. \tag{2.54}$$

The formal solution of this equation is

$$\psi(\mathbf{r},t) = \int d\mathbf{r}' \int dt' G_0(\mathbf{r},t;\mathbf{r}',t')\zeta(\mathbf{r}',t'), \tag{2.55}$$

where $G_0$ is the equilibrium Green's function (GF) which satisfies

$$\left[\partial_t - \frac{1}{2}D^2 + \varepsilon - \frac{b}{2}\right] G_0(\mathbf{r}, t; \mathbf{r}', t') = \delta(\mathbf{r} - \mathbf{r}')\delta(t - t'). \tag{2.56}$$

The easiest way to find $G_0$ is by Fourier transformation, which immediately gives

$$\left[i\Omega - \frac{1}{2}D^2 + \varepsilon - \frac{b}{2}\right] G_0(\mathbf{r}, \mathbf{r}', \Omega) = \delta(\mathbf{r} - \mathbf{r}'), \tag{2.57}$$

where

$$G_0(\mathbf{r}, \mathbf{r}', \Omega) = \int_{t'} G_0(\mathbf{r}, t; \mathbf{r}', t') e^{-i\Omega(t-t')}. \tag{2.58}$$

By expanding $G_0$ in term of the Landau eigenfunction one has

$$G_0(\mathbf{r}, \mathbf{r}', \Omega) = \sum_n \frac{\varphi_n(\mathbf{r})\varphi_n^*(\mathbf{r}')}{i\Omega + E_n}, \tag{2.59}$$

where $\varphi_n(\mathbf{r})$ satisfies

$$\left[-\frac{1}{2}\left(\frac{\partial}{\partial x} - iby\right)^2 - \frac{1}{2}\frac{\partial^2}{\partial y^2} + \varepsilon - \frac{b}{2}\right] \varphi_n(\mathbf{r}) = E_n \varphi_n(\mathbf{r}). \tag{2.60}$$

Equation (2.60) is solved exactly in Quantum mechanics, so one gets

$$G_0(\mathbf{r}, t; \mathbf{r}', t') = \frac{\sqrt{b}}{4\pi^2} \int_{\Omega, \widetilde{y}_0} G_0(\widetilde{y}, \widetilde{y}', \Omega, \widetilde{y}_0) e^{-i\sqrt{b}\widetilde{y}_0(x-x')} e^{i\Omega(t-t')}, \tag{2.61}$$

where $\widetilde{y} = \sqrt{b}y$ , and $\widetilde{y}_0 = -k_x/\sqrt{b}$, $k_x$ is the $x$ component of the vector momentum and

$$G_0(\widetilde{y}, \widetilde{y}', \Omega, \widetilde{y}_0) = \left(\frac{b}{\pi}\right)^{1/2} \exp\left[-(\widetilde{y} - \widetilde{y}_0)^2/2 - (\widetilde{y}' - \widetilde{y}_0)^2/2\right] \sum_n \frac{1}{2^n n!} \frac{H_n(\widetilde{y} - \widetilde{y}_0) H_n(\widetilde{y}' - \widetilde{y}_0)}{(i\Omega + E_n)}, \tag{2.62}$$

with the energy eigenvalues

$$E_n = nb + \varepsilon, \tag{2.63}$$

($H_n$ are the Hermite polynomials).

Averaging over the noise, Eq. (2.13), and Eq. (2.55), the equilibrium correlation function Eq. (2.51) is

$$\begin{aligned} C_0(\mathbf{r},t;\mathbf{r}',t') &= 2\eta_{2D}^{mf}\bar{t}_{mf}\int_{\mathbf{r}_1,t_1} G_0(\mathbf{r},t;\mathbf{r}_1,t_1)G_0^*(\mathbf{r}',t';\mathbf{r}_1,t_1) \\ &= -\frac{\eta_{2D}^{mf}\bar{t}_{mf}\sqrt{b}}{2\pi^2}\int_{\Omega,\widetilde{y}_0}\frac{ImG_0(\widetilde{y},\widetilde{y}',\Omega,\widetilde{y}_o)}{\Omega}e^{-i\sqrt{b}\widetilde{y}_0(x-x')}e^{i\Omega(t-t')}. \end{aligned} \tag{2.64}$$

which enters the self-consistent equation (sometimes called gap equation) Eq. (2.54), determining $\varepsilon$. In equilibrium, $\langle|\psi(\mathbf{r},t)|^2\rangle$ is

$$\langle|\psi(\mathbf{r},t)|^2\rangle = \frac{\eta_{2D}^{mf}\bar{t}_{mf}b}{2\pi}\sum_n\frac{1}{E_n}. \tag{2.65}$$

Thus Eq. (2.54) becomes

$$\varepsilon = -a_h + \frac{\eta_{2D}^{mf}\bar{t}_{mf}b}{\pi}\sum_n\frac{1}{nb+\varepsilon} = -a_h + \frac{\eta_{2D}^{mf}\bar{t}_{mf}b}{\pi}\sum_n\frac{1}{nb+\varepsilon}, \tag{2.66}$$

The sum in Eq. (2.66) diverge at large $n$. An ultraviolet (UV) cutoff $\Lambda$ was introduced for regularization in section 2.5.2. The interactions part, the "bubble" integral, was performed in Eq. (2.42). Thus, the the temperature $T_c$ will be renormalized:

$$a_h^r = a_h - \eta_{2D}\bar{t}/\pi\log\Lambda, \tag{2.67}$$

where note $\eta_{2D}^{mf} = \eta_{2D}\frac{T_c^{mf}}{T_c}$, and $\eta_{2D} = \sqrt{2Gi_{2D}}\pi$ with $Gi_{2D} = \frac{1}{2}\left(8e^2\kappa^2\xi^2T_c/c^2\hbar^2s'\right)^2(T_c^{mf}$

is now replaced by $T_c$) . The gap equation takes a form

$$\varepsilon = -a_h^r + 2\eta_{2D}\bar{t}u'(\varepsilon, b). \tag{2.68}$$

This coincides with the static approach presented in section 2.5.2.

### 2.5.4 Expectation value of the heat current in linear response to electric field

The heat and the electric current in section 2.4.3 in the vortex liquid phase can be rewritten as following:

$$\mathbf{j}^h = -\left[D\left(\mathbf{r}\right)\left(\frac{\partial}{\partial t'} - i\mathcal{E}y\right) + D^*\left(\mathbf{r}'\right)\left(\frac{\partial}{\partial t} + i\mathcal{E}y\right)\right] C(\mathbf{r}, t; \mathbf{r}', t')|_{\mathbf{r}=\mathbf{r}';t=t'}, \tag{2.69}$$

$$\mathbf{j}^e = -i\left[D\left(\mathbf{r}\right) - D^*\left(\mathbf{r}'\right)\right] C(\mathbf{r}, t; \mathbf{r}', t')|_{\mathbf{r}=\mathbf{r}';t=t'}, \tag{2.70}$$

where

$$C(\mathbf{r}, t; \mathbf{r}', t') = 2\eta_{2D}\bar{t}\int_{\mathbf{r}_1,t_1} G(\mathbf{r}, t; \mathbf{r}_1, t_1)G^*(\mathbf{r}', t'; \mathbf{r}_1, t_1), \tag{2.71}$$

with $G$ is the GF of the linearized TDGL equation in the presence of the scalar potential. One finds correction to the Green function to linear order in the electric field

$$G(\mathbf{r}, t; \mathbf{r}', t') = G_0(\mathbf{r}, t; \mathbf{r}', t') - i\mathcal{E}\int_{\mathbf{r}_1,t_1} y_1 G_0(\mathbf{r}, t; \mathbf{r}_1, t_1)G_0(\mathbf{r}_1, t_1; \mathbf{r}', t'). \tag{2.72}$$

The transverse thermoelectric conductivity is obtained by expanding the correlation function to linear order in the electric field. The correlation function $C$ in terms of the GF $G_0$ using Eqs. (2.64), ( 2.71) and (2.72) takes a form

$$C(\mathbf{r}, t; \mathbf{r}', t') = C_0(\mathbf{r}, t; \mathbf{r}', t') + C_1\left(\mathbf{r}, t; \mathbf{r}', t'\right), \tag{2.73}$$

where

$$\begin{aligned} C_1(\mathbf{r},t;\mathbf{r}',t') &= i\mathcal{E}\int_{\mathbf{r}_1,t_1} y_1\left[G_0(\mathbf{r},t;\mathbf{r}_1,t_1)C_0^*(\mathbf{r}',t';\mathbf{r}_1,t_1) - G_0^*(\mathbf{r}',t';\mathbf{r}_1,t_1)C_0(\mathbf{r},t;\mathbf{r}_1,t_1)\right] \\ &= i\frac{\mathcal{E}\eta_{2D}\bar{t}}{2\pi^2\sqrt{b}}\int\frac{d\Omega}{\Omega}\int_{\widetilde{y}_0,\widetilde{y}_1}\widetilde{y}_1[G_0^*(\widetilde{y}',\widetilde{y}_1,\Omega,\widetilde{y}_0)ImG_0(\widetilde{y},\widetilde{y}_1,\Omega,\widetilde{y}_0) \\ &- G_0(\widetilde{y},\widetilde{y}_1,\Omega,\widetilde{y}_0)ImG_0(\widetilde{y}',\widetilde{y}_1,\Omega,\widetilde{y}_0)]e^{-i\sqrt{b}\widetilde{y}_0(x-x')}e^{i\Omega(t-t')}, \end{aligned} \tag{2.74}$$

$C_0$ is the equilibrium correlation function which do not contribute to the currents take a form

In order to determine the transverse thermoelectric conductivity, we need to compute the $x$ component of the heat current to first order in the electric field. In the chosen gauge, the heat current along the $x$ direction under condition $j^e_{tr(x)} = 0$ also contains two terms. The term coming from $C_0$ vanishes

$$j^h_{0x} = \frac{\mathcal{E}\eta_{2D}\bar{t}\sqrt{b}}{2\pi^2}\int_{\Omega,\widetilde{y}_0}(\widetilde{y}-\widetilde{y}_0)\,ImG_0(\widetilde{y},\Omega,\widetilde{y}_0) = 0, \tag{2.75}$$

because $ImG_0(\widetilde{y},\Omega,\widetilde{y}_0)$ is a odd function of $\Omega$. It is possible to interpret easily that $C_0$ is the equilibrium correlation function which does not contribute to the current. Considering the $C_1$

$$\begin{aligned} j^h_{1x} &= \frac{2\mathcal{E}\eta_{2D}\bar{t}b}{\pi^2}\sum_{nm}\frac{1}{2^n n!}\frac{1}{2^m m!}\int_{-\infty}^{+\infty}\frac{d\Omega}{2\pi}\Omega^2\frac{1}{(E_n^2+\Omega^2)}\frac{1}{(E_m^2+\Omega^2)} \\ &\times\int_{-\infty}^{+\infty}d\widetilde{y}_0\int_{-\infty}^{+\infty}d\widetilde{y}_1\widetilde{y}_1\,(\widetilde{y}_0-\widetilde{y})\exp\left[-(\widetilde{y}-\widetilde{y}_0)^2-(\widetilde{y}_1-\widetilde{y}_0)^2\right] \\ &\times H_n(\widetilde{y}-\widetilde{y}_0)H_n(\widetilde{y}_1-\widetilde{y}_0)H_m(\widetilde{y}-\widetilde{y}_0)H_m(\widetilde{y}_1-\widetilde{y}_0) \\ &= \frac{\mathcal{E}\eta_{2D}\bar{t}(b-2\varepsilon)}{2b}\Big[u'(\varepsilon,b)-u'(\varepsilon+b,b)\Big]. \end{aligned} \tag{2.76}$$

where function $u'$ was defined in Eq. (2.42).

The heat current in physical units is therefore

$$j^h_x = \frac{cTE_y}{H_{c2}\xi^2 s'}\left(\frac{1}{2}-\frac{\varepsilon}{b}\right)\Big[u'(\varepsilon,b)-u'(\varepsilon+b/2,b)\Big]. \tag{2.77}$$

Using the Onsager relation and Eqs. (2.25), (2.47) and (2.77) one obtains the transverse thermoelectric conductivity

$$\alpha_{xy} \equiv \frac{\widetilde{\alpha}_{xy}}{T} = \frac{c}{2bH_{c2}\xi^2 s'}\Big\{ (b-2\varepsilon)\left[u'(\varepsilon,b) - u'(\varepsilon+b/2,b)\right] - 2b\partial_b u(\varepsilon,b) + 4b\eta_{2D}\bar{t}u'\partial_b u'\Big\}. \tag{2.78}$$

Similar calculation, the electrical conductivity in physical units $\sigma_{yy} = \frac{J_y^e}{E_y}$ (averaged over $\mathbf{r}$) takes a form

$$\begin{aligned}
\sigma_{yy} &= \frac{\eta_{2D}t}{2}\frac{\sigma_n}{k}\sum_n (n+1)\left(\frac{1}{nb+\varepsilon} + \frac{1}{(n+1)b+\varepsilon} - \frac{2}{(n+1/2)b+\varepsilon}\right) \\
&= \frac{\eta_{2D}\bar{t}}{4\pi b^2}\frac{\sigma_n}{k}\left[(b-\varepsilon)u'(\varepsilon,b) - \varepsilon u'(\varepsilon+b,b) - (b-2\varepsilon)u'(\varepsilon+b/2,b)\right] \\
&= \frac{\eta_{2D}\bar{t}}{4\pi b}\frac{\sigma_n}{k}\left\{2 - \left(1-\frac{2\varepsilon}{b}\right)\left[\psi_p\left(\frac{\varepsilon}{b}\right) - \psi_p\left(\frac{1}{2}+\frac{\varepsilon}{b}\right)\right]\right\},
\end{aligned} \tag{2.79}$$

where $\psi_p$ is the polygamma function introduced in section 2.5.2.

### 2.5.5 Extension to anisotropic 3D model

For 3D materials with asymmetry along the $z$ axis the GL model takes a form

$$F = \int d\mathbf{r}\frac{\hbar^2}{2m^*}|\mathbf{D}\Psi|^2 + \frac{\hbar^2}{2m_c}|\partial_z\Psi|^2 + a|\Psi|^2 + \frac{b'}{2}|\Psi|^4. \tag{2.80}$$

which can be again rescaled into

$$f = \frac{F}{T} = \frac{1}{\eta_{mf}\bar{t}_{mf}}\int d\mathbf{r}\left[\frac{1}{2}|D\psi|^2 + \frac{1}{2}|\partial_z\psi|^2 - \left(a_h + \frac{b}{2}\right)|\psi|^2 + \frac{1}{2}|\psi|^4\right], \tag{2.81}$$

by $x \to \xi x, y \to \xi y, z \to \xi z/\gamma, \Psi^2 \to (2\alpha T_c^{mf}/b')\psi^2$. The dimensionless coefficient is

$$\eta_{mf} = \sqrt{2Gi_{mf}}\pi. \tag{2.82}$$

where the Ginzburg number is defined by

$$Gi_{mf} = \frac{1}{2}\left(8e^2\kappa^2\xi T_c^{mf}\gamma/c^2\hbar^2\right)^2. \tag{2.83}$$

The gap equation takes a form

$$\varepsilon = -a_h^r + 2\eta\bar{t}\ u'_{3D}. \tag{2.84}$$

where note $\eta_{mf} = \eta\frac{T_c^{mf}}{T_c}$, and $\eta = \sqrt{2Gi}\pi$ with $Gi = \frac{1}{2}\left(8e^2\kappa^2\xi T_c\gamma/c^2\hbar^2\right)^2$($T_c^{mf}$ is now replaced by $T_c$).

The transverse thermoelectric conductivity is

$$\begin{aligned}\alpha_{xy} &= \frac{c\gamma}{2bH_{c2}\xi^3}\Big\{u_{3D}(\varepsilon,b)/2b - u_{3D}(\varepsilon+b/2,b)/2b + (b-2\varepsilon)[u'_{3D}(\varepsilon,b) - u'_{3D}(\varepsilon+b/2,b)] \\ &- 2b\partial_b u_{3D} + 4b\eta\bar{t}u'_{3D}\partial_b u'_{3D}\Big\},\end{aligned} \tag{2.85}$$

while the electrical conductivity

$$\begin{aligned}\sigma_{yy} &= \frac{\eta\bar{t}}{4b^2}\frac{\sigma_n}{k}\Big[u_{3D}(\varepsilon,b) + u_{3D}(\varepsilon+b,b) - 2u_{3D}(\varepsilon+b/2,b) + 2(b-\varepsilon)u'_{3D}(\varepsilon,b) \\ &- 2\varepsilon u'_{3D}(\varepsilon+b,b) - 2(b-2\varepsilon)u'_{3D}(\varepsilon+b/2,b)\Big].\end{aligned} \tag{2.86}$$

## 2.6 Comparison with experiment and MC simulation

Here we compare the results to $2D$ the simulation results of S. Mukerjee and D.A. Huse [14] and several recent experiments on high-$T_c$ cuprates.

### 2.6.1 Two dimensional thermal fluctuations: LaSCO

The experiment results of Y. Wang *et al.* [21] obtained from the Nernst effect and resistivity measurements on an overdoped LaSCO sample with $x = 0.20$ and $T_c$=28 K. The comparison is presented in Fig. 2.8 (low temperatures in (a) and close to $T_c$ in (b)). The

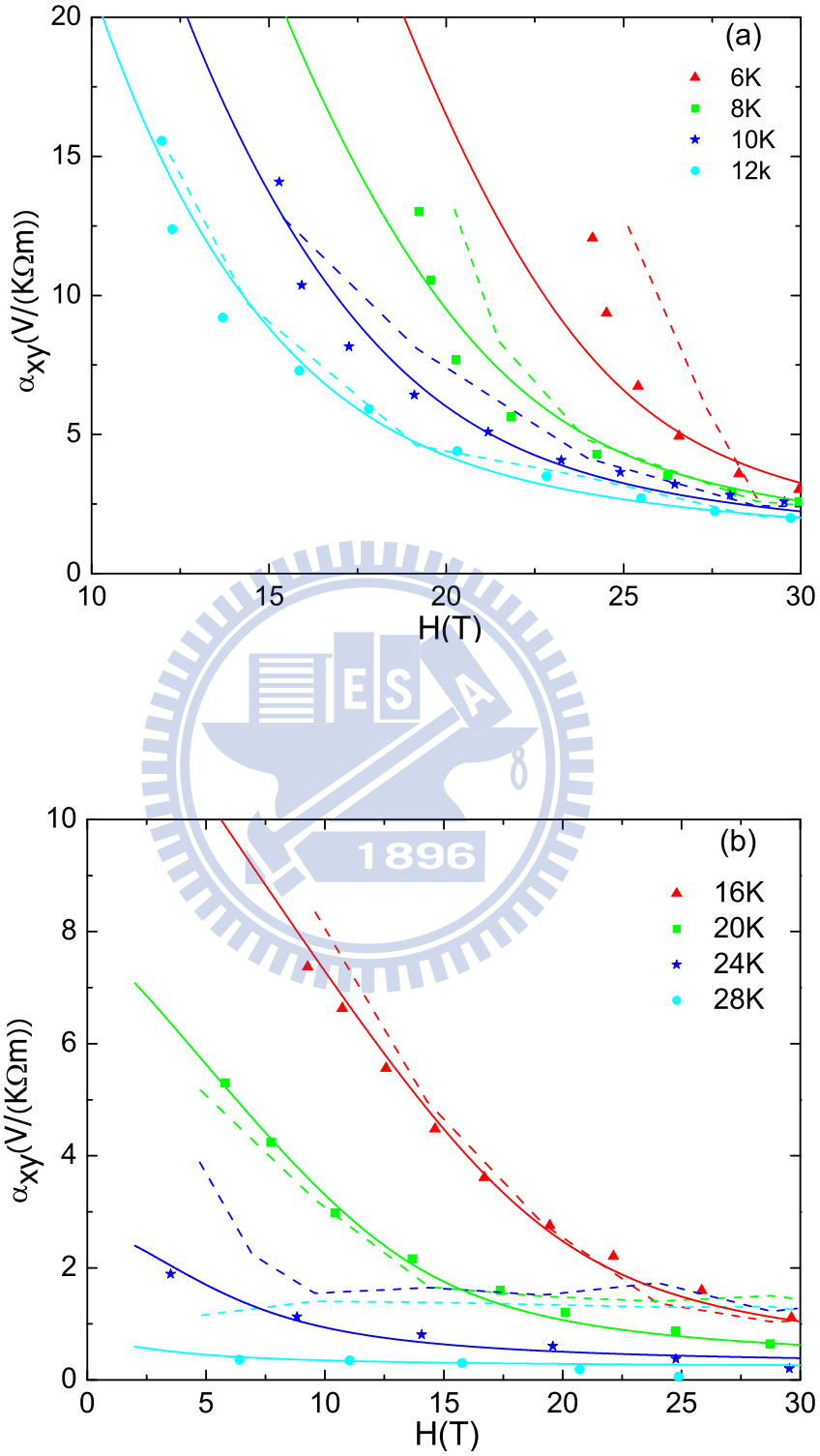


Figure 2.8: Points are $\alpha_{xy}$ for different temperatures of LaSCO in Ref. [21], with $x$=0.2 (overdoped, $T_c$=28 K). The dashed line is the simulation value of $\alpha_{xy}$ in Ref. [14]. The solid line is the theoretical value of $\alpha_{xy}$ with fitting parameters (see text).

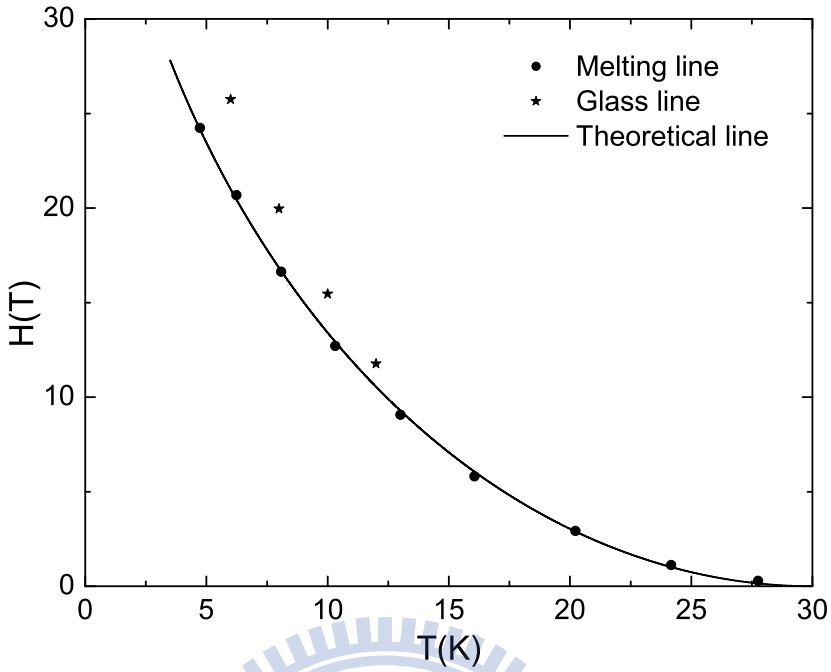


Figure 2.9: Comparison of the experimental melting line for overdoped LaSCO in Ref. [21] with our fitting.

parameters we obtain from the fit are: $H_{c2}(0) = T_c dH_{c2}(T)/dT|_{T_c} = 55$ T (corresponding to $\xi = 24.5$ Å), the Ginzburg-Landau parameter $\kappa = 56$, the order parameter effective thickness $s' = 6.8$ Å. Using those parameters we obtain $Gi_{2D} = 1.1 \times 10^{-4}$ (corresponding to $\eta_{2D} = 0.046$) and provides a reasonable quantitative agreement between theory and experiment. Below irreversibility line where the theory should be modified including both pining and crystalline phase in Fig. 2.8 (a). The deviation develops roughly at the location of the irreversibility line. However, our results are in good quantitative agreement with experimental data for temperature close to $T_c$ in Fig. 2.8 (b), where the numerical simulation gives a nearly constant $\alpha_{xy}$, while the experiment shows more variation. In Fig . 2.9 the melting line of overdoped LaSCO of Ref. [21] is fitted using $Gi_{2D} = 1.49 \times 10^{-4}$, corresponding to $\eta_{2D} \cong 0.054$ which is consistent with the adjusted value of $\eta_{2D}$ when we fit the transverse thermoelectric conductivity. The glass (irreversibility) line in Fig . 2.9 which is estimated from Fig. 2.8 (a), where values of $\alpha_{xy}$ are lower than simulation and experiment data.

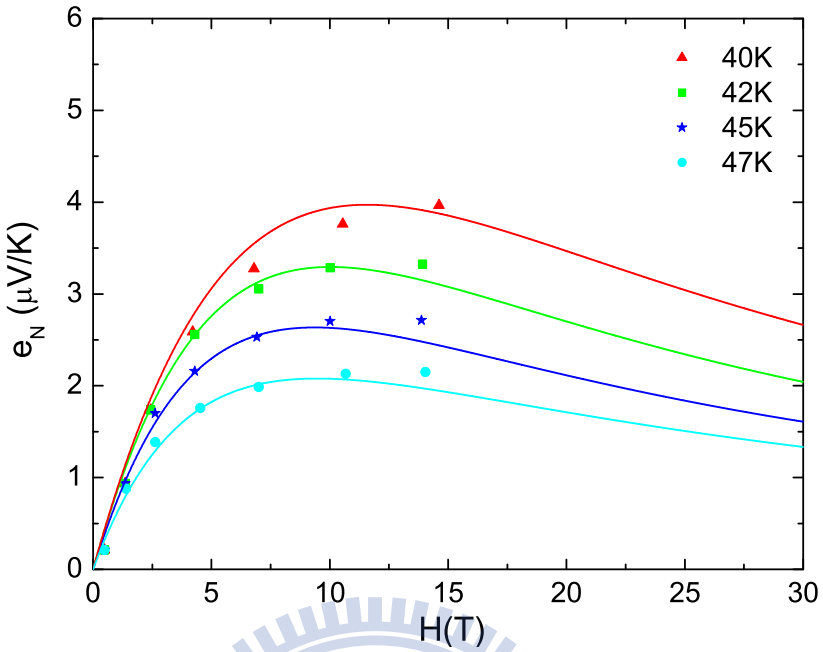


Figure 2.10: Points are $e_N$ for different temperatures of YBCO in Ref. [21], with $y$=6.5 (underdoped, $T_c$=50 K). The solid line is the theoretical value of $e_N$ with fitting parameters (see text).

### 2.6.2 Two dimensional thermal fluctuations: underdoped YBCO

We also compared the results to the experiment on an underdoped YBCO sample with $y = 6.5$ and $T_c$=50 K in Ref. [21], and the normal sate conductivity $\sigma_n = 7.14 \times 10^5$ $(\Omega\ \mathrm{m})^{-1}$ in Ref. [41]. The best fitting parameters are: $H_{c2}(0)$=97 T (thus $\xi = 18.4$ Å), $\kappa = 48.2$, and $s' = 4.8$ Å, and the factor $k = \sigma_n/\sigma_{GL} = 0.36$. Using those parameters we obtain $Gi_{2D} = 2.19 \times 10^{-4}$ (corresponding to $\eta_{2D} = 0.066$). Our values are in good quantitative agreement with experimental data for temperature close to $T_c$ in Fig. 2.10. We find that the theoretical value of $e_N$ has a characteristic "tilted-hill" profile observed in experiment [20, 21, 23]. In Fig. 2.11 we present the fitting of the melting line for underdoped YBCO in Ref. [21] that gives $Gi_{2D} = 3.14 \times 10^{-4}$, $\eta_{2D} \cong 0.078$ which is consistent with the adjusted value of $\eta_{2D}$ when we fit the Nernst signal $e_N$.

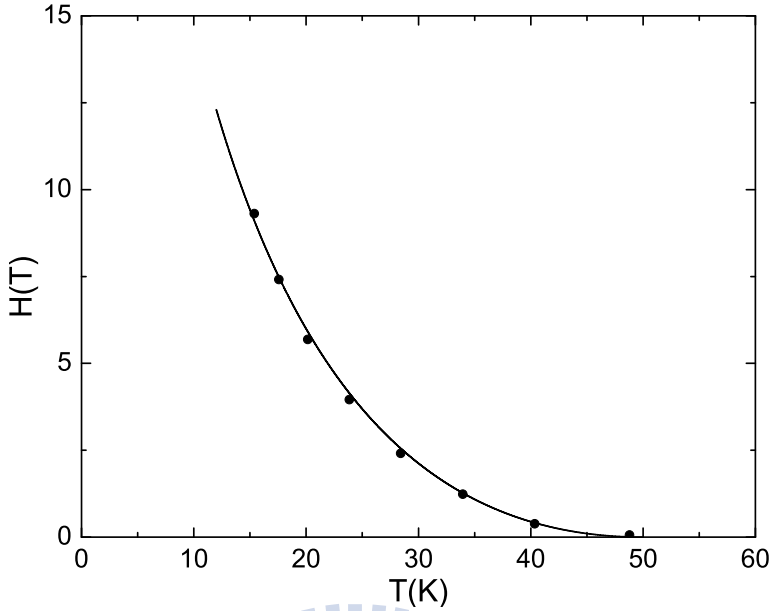


Figure 2.11: Comparison of the experimental melting line for underdoped YBCO in Ref. [21] with our fitting.

### 2.6.3 Three dimensional thermal fluctuations: overdoped YBCO

We also used the results calculated in the three dimensions to compare to the experiment on an overdoped YBCO sample with $y = 6.99$ and $T_c$=93 K in Ref. [21]. The normal-state conductivity and the anisotropy parameter the used in the calculation are $\sigma_n = 9.45 \times 10^5$ $(\Omega\ \mathrm{m})^{-1}$ in Ref. [41] and $\gamma = 7.8$ in Ref. [42], respectively. The best fitting parameters are: $H_{c2}(0)$=210 T (thus $\xi = 12.5$ Å), $\kappa = 55$, $k = 0.45$. Using those parameters we obtain $Gi = 2.24 \times 10^{-3}$ (corresponding to $\eta = 0.22$). Our results are also in good quantitative agreement with experimental data for temperature close to $T_c$ in Fig. 2.12. In Fig. 2.13 we also present the fitting of the melting line for overdoped YBCO in Ref. [21] that gives $Gi = 4.26 \times 10^{-3}$, $\eta \cong 0.29$ which is also consistent with the adjusted value of $\eta$ when we fit the Nernst signal $e_N$.

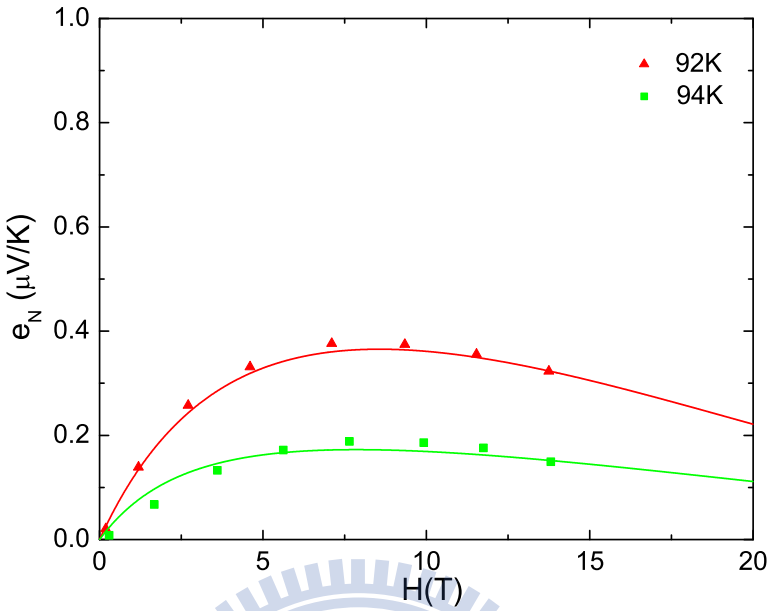


Figure 2.12: Points are $e_N$ for different temperatures of YBCO in Ref. [21], with $y$=6.99 (overdoped, $T_c$=93 K). The solid line is the theoretical value of $e_N$ with fitting parameters (see text)

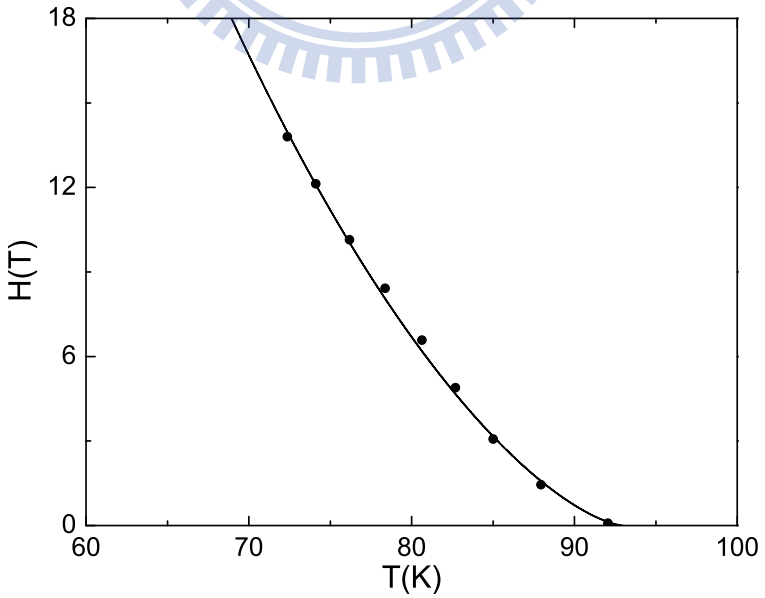


Figure 2.13: Comparison of the experimental melting line for overdoped YBCO in Ref. [21] with our fitting.

## 2.7 Summary

Time dependent Ginzburg-Landau equations with thermal noise describing strong thermal fluctuations on the mesoscopic scale is used to describe strongly Type-II superconductor in the vortex-liquid regime both in $2D$ (describing strongly layered high-$T_c$ superconductors) and $3D$ (less layered superconductors like optimally doped YBCO). Using GL theory developed earlier we estimated the region in the parameter space in which, on one hand vortex crystal is effectively destroyed by thermal fluctuations and, on the other hand disorder (significantly "weakened" by thermal fluctuations) is not strong enough to significantly affect the transport. Under these conditions we obtained explicit expressions for the transverse thermoelectric conductivity $\alpha_{xy}$ and the Nernst signal $e_N$ including all Landau levels were obtained using a gaussian approximation. It is very similar to the Hartree-Fock approximation utilized in Ref. [11], but has a virtue of being a variational principle.

The results are presented using both the strength of the thermal fluctuation $\eta$ and more often used Ginzburg number $Gi$ in the $2D$ and $3D$. The applicability region considered coincides with domain on the phase diagram in which the signal is large. We compared the results to the available $2D$ numerical simulations of the same model and the experiments on high-$T_c$ materials. Our results in $2D$ are significantly lower than the available numerical simulation in Ref. [14] below the irreversibility line at which theory should be modified by including both pinning and crystalline correlation effects. However within the applicability region theory is in good qualitative and even quantitative agreement with experimental data on both overdoped $La_{1.8}Sr_{0.2}CuO_4$ and underdoped $YBa_2Cu_3O_{6.5}$ Ref. [21] for temperatures close to $T_c$.

We also compared the values of $e_N$ calculated in the three dimensions with experiment data for temperature close to $T_c$ on overdoped $YBa_2Cu_3O_{6.99}$, and this comparison is also in good quantitative agreement. The Ginzburg numbers $Gi$ were taken out from the fitting of melting lines of $La_{1.8}Sr_{0.2}CuO_4$, $YBa_2Cu_3O_{6.5}$ and $YBa_2Cu_3O_{6.99}$ on the same

samples. The Ginzburg numbers $Gi$ are consistent with the adjusted values of $\eta$ when we fit the transverse thermoelectric conductivity and the Nernst signal. The irreversibility line of $La_{1.8}Sr_{0.2}CuO_4$ was fitted as well with the same set of parameters.

# Chapter 3

# Electrical conductivity beyond a linear response in layered superconductors under a magnetic field

## 3.1 Introduction

Electric response of a HTSC under magnetic field has been a subject of extensive experimental and theoretical investigation for years. Magnetic field in these layered strongly Type-II superconductors create magnetic vortices, which, if not pinned by inhomogeneities, move and let the electric field to penetrate the mixed state. The dynamic properties of fluxons appearing in the bulk of a sample are strongly affected by the combined effect of thermal fluctuations, anisotropy (dimensionality) and the flux pinning [29, 43]. Thermal fluctuations in these materials are far from negligible and in particular are responsible for existence of the first-order vortex lattice melting transition separating two thermodynamically distinct phases, the vortex solid and the vortex liquid. Magnetic field and reduced dimensionality due to pronounced layered structure (especially in materials like

$Bi_2Sr_2CaCuO_{8+\delta}$) further enhance the effect of thermal fluctuations on the mesoscopic scale. On the other hand the role of pinning in high-$T_c$ materials is reduced significantly compared to the low temperature one, leading to smaller critical currents. At elevated temperatures the thermal depinning [43] further diminishes effects of disorder.

Linear response to electric field in the mixed state of these superconductors has been thoroughly explored experimentally and theoretically over the last three decades. These experiments were performed at very small voltages in order to avoid effects of nonlinearity. Deviation from linearity however are interesting in their own right. These effects have also been studied in low-$T_c$ superconductors experimentally[44, 45] and theoretically [46, 47] and recently experiments were extended to HTSC compounds [48, 49].

Since thermal fluctuations in the low-$T_c$ materials are negligible compared to the inter-vortex interactions, the moving vortex matter is expected to preserve a regular lattice structure (for weak enough disorder). On the other hand, as mentioned above, the vortex lattice melts in HTSC over large portions of their phase diagram, so the moving vortex matter in the region of vortex liquid can be better described as an irregular flowing vortex liquid. In particular the nonlinear effects will also be strongly influenced by the thermal fluctuations.

A simpler case of a zero or very small magnetic field in the case of strong thermal fluctuations was in fact comprehensively studied theoretically [8] albeit in linear response only. In any superconductor there exists a critical region around the critical temperature $|T - T_c| \ll Gi \cdot T_c$, in which the fluctuations are strong (the Ginzburg number characterizing the strength of thermal fluctuations is just $Gi \sim 10^{-10} - 10^{-7}$ for low $T_c$, while $Gi \sim 10^{-5} - 10^{-1}$ for HTSC materials). Outside the critical region and for small electric fields, the fluctuation conductivity was calculated by Aslamazov and Larkin [50] by considering (noninteracting) Gaussian fluctuations within BCS and within a more phenomenological GL approach. In the framework of the GL approach (restricted to the lowest Landau level approximation), Ullah and Dorsey [11] computed the Ettingshausen coefficient by using the Hartree approximation. This approach was extended to other

transport phenomena like the Hall conductivity [11] and the Nernst effect [51].

The fluctuation conductivity within linear response can be applied to describe sufficiently weak electric fields, which do not perturb the fluctuations' spectrum [52]. Physically at electric field, which is able to accelerate the paired electrons on a distance of the order of the coherence length $\xi$ so that they change their energy by a value corresponding to the Cooper pair binding energy, the linear response is already inapplicable [8]. The resulting additional field dependent depairing leads to deviation of the current-voltage characteristics from the Ohm's law. The non-Ohmic fluctuation conductivity was calculated for a layered superconductor in an arbitrary electric field considering the fluctuations as noninteracting Gaussian ones [53, 54]. The fluctuations' suppression effect of high electric fields in HTSC was investigated experimentally for the in-plane paraconductivity in zero magnetic field [55–57], and a good agreement with the theoretical models [53, 54] was found. Theoretically the nonlinear fluctuation conductivity in HTSC has been treated by Puica and Lang [58]. Below we compare their approach and results to ours.

In this study the nonlinear electric response of the moving vortex liquid in a layered superconductor under magnetic field perpendicular to the layers is investegated using the TDGL approach. The layered structure is modeled via the Lawrence-Doniach discretization in the magnetic field direction. In the moving vortex liquid the long range crystalline order is lost due to thermal fluctuations and the vortex matter becomes homogeneous on a scale above the average inter-vortex distances. Although sometimes motion tends to suppress the fluctuations, they are still a dominant factor in flux dynamics. The TDGL approach is an ideal tool to study a combined effect of the dissipative (overdamped) flux motion and thermal fluctuations conveniently modeled by the Langevin white noise. The interaction term in dynamics is treated in self-consistent Gaussian approximation which is similar in structure to the Hartree approximation [8, 11, 58, 59].

Firstly the model of Ref. [58], is physically different from ours. The authors in Ref. [58] believe that the two quantities, layer distance and thickness in the Lawrence-Doniach for HTSC are equal (apparently not the case in HTSC), while we consider them as two

independent parameters. Another difference is we use so called self-consistent Gaussian approximation to treat the model while Ref. [58] used the Hartree approximation.

A main contribution of our paper is an explicit form of the Green's function incorporating all Landau levels. This allows to obtain explicit formulas without need to cutoff higher Landau levels. In Ref. [58], a nontrivial matrix inversion (of infinite matrices) or cutting off the number of Landau levels is required. Note that the exact analytical expression of Green function of the linearized TDGL equation in DC field can be even generalized also to AC field. The method is very general, and it allow us to study transport phenomena beyond linear response of Type-II superconductor like the Nernst effect, Hall effect. The renormalization of the models is also different from Ref. [58]. One of the main result of our work is that the conductivity formula is independent of UV cutoff (unlike in Ref. [58]) as it should be as the standard $|\Psi|^4$ theory is renormalizable. Furthermore self-consistent Gaussian approximation used in this paper is consistent to leading order with perturbation theory, see Ref. [40] in which it is shown that this procedure preserved a correct the ultraviolet (UV) renormalization (is RG invariant). Without electric field the issue was comprehensively discussed in a textbook Kleinert [40]. One can use Hartree procedure only when UV issues are unimportant. We can also show, if there is no electric field, the result obtained using TDGL model and self-consistent Gaussian approximation will lead the same thermodynamic equation using self-consistent Gaussian approximation.

## 3.2 Thermal fluctuations in the time dependent GL Lawrence-Doniach model

To describe fluctuation of order parameter in layered superconductors, one can start with the Lawrence-Doniach expression of the GL free energy of the $2D$ layers with a Josephson

coupling between them:

$$F_{GL} = s' \sum_n \int d\mathbf{r} \Big\{ \frac{\hbar^2}{2m^*} |\mathbf{D}\Psi_n|^2 + \frac{\hbar^2}{2m_c d'^2} |\Psi_n - \Psi_{n+1}|^2 + a|\Psi_n|^2 + \frac{b'}{2}|\Psi_n|^4 \Big\}, \quad (3.1)$$

where $s'$ is the order parameter effective "thickness" of layer and $d'$ distance between layers labeled by $n$. The Lawrence-Doniach model approximates paired electrons DOS by homogeneous infinitely thin planes separated by distance $d'$. While discussing thermal fluctuations, we have to introduce a finite thickness, otherwise the fluctuations will not allow the condensate to exist (Mermin-Wagner theorem). The thickness is of course smaller than the distance between the layers (otherwise we would not have layers). The order parameter is assumed to be non-zero within $s'$. Effective Cooper pair mass in the $ab$ plane is $m^*$ (disregarding for simplicity the anisotropy between the crystallographic $a$ and $b$ axes), while along the $c$ axis it is much larger-$m_c$. For simplicity we assume $a = \alpha T_c^{mf}(\bar{t}_{mf} - 1)$, $\bar{t}_{mf} \equiv T/T_c^{mf}$, although this temperature dependence can be easily modified to better describe the experimental coherence length. The "mean field" critical temperature $T_c^{mf}$ depends on UV cutoff, $\tau_{cut}$, of the "mesoscopic" or "phenomenological" GL description, specified later. This temperature is higher than measured critical temperature $T_c$ due to strong thermal fluctuations on the mesoscopic scale.

The covariant derivatives are defined by $\mathbf{D} \equiv \nabla + i(2\pi/\Phi_0)\mathbf{A}$, where the vector potential describes constant and homogeneous magnetic field $\mathbf{A} = (-By, 0)$. The two scales, the coherence length $\xi^2 = \hbar^2/(2m^*\alpha T_c)$, and the penetration depth $\lambda^2 = c^2 m^* b'/(4\pi e^{*2}\alpha T_c)$ define the GL ratio $\kappa \equiv \lambda/\xi$, which is very large for HTSC. In this case of strongly Type-II superconductors the magnetization is by a factor $\kappa^2$ smaller than the external field for magnetic field larger than the first critical field $H_{c1}(T)$, so that we take $B \approx H$. The electric current, $\mathbf{J} = \mathbf{J}_n + \mathbf{J}_s$, includes both the Ohmic normal part

$$\mathbf{J}_n = \sigma_n \mathbf{E}, \quad (3.2)$$

and the supercurrent

$$\mathbf{J}_s = \frac{ie^*\hbar}{2m^*}\left(\Psi_n^*\mathbf{D}\Psi_n - \Psi_n\mathbf{D}\Psi_n^*\right). \tag{3.3}$$

Since we are interested in a transport phenomenon, it is necessary to introduce a dynamics of the order parameter. The simplest one is a gauge-invariant version of the "type A" relaxational dynamics [8, 34]. In the presence of thermal fluctuations, which on the mesoscopic scale are represented by a complex white noise [8, 35], it reads:

$$\frac{\hbar^2\gamma'}{2m^*}D_t\Psi_n = -\frac{1}{s'}\frac{\delta F_{GL}}{\delta\Psi_n^*} + \zeta_n, \tag{3.4}$$

where $D_t \equiv \partial/\partial t - i(e^*/\hbar)\Phi$ is the covariant time derivative, with $\Phi = -Ey$ being the scalar electric potential describing the driving force in a purely dissipative dynamics. The electric field is therefore directed along the $y$ axis and consequently the vortices are moving in the $x$ direction. For magnetic fields that are not too low, we assume that the electric field is also homogeneous [35]. The inverse diffusion constant $\gamma'/2$, controlling the time scale of dynamical processes via dissipation, is real, although a small imaginary (Hall) part is also generally present [36]. The variance of the thermal noise, determining the temperature $T$ is taken to be the Gaussian white noise:

$$\langle\zeta_n^*(\mathbf{r},t)\zeta_m(\mathbf{r}',t')\rangle = \frac{\hbar^2\gamma'}{m^*s'}T\delta(\mathbf{r}-\mathbf{r}')\delta(t-t')\delta_{nm}. \tag{3.5}$$

Keeping the same notation as in section 2.4.2. The dimensionless Boltzmann factor in these units is:

$$\frac{F_{GL}}{T} = \frac{s}{\eta_{mf}\bar{t}_{mf}}\sum_n\int d\mathbf{r}\Big\{\frac{1}{2}|D\psi_n|^2 + \frac{1}{2d^2}|\psi_n-\psi_{n+1}|^2 - \frac{1-\bar{t}_{mf}}{2}|\psi_n|^2 + \frac{1}{2}|\psi_n|^4\Big\}, \tag{3.6}$$

where the covariant derivatives in dimensionless units in Landau gauge are $D_x = \frac{\partial}{\partial x} - iby$, $D_y = \frac{\partial}{\partial y}$, and the order parameter field was rescaled: $\Psi_n^2 = (2\alpha T_c^{mf}/b')\psi_n^2$. The

dimensionless fluctuations' strength coefficient $\eta_{mf}$ was defined in Eq. 2.82.

The relation between parameters of the two models, the Lawrence-Doniach and the 3D anisotropic GL model, is $d' = d\xi_z = d\xi/\gamma$, $s' = s\xi_z = s\xi/\gamma$. The TDGL Eq. (3.4) written in dimensionless units introduced in section 2.4.2 reads

$$\widehat{H}\psi_n + \frac{1}{2d^2}(2\psi_n - \psi_{n+1} - \psi_{n-1}) - \frac{1-\bar{t}_{mf}}{2}\psi_n + |\psi_n|^2\psi_n = \overline{\zeta}_n, \tag{3.7}$$

$$\widehat{H} = D_t - \frac{1}{2}D^2,$$

while the Gaussian white-noise correlation takes a form

$$\left\langle \overline{\zeta}_n^*(\mathbf{r},t)\overline{\zeta}_m(\mathbf{r}',t')\right\rangle = \frac{2\eta_{mf}\bar{t}_{mf}}{s}\delta(\mathbf{r}-\mathbf{r}')\delta(t-t')\delta_{nm}. \tag{3.8}$$

The covariant time derivative in dimensionless units is $D_t = \frac{\partial}{\partial t} + ivby$ with $v = \mathcal{E}/b$ being the vortex velocity and the thermal noise was rescaled as $\zeta_n = \overline{\zeta}_n(2\alpha T_c^{mf})^{3/2}/b'^{1/2}$. The dimensionless current density is $\mathbf{J}_s^e = J_{GL}\mathbf{j}_s^e$ where

$$\mathbf{j}_s^e = \frac{i}{2}\left(\psi_n^* D\psi_n - \psi_n D\psi_n^*\right). \tag{3.9}$$

with $J_{GL} = cH_{c2}/(2\pi\xi\kappa^2)$ being the unit of the current density was introduced in section 2.4.2.

## 3.3 Vortex liquid within the gaussian approximation

### 3.3.1 Gap equation

Thermal fluctuations in vortex liquid frustrate the phase of the order parameter, so that $\langle\psi_n(\mathbf{r},t)\rangle = 0$. Therefore the contributions to the expectation values of physical quantities like the electric current come exclusively from the correlations, the most important being the quadratic one $\langle\psi_n(\mathbf{r},t)\psi_n^*(\mathbf{r}',t')\rangle$. In particular, $\langle|\psi_n(\mathbf{r},t)|^2\rangle$ is the superfluid density.

A simple approximation which captures the most interesting fluctuations effects in the Gaussian approximation, in which the cubic term in the TDGL Eq. (3.7), $|\psi_n|^2\psi_n$, is replaced by a linear one $2\left\langle|\psi_n|^2\right\rangle\psi_n$

$$\left(\widehat{H}-\frac{b}{2}\right)\psi_n+\frac{1}{2d^2}(2\psi_n-\psi_{n+1}-\psi_{n-1})+\varepsilon\psi_n=\overline{\zeta}_n, \tag{3.10}$$

leading the "renormalized" value of the coefficient of the linear term:

$$\varepsilon=-a_h+2\left\langle|\psi_n|^2\right\rangle, \tag{3.11}$$

where the constant is defined as $a_h=(1-\bar{t}_{mf}-b)/2$. The average $\langle|\psi_n|^2\rangle$ is expressed via the parameter $\varepsilon$ below and will be determined self-consistently together with $\varepsilon$. It differs slightly from a well known Hartree-Fock procedure in which the coefficient of the linearized term is generally different (see Refs. [35, 40] and Appendix B for details ).

Due to the discrete translation invariance in the field direction $z$, it is convenient to work with the Fourier transform with respect to the layer index:

$$\begin{aligned}\psi_n(\mathbf{r},t) &= \int_0^{2\pi/d}\frac{dk_z}{2\pi}e^{-ink_zd}\psi_{k_z}(\mathbf{r},t),\\ \psi_{k_z}(\mathbf{r},t) &= d\sum_n e^{ink_zd}\psi_n(\mathbf{r},t),\end{aligned} \tag{3.12}$$

and similar transformation for $\overline{\zeta}$.

In terms of Fourier components, second term of the TDGL Eq. (3.10) can be written as

$$2\psi_n-\psi_{n+1}-\psi_{n-1}=\int_0^{2\pi/d}\frac{dk_z}{2\pi}\psi_{k_z}(\mathbf{r},t)\exp\left[-ink_zd\right]\left\{2-2\cos(k_zd)\right\}, \tag{3.13}$$

Then the TDGL Eq. (3.10) becomes

$$\left\{\widehat{H}-\frac{b}{2}+\frac{1}{d^2}[1-\cos(k_zd)]+\varepsilon\right\}\psi_{k_z}(\mathbf{r},t)=\overline{\zeta}_{k_z}(\mathbf{r},t). \tag{3.14}$$

The noise correlation is

$$\begin{aligned}\left\langle \overline{\zeta}^*_{k_z}(\mathbf{r},t)\overline{\zeta}_{k'_z}(\mathbf{r}',t')\right\rangle &= \left\langle d\sum_n \overline{\zeta}^*_n(\mathbf{r},t)\exp\left[-ink_zd\right] d\sum_{n'}\overline{\zeta}_{n'}(\mathbf{r},t)\exp\left[in'k'_zd\right]\right\rangle \\ &= d^2\frac{2\eta_{mf}\bar{t}_{mf}}{s}\delta(\mathbf{r}-\mathbf{r}')\delta(t-t')\sum_n\exp\left[ind(k'_z-k_z)\right] \\ &= 4\pi\eta_{mf}\bar{t}_{mf}\frac{d}{s}\delta(\mathbf{r}-\mathbf{r}')\delta(t-t')\delta(k_z-k'_z), \qquad (3.15)\end{aligned}$$

Note that

$$\sum_n \exp\left[idn(k_z-k'_z)\right] = \frac{2\pi}{d}\delta(k_z-k'_z), \qquad (3.16)$$

The relaxational linearized TDGL equation with a Langevin noise, Eq. (3.14), is solved using the retarded ($G=0$ for $t<t'$) GF $G_{k_z}(\mathbf{r},t;\mathbf{r}',t')$:

$$\psi_{k_z}(\mathbf{r},t) = \int d\mathbf{r}'\int d\tau' G_{k_z}(\mathbf{r},t;\mathbf{r}',t')\overline{\zeta}_{k_z}(\mathbf{r}',t'). \qquad (3.17)$$

The GF satisfies

$$\left\{\widehat{H}-\frac{b}{2}+\frac{1}{d^2}[1-\cos(k_zd)]+\varepsilon\right\}G_{k_z}(\mathbf{r},\mathbf{r}',t-t') = \delta(\mathbf{r}-\mathbf{r}')\delta(t-t'). \qquad (3.18)$$

The GF is computed in Appendix A:

$$G_{k_z}\left(\mathbf{r},\mathbf{r}',\tau\right) = \exp\left[\frac{ib}{2}X\left(y+y'\right)\right]g_{k_z}\left(X,Y,\tau\right), \qquad (3.19)$$

where

$$g_{k_z}\left(X,Y,\tau\right) = C_{k_z}(\tau)\theta\left(\tau\right)\exp\left(-\frac{X^2+Y^2}{2\beta}-vX\right), \qquad (3.20)$$

with $X=x-x'-v\tau, Y=y-y'$, and $\tau=t-t'$. $\theta\left(\tau\right)$ is the Heaviside step function, $C$

and $\beta$ are coefficients as follows:

$$C = \frac{b}{4\pi}\exp\left\{-\left(\varepsilon - \frac{b}{2} + \frac{v^2}{2} + \frac{1}{d^2}[1-\cos(k_z d)]\right)\tau\right\}\sinh^{-1}\left(\frac{b\tau}{2}\right), \tag{3.21}$$

$$\beta = \frac{2}{b}\tanh\left(\frac{b\tau}{2}\right). \tag{3.22}$$

The thermal average of the superfluid density (density of Cooper pairs) is

$$\begin{aligned}\left\langle|\psi_n(\mathbf{r},t)|^2\right\rangle &= \int_0^{2\pi/d}\frac{dk_z}{2\pi}\int_0^{2\pi/d}\frac{dk_z'}{2\pi}\exp\left[ind(k_z'-k_z)\right]\left\langle\psi_{k_z}(\mathbf{r},t)\psi_{k_z'}^*(\mathbf{r},t)\right\rangle \\ &= \int_0^{2\pi/d}\frac{dk_z}{2\pi}\int_0^{2\pi/d}\frac{dk_z'}{2\pi}\exp\left[ind(k_z'-k_z)\right]\int d\mathbf{r}'\int_{-\infty}^{\tau}dt' G_{k_z}(\mathbf{r},t;\mathbf{r}',t') \\ &\quad\times\int d\mathbf{r}''\int_{-\infty}^{\tau}dt'' G_{k_z'}(\mathbf{r},t;\mathbf{r}'',t'')\left\langle\overline{\zeta}_{k_z}(\mathbf{r}',t')\overline{\zeta}_{k_z'}^*(\mathbf{r}'',t'')\right\rangle. \end{aligned}\tag{3.23}$$

Substituting the noise correlation (3.8) into expression (3.23), one has

$$\begin{aligned}\left\langle|\psi_n(\mathbf{r},t)|^2\right\rangle &= 4\pi\eta_{mf}\bar{t}_{mf}\frac{d}{s}\int_0^{2\pi/d}\frac{dk_z}{2\pi}\int_0^{2\pi/d}\frac{dk_z'}{2\pi}\exp\left[ind(k_z'-k_z)\right]\int d\mathbf{r}'\int_{-\infty}^{t}dt' \\ &\quad\times G_{k_z}(\mathbf{r},t;\mathbf{r}',t')\int d\mathbf{r}''\int_{-\infty}^{t}dt'' G_{k_z'}^*(\mathbf{r},t;\mathbf{r}'',t'')\delta(\mathbf{r}'-\mathbf{r}'')\delta(k_z-k_z')\delta(t'-t'') \\ &= 2\eta_{mf}\bar{t}_{mf}\frac{d}{s}\int_0^{2\pi/d}\frac{dk_z}{2\pi}\int d\mathbf{r}'\int_{-\infty}^{\tau}dt'\left|G_{k_z}(\mathbf{r},t;\mathbf{r}',t')\right|^2. \end{aligned}\tag{3.24}$$

Substituting the GF (3.19) into expression (3.24), one obtains

$$\begin{aligned}\left\langle|\psi_n(\mathbf{r},t)|^2\right\rangle &= 2\pi\eta_{mf}\bar{t}_{mf}\frac{d}{s}\int_0^{2\pi/d}\frac{dk_z}{2\pi}\int_0^{\infty}d\tau C^2\int dX\,dY\exp\left(-\frac{X^2+Y^2}{\beta}-2vX\right) \\ &= 2\pi\eta_{mf}\bar{t}_{mf}\frac{d}{s}\int_0^{\infty}d\tau\beta\exp\left(\beta v^2\right)\int_0^{2\pi/d}\frac{dk_z}{2\pi}|C|^2. \end{aligned}\tag{3.25}$$

Note that

$$\begin{aligned}\int_0^{2\pi/d}\frac{dk_z}{2\pi}|C|^2 &= \left(\frac{b}{4\pi}\right)^2\int_0^{2\pi/d}\frac{dk_z}{2\pi}\exp\left\{-\left(2\varepsilon - b + v^2 + \frac{2}{d^2}[1-\cos(k_z d)]\right)\tau\right\} \\ &= \frac{1}{d}\left(\frac{b}{4\pi}\right)^2\exp\left\{-\left(2\varepsilon - b + v^2 + \frac{2}{d^2}\right)\tau\right\}I_0\left(2\tau/d^2\right). \end{aligned}\tag{3.26}$$

Here $I_0(x) = (1/2\pi)\int_0^{2\pi}e^{x\cos\theta}d\theta$ is the modified Bessel function. Then the expression

(3.25) takes form

$$\left\langle |\psi_n(\mathbf{r},t)|^2 \right\rangle = \frac{\eta_{mf}\bar{t}_{mf}b}{2\pi s}\int_0^\infty \frac{f(\varepsilon,\tau)}{\sinh(b\tau)} \tag{3.27}$$

where

$$f(\varepsilon,\tau) = \exp\left[\frac{2v^2}{b}\tanh\left(\frac{b\tau}{2}\right)\right] e^{-\left(2\varepsilon-b+v^2\right)\tau} e^{-2\tau/d^2} I_0\left(2\tau/d^2\right). \tag{3.28}$$

The first pair of multipliers in Eq. (3.28) is independent of the inter-plane distance $d$ and exponentially decreases for $\tau > (2\varepsilon - b + v^2)^{-1}$, while the last pair of multipliers depends on the layered structure. The expression (3.25) is divergent at small $\tau$, so an UV cutoff $\tau_{cut}$ is necessary for regularization. Substituting the expectation value into the "gap equation", Eq. (3.11), the later takes a form

$$\varepsilon = -a_h + \frac{\eta_{mf}\bar{t}_{mf}b}{\pi s}\int_{\tau=\tau_{cut}}^\infty \frac{f(\varepsilon,\tau)}{\sinh(b\tau)}. \tag{3.29}$$

### 3.3.2 Renormalization

Let us first consider the expression of the superfluid density. In the case $v = 0$, we shall obtain the thermodynamic limit

$$\left\langle |\psi_n(\mathbf{r},\tau)|^2 \right\rangle = \frac{\eta_{mf}\bar{t}_{mf}b}{2\pi s}\int_{\tau=\tau_{cut}}^\infty \frac{\exp\left\{-\left(2\varepsilon - b + \frac{2}{d^2}\right)\tau\right\} I_0\left(\frac{2\tau}{d^2}\right)}{\sinh(b\tau)}. \tag{3.30}$$

We take b to zero limit:

$$\begin{aligned}\left\langle |\psi_n(\mathbf{r},\tau)|^2 \right\rangle &= \frac{\eta_{mf}\bar{t}_{mf}}{2\pi s}\int_{\tau=\tau_{cut}}^\infty \frac{\exp\left\{-\left(2\varepsilon + \frac{2}{d^2}\right)\tau\right\} I_0\left(\frac{2\tau}{d^2}\right)}{\tau} \\ &= \frac{\eta_{mf}\bar{t}_{mf}}{2\pi s}\int_{\tau_{cut}/d^2}^\infty \exp\left\{-\left(2\varepsilon d^2 + 2\right)\tau\right\} I_0\left(2\tau\right) d\ln\tau. \end{aligned} \tag{3.31}$$

We make an integration by parts

$$\int_{\tau_{cut}/d^2}^{\infty} \exp\left\{-\left(2\varepsilon d^2+2\right)\tau\right\} I_0\left(2\tau\right) d\ln\tau$$
$$= -\exp\left\{-\left(2\varepsilon d^2+2\right)\frac{\tau_{cut}}{d^2}\right\} I_0\left(2\tau_{cut}/d^2\right)\ln\left(\frac{\tau_{cut}}{d^2}\right)$$
$$-\int_{\tau_{cut}/d^2}^{\infty} \frac{d\left[\exp\left\{-\left(2\varepsilon d^2+2\right)\tau\right\} I_0\left(2\tau\right)\right]}{d\tau}\ln\tau d\tau. \tag{3.32}$$

For small $\tau_{cut}$, one obtains

$$\int_{\tau_{cut}/d^2}^{\infty} \exp\left\{-\left(2\varepsilon d^2+2\right)\tau\right\} I_0\left(2\tau\right) d\ln\tau \simeq -\int_0^{\infty} \frac{d\left[\exp\left\{-\left(2\varepsilon d^2+2\right)\tau\right\} I_0\left(2\tau\right)\right]}{d\tau}\ln\tau d\tau$$
$$-\ln\left(\frac{\tau_{cut}}{d^2}\right). \tag{3.33}$$

If $\varepsilon = 0$, one has

$$\int_{\tau_{cut}/d^2}^{\infty} \exp\left\{-2\tau\right\} I_0\left(2\tau\right) d\ln\tau \simeq -\gamma_E - \ln\left(\tau_c/d^2\right), \tag{3.34}$$

where

$$\int_0^{\infty} \frac{d\left[\exp\left\{-2\tau\right\} I_0\left(2\tau\right)\right]}{d\tau}\ln\tau d\tau = \gamma_E = 0.577. \tag{3.35}$$

Therefore, the expression of the superfluid density in the case $\nu, b, \varepsilon = 0$ is

$$\left\langle|\psi_n(\mathbf{r},\tau)|^2\right\rangle \simeq -\frac{\eta_{mf}\bar{t}_{mf}}{2\pi s}\{\ln\left(\tau_{cut}/d^2\right)+\gamma_E\}. \tag{3.36}$$

Physically the renormalization corresponds to reduction of the critical temperature by the thermal fluctuations from $T_c^{mf}$ to $T_c$. The thermal fluctuations occur on the mesoscopic scale. The critical temperature $T_c$ is defined at $\varepsilon = 0$, and $\upsilon = 0$, and at low magnetic field less than $H_{c1} = \frac{H_{c2}}{2\kappa^2}\ln(\kappa)$ (for a typical high-$T_c$ superconductor, $\kappa \simeq 50$, $H_{c1} =$

$7.8 \times 10^{-4} H_{c2}$ ), the superconductor is at Meissner phase, $b = 0$, the Eq. (3.29) leads to

$$0 = \left(1 - \frac{T_c}{T_c^{mf}}\right) + \frac{2\eta}{\pi s}\{\ln\left(\tau_{cut}/d^2\right) + \gamma_E\}. \tag{3.37}$$

Then one obtains relation between $T_c$ and $T_c^{mf}$:

$$T_c = T_c^{mf}\left\{1 + \left[\frac{2\eta}{\pi s}\ln\left(\tau_{cut}/d^2\right) + \gamma_E\right]\right\}, \tag{3.38}$$

where note once again that $\eta_{mf} = \eta\frac{T_c^{mf}}{T_c}$, and $\eta = \sqrt{2Gi}\pi$ with $Gi = \frac{1}{2}\left(8e^2\kappa^2\xi T_c\gamma/c^2\hbar^2\right)^2$($T_c^{mf}$ is now replaced by $T_c$).

In order to absorb the divergence into a "renormalized" value $a_h^r$ of the coefficient $a_h$ in the Eq. (3.29), it is convenient to make an integration by parts in the last term for small $\tau_{cut}$:

$$b\int_{\tau=\tau_{cut}}^{\infty}\frac{f(\varepsilon,\tau)}{\sinh(b\tau)} = \ln[\sinh(b\tau)]\frac{f(\varepsilon,\tau)}{\cosh(b\tau)}|_{\tau_{cut}}^{\infty} - \int_0^{\infty}\ln[\sinh(b\tau)]\frac{d}{d\tau}\left[\frac{f(\varepsilon,\tau)}{\cosh(b\tau)}\right], \tag{3.39}$$

For small $b$ and $\tau_c$, the first term in right side of Eq. (3.39) can be made approximative

$$b\int_{\tau=\tau_{cut}}^{\infty}\frac{f(\varepsilon,\tau)}{\sinh(b\tau)} \simeq -\int_0^{\infty}\ln[\sinh(b\tau)]\frac{d}{d\tau}\left[\frac{f(\varepsilon,\tau)}{\cosh(b\tau)}\right] - \ln(b\tau_{cut}). \tag{3.40}$$

Then Eq. (3.29) can be rewritten as

$$\begin{aligned}\varepsilon &= -a_h - \frac{\eta_{mf}\bar{t}_{mf}}{\pi s}\left\{\int_0^{\infty}\ln[\sinh(b\tau)]\frac{d}{d\tau}\left[\frac{f(\varepsilon,\tau)}{\cosh(b\tau)}\right] + \ln(b\tau_{cut})\right\} \\ &= -a_h - \frac{\eta\bar{t}}{\pi s}\left\{\int_0^{\infty}\ln[\sinh(b\tau)]\frac{d}{d\tau}\left[\frac{f(\varepsilon,\tau)}{\cosh(b\tau)}\right] - \gamma_E + \ln(bd^2)\right\} \\ &\quad -\frac{\eta\bar{t}}{\pi s}\left[\ln\left(\tau_{cut}/d^2\right) + \gamma_E\right],\end{aligned} \tag{3.41}$$

Let's consider the first and last term in the right hand side of Eq. (3.41)

$$\begin{aligned} -a_h - \frac{\eta\bar{t}}{\pi s}\left[\ln\left(\tau_{cut}/d^2\right)+\gamma_E\right] &= -\frac{1-\bar{t}_{mf}-b}{2} - \frac{\eta\bar{t}}{\pi s}\left[\ln\left(\tau_{cut}/d^2\right)+\gamma_E\right] \\ &= -\frac{1-\bar{t}-b}{2} - \bar{t}\left\{\frac{1-\frac{T_c}{T_c^{mf}}}{2} + \frac{\eta}{\pi s}\left[\ln\left(\tau_{cut}/d^2\right)+\gamma_E\right]\right\}. \end{aligned} \tag{3.42}$$

Substituting Eq. (3.38) into Eq. (3.42), then this becomes

$$-a_h - \frac{\eta\bar{t}}{\pi s}\left[\ln\left(\tau_{cut}/d^2\right)+\gamma_E\right] = -\frac{1-\bar{t}-b}{2}. \tag{3.43}$$

Then Eq. (3.41) becomes

$$\varepsilon = -a_h^r - \frac{\eta\bar{t}}{\pi s}\left\{\int_0^\infty \ln[\sinh(b\tau)]\frac{d}{d\tau}\left[\frac{f(\varepsilon,\tau)}{\cosh(b\tau)}\right] - \gamma_E + \ln(bd^2)\right\}, \tag{3.44}$$

where $a_h^r = \frac{1-\bar{t}-b}{2}$. The formula is cutoff independent. In terms of energy UV cutoff $\Lambda$, introduced for example in [51], the cutoff "time" $\tau_{cut}$ can be expressed as

$$\tau_{cut} = \frac{1}{2e^{\gamma_E}\Lambda}. \tag{3.45}$$

This is obtained by comparing a thermodynamic result for a physical quantity like superfluid density with the dynamic result (see Appendix C). The temporary UV cutoff used is completely equivalent to the standard energy or momentum cutoff Lambda used in thermodynamics (in which the time dependence does not appear). Physically one might think about momentum cutoff as more basic and this would be universal and independent of particular time dependent realization of thermal fluctuations (TDGL with white noise in our case). Roughly (in physical units) $\Lambda \simeq \varepsilon_F = \hbar^2 k_F^2/(2m^*)$. In the next section we will discuss the estimate of $T_c^{mf}$ using this value due to the following reason. For high-$T_c$ materials ordinary BCS is invalid and coherence length is of order of lattice spacing (the cutoff becomes microscopic) and therefore the energy cutoff is of order $\varepsilon_F$. Except the

formula to calculate $T_c^{mf}$, all other formulas in this paper is independent of energy cutoff.

## 3.4 $I-V$ curve

### 3.4.1 Current density

The supercurrent density, defined by Eq. (3.9), can be expressed via the GF by substituting Eq. (3.17) and Eq.(3.12) into Eq. (3.9):

$$\begin{aligned} j_y^s &= \frac{i}{2}\int_0^{2\pi/d}\frac{dk_z}{2\pi}\int_0^{2\pi/d}\frac{dk_z'}{2\pi}\exp\left[ind(k_z-ik_z')\right] \\ &\quad\times\left\langle\int_{\mathbf{r}',t'}G_{k_z}^*\left(\mathbf{r},t;\mathbf{r}',t'\right)\overline{\zeta}_{k_z}^*\left(\mathbf{r}',t'\right)\frac{\partial}{\partial y}\int_{\mathbf{r}'',t''}G_{k_z'}\left(\mathbf{r},t;\mathbf{r}'',t''\right)\overline{\zeta}_{k_z'}\left(\mathbf{r}'',t''\right)\right\rangle+cc \\ &= \frac{i}{2}\int_0^{2\pi/d}\frac{dk_z}{2\pi}\int_0^{2\pi/d}\frac{dk_z'}{2\pi}\exp\left[ind(k_z-ik_z')\right]\int_{\mathbf{r}',t',\mathbf{r}'',t''}G_{k_z}^*\left(\mathbf{r},t;\mathbf{r}',t'\right) \\ &\quad\times\frac{\partial}{\partial y}G_{k_z'}\left(\mathbf{r},t;\mathbf{r}'',t''\right)\left\langle\overline{\zeta}_{k_z}^*\left(\mathbf{r}',t'\right)\overline{\zeta}_{k_z'}\left(\mathbf{r}'',t''\right)\right\rangle+cc. \end{aligned} \tag{3.46}$$

Substituting the noise correlation (3.8) into expression (3.46), the supercurrent density takes form:

$$j_y^s = i\eta\bar{t}\frac{d}{s}\int_0^{2\pi/d}\frac{dk_z}{2\pi}\int_{\mathbf{r}',t'}G_{k_z}^*\left(\mathbf{r},t;\mathbf{r}',t'\right)\frac{\partial}{\partial y}G_{k_z}\left(\mathbf{r},t;\mathbf{r}',t'\right)+c.c. \tag{3.47}$$

Substituting Eq. (3.19) into Eq. (3.47), one has

$$\begin{aligned} j_y^s &= i\eta\bar{t}\frac{d}{s}\int_0^{2\pi/d}\frac{dk_z}{2\pi}\int d\mathbf{r}'\int_{\tau=0}^{\infty}\left[\left\{\frac{ib}{2}X-\frac{1}{\beta}Y\right\}g_{k_z}^2\left(X,Y,\tau\right)\right]+c.c \\ &= i\eta b\bar{t}\frac{d}{s}\int_0^{2\pi/d}\frac{dk_z}{2\pi}\int_{\tau=0}^{\infty}|C|^2\int dXdY\left\{\frac{ib}{2}X-\frac{1}{\beta}Y\right\}\exp\left[-\frac{X^2+Y^2}{\beta}-2vX\right]+cc. \end{aligned} \tag{3.48}$$

Performing the Gaussian integrals over $X$ and $Y$, one obtains:

$$j_y^s = \frac{\eta\bar{t}}{4\pi s}v\int_{\tau=0}^{\infty}\frac{f(\varepsilon,\tau)}{\cosh^2(\frac{b\tau}{2})}, \tag{3.49}$$

where the function $f$ was defined in Eq. (3.28). Consequently the contribution to the conductivity is $\sigma_s = j_y^s/\mathcal{E}$. The conductivity expression is not divergent when expressed as a function of renormalized $T_c$ (the real transition temperature), so it is independent of the cutoff. This is considered in detail in section 3.3.2 and is indeed different from the Ref. [58]. In physical units the current density reads

$$J_y = \sigma_n E \left[ 1 + \frac{\eta \bar{t}}{4\pi s} \frac{1}{k} \int_{\tau=0}^{\infty} \frac{f(\varepsilon, \tau)}{\cosh^2(\frac{b\tau}{2})} \right]. \tag{3.50}$$

This is the main result of the present paper. We also obtained the conductivity expression in $2D$ in linear response which do match the linear response conductivity expression (2.79) and [51].

$$\sigma_{2D}^s = \frac{\eta_{2D} \bar{t}}{4\pi b} \frac{\sigma_n}{k} \left\{ 2 - \left( 1 - \frac{2\varepsilon}{b} \right) \left[ \psi_p \left( \frac{\varepsilon}{b} \right) - \psi_p \left( \frac{1}{2} + \frac{\varepsilon}{b} \right) \right] \right\}. \tag{3.51}$$

### 3.4.2 Comparison with experiment

The experiment results of I. Puica *et al.* [49], obtained from the resistivity and Hall effect measurements on an optimally doped YBCO films of thickness 50 nm and $T_c = 86.8$ K. The distance between the bilayers used the calculation is $d' = 11.68$ Å in Ref. [60]. The number of bilayers is 50, large enough to be described by the Lawrence-Doniach model without taking care of boundary conditions. In order to compare the fluctuation conductivity with experimental data in HTSC, one cannot use the expression of relaxation time $\gamma'$ in BCS which may be suitable for low-$T_c$ superconductor. Instead of this, we use the factor $k$ as fitting parameter.

The comparison is presented in Fig. 3.1. The resistivity in physical units

$$\rho = \frac{1}{\sigma_{GL}\sigma_s + \sigma_n} = \frac{1}{\sigma_n(\sigma_s/k + 1)}, \tag{3.52}$$

curves were fitted to Eq. (3.52) with the normal-state conductivity measured in Ref. [49]

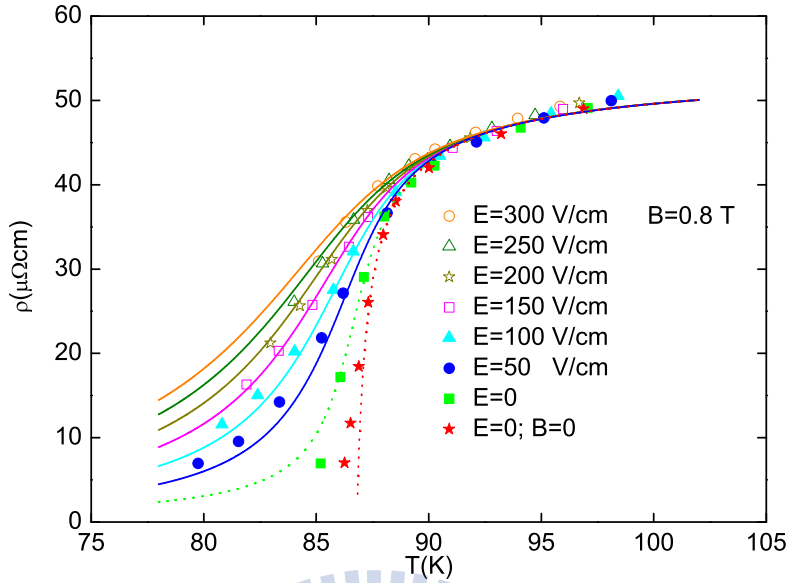


Figure 3.1: Points are resistivity for different electric fields of an optimally doped YBCO in Ref. [49]. The solid line is the theoretical value of resistivity calculated from Eq. (3.52) with fitting parameters (see text).

to be $\sigma_n = 1.9 \times 10^4$ $(\Omega\text{cm})^{-1}$. The parameters we obtain from the fit are: $H_{c2}(0) = 190$ T (corresponding to $\xi = 13.2$ Å), $\kappa = 43.6$, $s' = 8.5$ Å, $k = 0.55$, where we take $\gamma = 7.8$ for optimally doped YBCO in Ref. [42]. Using those parameters, we obtain $Gi = 9.32 \times 10^{-4}$ (corresponding to $\eta = 0.136$). The order parameter effective thickness $s'$ can be taken to be equal to the layer thickness (see in Ref. [61]) of the superconducting $CuO_2$ plane plus the coherence length $2\xi_z = 2\frac{\xi}{\gamma}$ due to the proximity effect: 3.18 Å+$2\frac{13.2}{7.8}$ Å= 6.9 Å, roughly in agreement in magnitude with the fitting value of $s'$.

We will now estimate $T_c^{mf}$ for this sample. For the underdoped YBCO, the radius of the Fermi surface of YBCO was measured in Ref. [62], $k_F = 0.7$ Å$^{-1}$, while the effective mass is $m^* = 1.9 m_e$. We will assume that the Fermi energy for underdoped YBCO of Ref. [62] is $\varepsilon_F = \hbar^2 k_F^2/(2m^*)$ and is roughly the same for the optimal YBCO studied in this paper. The cutoff "time" in physical units is then, according to Eq. (3.45), $\tau_{cut} = 2 \times 10^{-16}$ s. Equation (3.38) gives then $T_c^{mf} = 101.15$ K.

Using the parameters specified above we plot several theoretical $I - V$ curves. As expected the $I - V$ curve shown in Fig. 3.2 and Fig. 3.3 has two linear portions, the flux

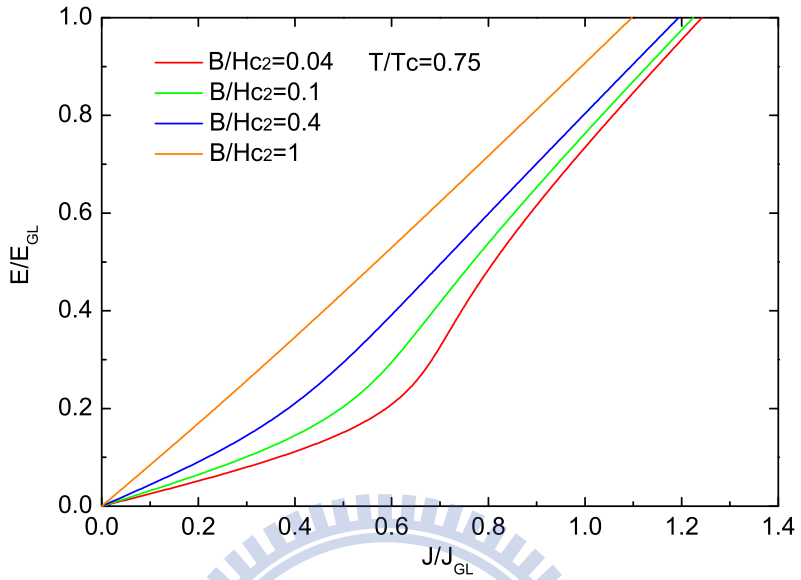


Figure 3.2: The current-voltage curves calculated from Eq. (3.50) by using the parameters (see text) for different magnetic fields $b = B/Hc2$ at temperature $\bar{t} = 0.75$.

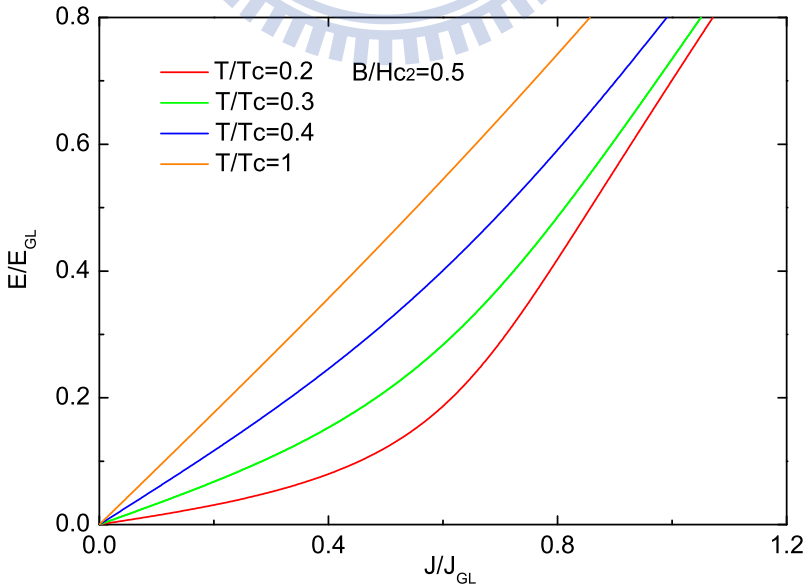


Figure 3.3: The current-voltage curves calculated from Eq. (3.50) by using the parameters (see text) for different temperatures $\bar{t} = T/Tc$ at magnetic flied $b = 0.5$.

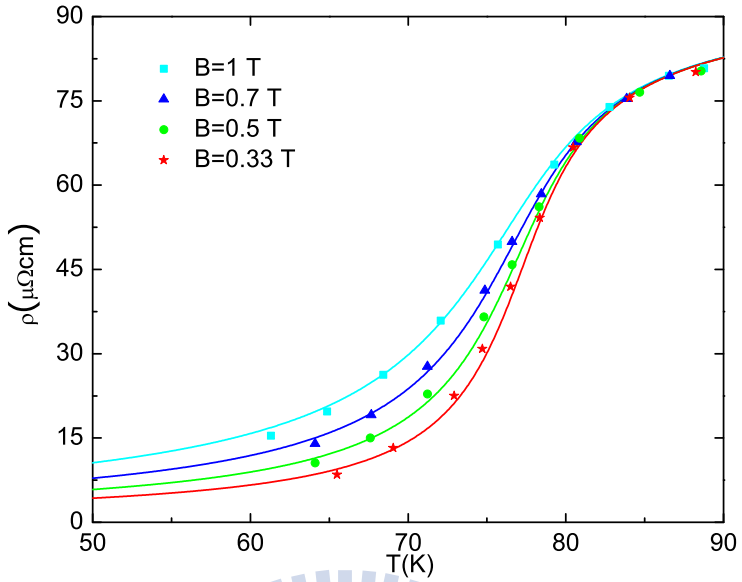


Figure 3.4: Points are resistivity for different magnetic fields of Bi2212 in Ref. [48]. The solid line is the theoretical value of resistivity calculated from Eq. (3.52) in linear case with fitting parameters (see text).

flow part for $E \ll E_{GL}$ and the normal Ohmic part for $E \gg E_{GL}$. In the crossover region, $E \sim E_{GL}$, a $I-V$ curve becomes nonlinear due to destruction of superconductivity (the normal area inside the vortex cores increases to fill all the space). In Fig. 3.2 the $I-V$ curves are shown for different the magnetic fields, at a fixed temperature $T = 0.75T_c$. At given electric field, as the magnetic field increases, the supercurrent decreases. When the magnetic field reaches $H_{c2}$, the $I-V$ curve becomes linear. In Fig. 3.3 the $I-V$ curves are shown for different temperatures, at a fixed magnetic field $H = 0.5H_{c2}$. At given electric field, as the temperature increases, the supercurrent decreases. When the temperature reaches $T_c$, the $I-V$ curve becomes linear. With decreasing temperature the crossover becomes steeper.

Our the results in linear response is also compared to the experiment data on Bi2212 [48] with $T_c = 81$. The layer distance used the calculation is $d' = 19.6$ Å in Ref. [61]. The comparison is presented in Fig. 3.4. The resistivity curves were fitted to Eq. (3.52) with the normal-state conductivity in Ref. [48] to be $\sigma_n = 1.42 \times 10^4\ (\Omega\text{cm})^{-1}$. The best fitting parameters are: $H_{c2}(0) = 150$ T (corresponding to $\xi = 14$ Å), $\kappa = 47.8$, $s' = 4.31$

Å, $k = 0.61$, and $\gamma = 25$ which give $Gi = 0.015$. The order parameter effective thickness $s'$ can be also roughly estimated: 3.32 Å+$2\frac{14}{25}$ Å= 4.5 Å, consistent with the fitting value of $s'$.

## 3.5 Summary

We calculated electrical conductivity and the $I - V$ curve in a layered Type-II superconductor in magnetic field in the presence of strong thermal fluctuations on the mesoscopic scale beyond the linear response. Time dependent Ginzburg-Landau equations with thermal noise describing the thermal fluctuations is used to describe the vortex-liquid regime and arbitrary flux flow velocities. The nonlinear term in dynamics is treated using the self-consistent Gaussian approximation. Thus exact analytical expression of Green's function of the linearized TDGL equation incorporating all Landau levels was obtained. The method is very general, and it allow us to study transport phenomena beyond linear response of Type-II superconductor such as the Nernst effect and Hall effect.

The renormalization of the critical temperature is calculated and is strong in layered high $T_c$ materials. The results were compared to the experimental data on HTSC. Our the resistivity results are in good qualitative and even quantitative agreement with experimental data on YBCO in strong electric fields and Bi2212 in linear case.

# Chapter 4

# Fluctuation Hall conductivity beyond a linear response in layered superconductor under a magnetic field

## 4.1 Introduction

### 4.1.1 Hall effect

The Hall effect is the production of a voltage difference (the Hall voltage) across an electrical conductor, transverse to an electric current in the conductor and a magnetic field perpendicular to the current. Edwin Hall discovered this effect in 1879. The Hall effect provides information on the sign, concentration, and mobility of charge carrier in the normal state. The experimental arrangement illustrated in Fig. 4.1 shows a magnetic field $\mathbf{B}$ applied in the $z$ direction perpendicular to a slab and a battery that establishes an electric field $E_y$ in the $y$ direction that causes a current $\mathbf{I} = \mathbf{J}A$ to flow, where $\mathbf{J} = ne\mathbf{v}$

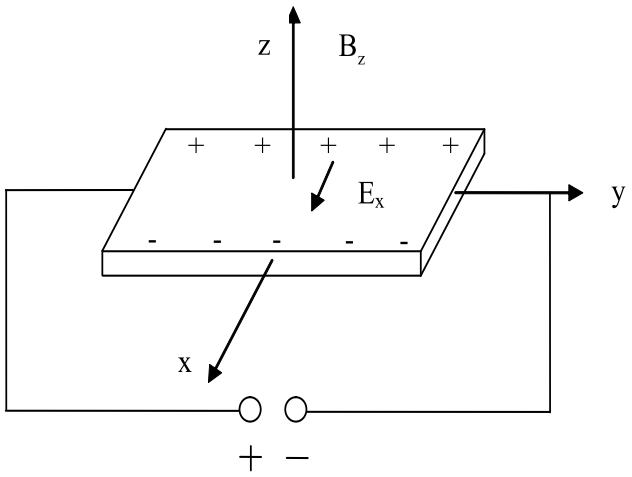


Figure 4.1: Experimental arrangement for Hall effect measurements.

is the current density. The Lorentz force

$$\mathbf{F} = q\mathbf{v} \times \mathbf{B}, \tag{4.1}$$

of the magnetic field on each moving charge $q$ is in the positive $x$ direction for both positive and negative charge carriers. This causes a charge separation to build up on the sides of the plate, which produces an electric field $\mathbf{E}_x$ perpendicular to the directions of the current $y$ and magnetic $z$ fields. The induced electric field is in the negative $x$ direction for positive $q$, and in the positive $x$ direction for negative $q$. After the charge separation has built up, the electric force $q\mathbf{E}_x$ balances the magnetic force $q\mathbf{v} \times \mathbf{B}$,

$$q\mathbf{E}_x = q\mathbf{v} \times \mathbf{B}, \tag{4.2}$$

and the charge carriers $q$ proceed along the wire undeflected.

The Hall coefficient $R_H$ is defined as a ratio

$$R_H = \frac{E_x}{J_y B_z} = \pm\frac{1}{ne}, \tag{4.3}$$

with a positive sign (+) for holes a negative sign (-) for electrons.

In the superconducting state, the Hall voltage arises from the electric field induced by flux motion. Perhaps the most important results that has been obtained from Hall effect measurement above $T_c$ is that the charge carriers in the copper-oxide planes of most of the HTSC are holes. Included in this group are the lanthanum, yttrium, bismuth, thallium, and mercury classes of compounds. The major exception is compounds with the $Nd_2CuO_4$, their charge carriers are electron-like. Below $T_c$, flux flow arising from a transport current in a superconductor induces an electric field **E**. The component of this electric field perpendicular to the direction of the current produces a Hall-effect voltage. The Hall resistivity $\rho_{xy}$ is defined as

$$\rho_{xy} = \frac{E_x}{J}, \tag{4.4}$$

is close to zero for low applied fields in the mixed state below $T_c$ and negative for higher fields. Thereafter, it becomes positive and increase linearly with further increase in fields [63–65].

### 4.1.2 Hall conductivity

The influence of superconducting fluctuations on off-diagonal components of the magnetoconductivity tensor (usually denoted as the excess Hall effect) in HTSC has received considerable experimental and theoretical attention over the past few years [8, 63–78] . Though a general consensus seems to be achieved now regarding the existence and the temperature dependence of the excess Hall effect, theoretical predictions of its sign are still controversial. Experimentally, the Hall resistivity shows a peculiar temperature dependence. Specifically, as the temperature is decreased through the fluctuation region, the Hall resistivity decreases and changes its sign relatively to the normal-state one, exhibits a negative minimum, and eventually reaches zero at low temperatures. This simple sign change was detected in many different HTSC in Refs. [70, 73, 79, 80] and even in

conventional superconductors Ref. [71, 72]. Furthermore, a double-sign reversal, which is a subsequent return of the Hall resistivity to the positive value before vanishing, has been observed in highly anisotropic HTSC, such as Bi2212 crystals [81] and films [82], $Tl_2Ba_2CaCu_2O_x$ films [83], or $HgBa_2CaCu_2O_6$ films [84]. Recently, the existence of the second sign change was also reported in YBCO films, either at high current densities [85] or in the strong pinning limit at low magnetic fields [86]. Finally, even a triple-sign reversal was reported in $HgBa_2CaCu_2O_6$ films with columnar defects induced by high-density ion irradiation [87].

Several theoretical approaches have attempted to explain the complex features of the Hall resistivity temperature dependence, but no consensus has been achieved. The Hall anomaly might originate from the pinning force [66], nonuniform carrier density in the vortex core [88, 89], or can be calculated in the TDGL model [90, 91]. Most recent theories claim to predict the double or triple-sign reversal, based either on entirely intrinsic mechanism of vortex motion and electronic spectrum [92], or on hydrodynamic interaction between vortices and the superconducting and normal-state fluids [93]. Some theories invoke superconducting fluctuations alone to account for the Hall effect sign reversal [11, 94], while others present a more extended picture based on the same foundations of TDGL using both the hydrodynamics and the vortex charging effect, arising from the difference in electron density between the core and the far outside region of the vortex [88, 89, 95]. Thus, the Hall effect in the mixed state of HTSC reflects a complex interplay between electronic properties of quasiparticles, thermodynamic fluctuations, hydrodynamic effects of vortices, and pinning.

From a considerable part of the published theoretical work, it appears that at least the first sign reversal, which occurs near the critical region, where vortex pinning is negligible and the superconducting order-parameter fluctuations play an important role, should be ascribed to a microscopic origin of superconductivity [68, 96, 97]. From the viewpoint of the TDGL formalism [11, 91, 94], to which any theory of vortex dynamics must reduce near the critical temperature $T_c$ [92, 98], the Hall anomaly is a consequence

of the difference in sign between the normal (quasiparticle) part and the superconducting fluctuation (or vortex flow) part of the total Hall conductivity. These two components have opposite signs, if the energy derivative of the density of states averaged over the Fermi surface is positive when the carriers are holes in the normal state [99]. Thus, the sign reversal can be intrinsic and depends on the details of the structure of the normal-state electronic spectrum. Such notion is further supported by the fact that in several HTSC, the sign reversal disappears when the material is strongly overdoped and the band structure approaches that of a conventional metal [100].

The possibility of the Hall angle sign change in the critical region was first discussed by Fukuyama, Ebisawa, and Tsuzuki (FET) [101], who pointed out that the origin of a nonvanishing Hall current due to fluctuating Cooper pairs could come from a hole-particle asymmetry, which reveals a complex relaxation time in the TDGL theory. In this early work, it was implicitly assumed that the fluctuations did not interact; that is, only Gaussian fluctuations were considered. Accordingly, the fluctuation parts of the conductivity tensor elements were predicted to diverge at $T_c$ in the presence of magnetic field. However, this predicted divergence has not been observed. A great improvement was obtained when the interaction between fluctuations was taken into account by incorporating the quartic term $|\Psi|^4$ from the GL expression of the free energy. Such a treatment was performed by Ullah and Dorsey [11] (UD) in the frame of a simple Hartree approach of the TDGL theory. More recently, Nishio and Ebisawa [94] (NE) extended the FET calculations of the weak (Gaussian) fluctuation contribution of the Hall conductivity to the strong (non-Gaussian) fluctuation regime, based on more sophisticated renormalization theory by Ikeda, Ohmi, and Tsuneto [102] (IOT). The renormalized, non- Gaussian fluctuation regime connects therefore the weak (Gaussian) fluctuation regime in the paraconducting region above $T_{c2}(H)$ to the vortex liquid (flux-flow) regime below the mean-field transition, interpolating smoothly without the $T_c$ divergence predicted by the Gaussian theory. The comparison between experimentally observed Hall anomaly in HTSC and the full quantitative application of the TDGL theory was done well by Puica *et. al.* [65].

However, all theories mentioned above is linear response. Recently, non-Ohmic fluctuation Hall conductivity was treated theoretically [58] and experimentally [49]. The non-Ohmic fluctuation Hall conductivity calculated in [58] was in good qualitative correspondence with the theoretical one [49], but the magnitude of the effect is somewhat smaller. The authors in [58] believe that the two quantities, layer distance and thickness in the Lawrence-Doniach for HTSC, are equal. They also made assumption that the imaginary part of the relaxation time $\gamma_1$ in the TDGL equation is small in comparison with the real one $\gamma$ as calculating the fluctuation Hall conductivity.

In this study the non-Ohmic fluctuation Hall conductivity of the moving vortex liquid in a layered superconductor under magnetic field perpendicular to the layers is studied using the TDGL approach. The layered structure is modeled via the Lawrence-Doniach discretization in the magnetic field direction. We consider layer distance and thickness in the Lawrence-Doniach as two independent parameters. The self-consistent Gaussian approximation mentioned in section 3.3.1 is used to treat the model while Ref. [58] used the Hartree approximation. A main contribution of this study is an explicit form of the Green's function incorporating all Landau levels. This allows to obtain explicit formulas without need to cutoff higher Landau levels and any assumption about the imaginary part of the relaxation time $\gamma_1$ in the TDGL equation. In Ref. [58], a nontrivial matrix inversion (of infinite matrices) or cutting off the number of Landau levels is required. The renormalization of the models is also different from Ref. [58]. One of the main result of our work is that the Hall conductivity formula is independent of UV cutoff (unlike in Ref. [58]).

### 4.1.3 Dissipative dynamics of vortices and electric fields in the mixed state for Hall effect

In order to calculate the Hall conductivity the imaginary part of the relaxation time in the TDGL equation must be introduced to break the particle-hole symmetry and allow

for a nonvanishing Hall current [8, 11, 58, 94, 101]. The TDGL equation (3.4) then takes form:

$$\frac{\hbar^2(\gamma' + i\gamma'')}{2m^*} D_t \Psi_n = -\frac{\delta}{\delta \Psi_n^*} \frac{F_{GL}}{s'} + \xi_n \tag{4.5}$$

The particle-hole symmetry exists for $\gamma'' = 0$. By particle-hole symmetry we mean that, under transformation of complex conjugation and $H \to -H$, the equation motion for $\Psi^*$, Eq. (4.5), is the same as that for $\Psi$, provided $\gamma'' = 0$. This result would, in turn, imply that $\sigma_{xy}(H) = \sigma_{xy}(-H)$; however, we know that, on general grounds, $\sigma_{xy}(H) = -\sigma_{xy}(-H)$, so that $\sigma_{xy}(H) = 0$ if $\gamma'' = 0$. Therefore, $\gamma'' \neq 0$ is necessary in order that the Hall conductivity be nonzero. Such an imaginary relaxation rate can arise from microscopic considerations [8, 101] or might be generated by coupling the order parameter to conserved densities, as in critical dynamics of neutral superfluids [103]. Keeping the same notation as in section 3.2, the TDGL equation in dimensionless units in the Gaussian approximation reads

$$(1 + i\vartheta) D_t \psi_n - \left( \frac{1}{2} D^2 + \frac{b}{2} \right) \psi_n + \frac{1}{2d^2} (2\psi_n - \psi_{n+1} - \psi_{n-1}) + \varepsilon \psi_n = \overline{\zeta}_n \tag{4.6}$$

where $\vartheta = \gamma''/\gamma'$. Usually $\gamma''$ is small in comparison with $\gamma'$ by a ratio of the order of $T_c/E_F$ [8].

In a similar way the relaxational linearized TDGL equation with a Langevin noise, Eq. (4.6), is solved using the retarded ($G' = 0$ for $t < t'$) GF $G'_{k_z}(\mathbf{r}, t; \mathbf{r}', t')$:

$$\psi_n(\mathbf{r}, t) = \int_0^{2\pi/d} \frac{dk_z}{2\pi} e^{-ink_z d} \int d\mathbf{r}' \int d\tau' G'_{k_z}(\mathbf{r}, t; \mathbf{r}', t') \overline{\zeta}_{k_z}(\mathbf{r}', t'). \tag{4.7}$$

The GF satisfies

$$\left[ (1 + i\vartheta) D_t - \frac{1}{2} D^2 - \frac{b}{2} + \frac{1}{d^2} [1 - \cos(k_z d)] + \varepsilon \right] G'_{k_z}(\mathbf{r}, \mathbf{r}', t - t') = \delta(\mathbf{r} - \mathbf{r}') \delta(t - t'), \tag{4.8}$$

and is computed in Appendix D. The result (see Appendix D) is:

$$G'_{k_z}(\mathbf{r},\mathbf{r}',\tau) = C'(k_z)\theta(\tau)\exp\left[\frac{ib}{2}X(y+y')\right]\exp\left(-\frac{X^2+Y^2}{2\beta'} - v(1+i\vartheta)X\right), \quad (4.9)$$

where

$$\begin{aligned} C'(k_z) &= \frac{b}{4\pi}\exp\left\{-\left(\varepsilon - \frac{b}{2} + \frac{v^2(1+i\vartheta)^2}{2} + \frac{1}{d^2}[1-\cos(k_z d)]\right)\frac{\tau}{(1+i\vartheta)}\right\} \\ &\quad \times \sinh^{-1}\left(\frac{b}{2}\frac{\tau}{(1+i\vartheta)}\right), \end{aligned} \quad (4.10)$$

$$\beta' = \frac{2}{b}\tanh\left(\frac{b}{2}\frac{\tau}{(1+i\vartheta)}\right), \quad (4.11)$$

with $X = x - x' - v\tau; Y = y - y'$; and $\tau = t - t'$.

## 4.2 The gap equation

In the same way the thermal average of the superfluid density (density of Cooper pairs) can be expressed via the GF $G'_{k_z}(\mathbf{r},t;\mathbf{r}',t')$

$$\begin{aligned} \left\langle|\psi_n(\mathbf{r},\tau)|^2\right\rangle &= 2\eta_{mf}\bar{t}_{mf}\frac{d}{s}\int_0^{2\pi/d}\frac{dk_z}{2\pi}\int d\mathbf{r}'\int_{-\infty}^{\tau}dt'\left|G'_{k_z}(\mathbf{r},t;\mathbf{r}',t')\right|^2 \\ &= 2\eta_{mf}\bar{t}_{mf}\frac{d}{s}\int_0^{2\pi/d}\frac{dk_z}{2\pi}\int d\mathbf{r}'\int_0^{\infty}d\tau\left|C'\right|^2\exp\left(-\frac{X^2+Y^2}{\beta''} - 2vX\right) \\ &= 2\pi\eta_{mf}\bar{t}_{mf}\frac{d}{s}\int_0^{\infty}d\tau\beta''\exp\left(\beta''v^2\right)\int_0^{2\pi/d}\frac{dk_z}{2\pi}\left|C'\right|^2, \end{aligned} \quad (4.12)$$

where

$$\beta'' = \frac{2\beta'\beta'^*}{\beta'+\beta'^*} = \frac{4}{b}\frac{\cosh\left(\frac{b\tau}{(1+\vartheta^2)}\right) - \cosh\left(i\vartheta\frac{b\tau}{(1+\vartheta^2)}\right)}{\cosh\left(\frac{b\tau}{(1+\vartheta^2)}\right)}, \quad (4.13)$$

$$|C'|^2 = \left(\frac{b}{4\pi}\right)^2 \exp\left\{-\left(2\varepsilon - b + v^2(1-\vartheta^2) + \frac{2}{d^2}[1-\cos(k_z d)]\right)\frac{\tau}{(1+\vartheta^2)}\right\} \times \sinh^{-1}\left(\frac{b}{2}\frac{\tau}{(1+i\vartheta)}\right)\sinh^{-1}\left(\frac{b}{2}\frac{\tau}{(1-i\vartheta)}\right). \quad (4.14)$$

Note that

$$\int_0^{2\pi/d}\frac{dk_z}{2\pi}|C'|^2 = \frac{1}{d}\left(\frac{b}{4\pi}\right)^2 \exp\left\{-\left(2\varepsilon - b + v^2(1-\vartheta^2) + \frac{2}{d^2}\right)\frac{\tau}{(1+\vartheta^2)}\right\} \times \sinh^{-1}\left(\frac{b}{2}\frac{\tau}{(1+i\vartheta)}\right)\sinh^{-1}\left(\frac{b}{2}\frac{\tau}{(1-i\vartheta)}\right) I_0\left[\frac{2\tau}{(1+\vartheta^2)d^2}\right], \quad (4.15)$$

where the Gamma function $I_0$ was introduced in section 3.3.2. Then the expression (4.12) takes form

$$\left\langle|\psi_n(\mathbf{r},t)|^2\right\rangle = \frac{\eta_{mf}\bar{t}_{mf}b}{2\pi s}\int_{\tau=\tau_{cut}}^{\infty}\frac{f'(\varepsilon,\tau)}{\sinh\left(\frac{b\tau}{(1+\vartheta^2)}\right)} \quad (4.16)$$

where

$$f'(\varepsilon,\tau) = \exp\left[\frac{4v^2}{b}\frac{\cosh\left(\frac{b\tau}{(1+\vartheta^2)}\right)-\cosh\left(i\vartheta\frac{b\tau}{(1+\vartheta^2)}\right)}{\cosh\left(\frac{b\tau}{(1+\vartheta^2)}\right)}\right] e^{-\left[2\varepsilon-b+v^2(1-\vartheta^2)\right]\tau} \times e^{-2\tau/(1+\vartheta^2)d^2} I_0\left(2\tau/(1+\vartheta^2)d^2\right). \quad (4.17)$$

The value of $\vartheta$ can be inferred from the microscopical theory if one considers the energy derivative $\mathcal{N}'$ of the density of states $\mathcal{N}$ at the Fermi level $\varepsilon_F$, and it writes [8, 94]

$$\vartheta = \frac{k_B T}{\varepsilon_F}\alpha, \quad (4.18)$$

where the parameter $\alpha$ amounts in the BCS model to

$$\alpha = -\frac{4\varepsilon_F \mathcal{N}'}{\pi g_{BCS}\mathcal{N}^2}, \quad (4.19)$$

with $g_{BCS} > 0$ the BCS coupling constant [94, 101]. Since $\varepsilon_F$ is for HTSC of the order of $10^3$ K (in $k_B$ units) [104], and the hole-particle asymmetry parameter $\alpha$, inferred from fits of excess Hall effect data [74] with the models from Refs. [94, 101] its absolute value turns out to be of the order of $10^{-2} \div 10^{-1}$, we conclude that $\vartheta$ is a small parameter (the order of $10^{-3} \div 10^{-2}$), reflecting also the small Hall angle. Therefore, the expression (4.16) can be expanded in first order in small $\vartheta$. Keeping zero order, the expression (4.16) get back to the expression (3.29). Therefore, the gap equation in this case is the same Eq. (3.44) after renormalization.

$$\varepsilon = -a_h^r - \frac{\eta\bar{t}}{\pi s}\left\{\int_0^\infty \ln[\sinh(b\tau)]\frac{d}{d\tau}\left[\frac{f(\varepsilon,\tau)}{\cosh(b\tau)}\right] - \gamma_E + \ln(bd^2)\right\}. \tag{4.20}$$

## 4.3 Fluctuation Hall conductivity

### 4.3.1 Hall current density

In the same way the supercurrent density, defined by Eq. (3.9), can be expressed via the GF by substituting Eq. (4.7) into Eq. (3.9):

$$\begin{aligned} j_x^s &= \frac{i}{2}\left\langle \psi_n^*(\mathbf{r},\tau)\left(\frac{\partial}{\partial x} - iby\right)\psi_n(\mathbf{r},\tau)\right\rangle + cc \\ &= i\eta\bar{t}\frac{d}{s}\int_0^{2\pi/d}\frac{dk_z}{2\pi}\int_{\mathbf{r}',\tau'} G'^*_{k_z}(\mathbf{r},\mathbf{r}',\tau)\left(\frac{\partial}{\partial x} - iby\right)G'_{k_z}(\mathbf{r},\mathbf{r}',\tau) + c.c. \end{aligned} \tag{4.21}$$

Substituting Eq. (4.9) into Eq. (4.21), one has

$$\begin{aligned} j_x^s &= -i\eta\bar{t}\frac{d}{s}\int_0^{2\pi/d}\frac{dk_z}{2\pi}\int_{\tau=0}^\infty |C'|^2\int dXdY\left\{\frac{X}{\beta'} + v(1+i\vartheta)\right\} \\ &\quad \times \exp\left[-\frac{X^2+Y^2}{\beta''} - 2vX\right] + c.c \end{aligned} \tag{4.22}$$

Performing the Gaussian integrals over $X$ and $Y$, one obtains:

$$j_x = \eta\bar{t}\frac{d}{s}\pi v\int_{\tau=0}^\infty \beta''\left[2\vartheta + i\beta''\left(\frac{1}{\beta'} - \frac{1}{\beta'^*}\right)\right]\exp(v^2\beta'')f'(\varepsilon,\tau), \tag{4.23}$$

where $f'(\varepsilon,\tau)$ was introduced in Eq. (4.17).

The expression (4.23) for Hall current is obtained without any assumption about the imaginary part of the relaxation time $\gamma''$ in the TDGL equation. Under the assumption $\vartheta = 0$, the hall current density Eq. (4.23) is exactly equal to zero. That is why as the next step we expand the expression (4.23) up to the first order over small $\vartheta$ and obtain:

$$\begin{aligned} j_x^s &= 2\eta\bar{t}\frac{d}{s}\pi v\vartheta\int_0^{2\pi/d}\frac{dk_z}{2\pi}\int_{\tau=0}^{\infty}\beta\left|C'\right|^2\left[1-\frac{b}{2}\frac{\tau[1-\tanh^2(b\tau/2)]}{\tanh(b\tau/2)}\right]\exp(v^2\beta) \\ &= \frac{b}{8\pi s}\eta\bar{t}v\vartheta\int_{\tau=0}^{\infty}\frac{2\tanh(b\tau/2)-b\tau[1-\tanh^2(b\tau/2)]}{\sinh^2(b\tau/2)}f(\tau), \end{aligned} \tag{4.24}$$

where $f(\tau)$ was introduced in Eq. (3.28).

The fluctuation Hall conductivity in physical units is given by

$$\sigma_{xy}^s = \frac{J_x^s}{E} = \frac{\sigma_{GL}\eta\bar{t}\vartheta}{8\pi s}\int_{\tau=0}^{\infty}\frac{2\tanh(b\tau/2)-b\tau[1-\tanh^2(b\tau/2)]}{\sinh^2(b\tau/2)}f(\tau), \tag{4.25}$$

In order to compare with experimental data, normal conductivity $\sigma_{xy}^n$ should be added. Thus, the total Hall conductivity will be consequently

$$\sigma_{xy} = \sigma_{xy}^s + \sigma_{xy}^n \tag{4.26}$$

### 4.3.2 Comparison with experiment and discussion

Hall effect measurements on an optimally doped YBCO films of thickness 50 nm and $T_c = 86.8$ K was done in Ref. [49] in which the resistivity of the same sample was fitted in section 3.4.2. The parameters, namely, $\xi, \kappa, s', k, \gamma, \sigma_n$, remained the same, as used in the fits shown in Fig. 3.1 The comparison is presented in Fig. 4.2. The Hall conductivity curves were fitted to Eq. (4.26) with the normal-state conductivity measured in Ref. [49] to be $\sigma_{xy}^n = 42\ (\Omega\text{cm})^{-1}$. We found that the best fits were obtained with $\vartheta = -0.0017$, and inferred empirically. The absolute value of $\vartheta$ obtained from our fitting is consistent with its value [74]. The negative value of the hole-particle asymmetry parameter $\vartheta$ (this means

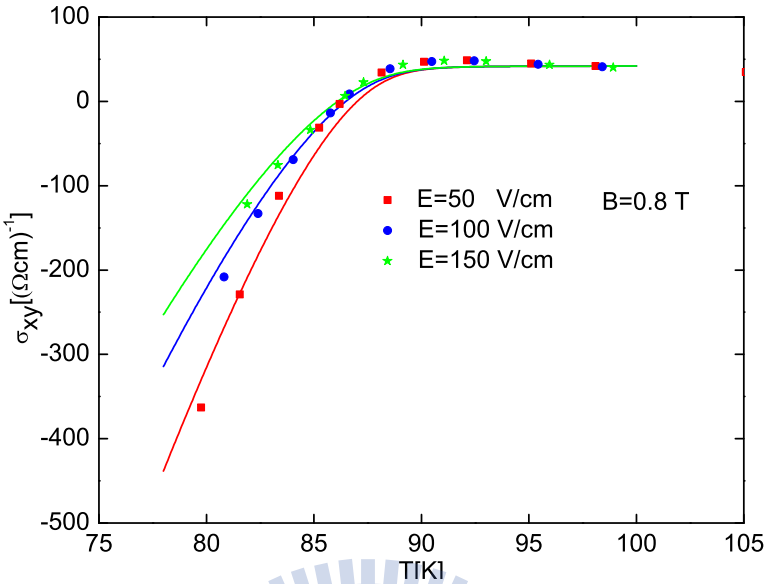


Figure 4.2: Points are Hall conductivity for different electric fields of an optimally doped YBCO in Ref. [49]. The solid line is the theoretical value of resistivity calculated from Eq. (4.26) with fitting parameters (see text).

a negative $\sigma_{xy}^{s}$) implies a positive energy-derivative of the density of states at $\varepsilon_F$ when the carriers are holes in the normal state. As suggested by Kopnin and Vinokur [105],one possibility to explain this behavior is that the Fermi surface of a metal in the normal state has both hole-like and electronic pockets. The Hall anomaly may thus depend on the doping level, as it was reported by Nagaoka *et al.* [100]. Very recently, Angilella *et al.* [106] have found that, close to an electronic topological transition of the Fermi surface, in the hole-like doping range, the fluctuation Hall conductivity has indeed an opposite sign with respect to the normal-state one, giving additional strong support that the Hall resistivity sign reversal is intrinsic and depends on the details of the structure of the electronic spectrum.

## 4.4 Summary

We have calculated the fluctuation Hall conductivity for a layered superconductor in an arbitrary in-plane electric field and perpendicular magnetic field in the frame of the TDGL

theory with thermal noise describing the thermal fluctuations using the self-consistent Gaussian approximation. We have obtained explicit formulas including all Landau levels without any assumption about the imaginary part of the relaxation time $\gamma''$ in the TDGL equation. It is then easy to get the expression for the fluctuation Hall conductivity under assumption that the imaginary part of the relaxation time is very small.

The renormalization of the critical temperature is calculated and is strong in layered high-$T_c$ materials. The results were compared to the experimental data on HTSC. Our the fluctuation Hall conductivity results are in good qualitative and even quantitative agreement with experimental data on YBCO in strong electric fields.

# Chapter 5

# Fluctuation ac conductivity in linear response

## 5.1 Introduction

The analysis of fluctuations conductivity has stimulated in the past years a considerable amount of work. Theoretical investigations of the dc as well as the finite-frequency conductivity have been a subject for years and development of this topic proceeded until the discovery of HTSC. Experimental investigations have been reported showing clear signs of fluctuations in both the real and imaginary parts of the ac conductivity in zero magnetic field [107–110]. The real part $\sigma_1$ of the complex conductivity ($\sigma = \sigma_1 + i\sigma_2$) has a sharp peak at $T_c$ , which is not observed in, e.g., $Nb$ as representative of low temperature classical superconductors [111]. The salient feature of the ac case is that the fluctuation conductivity does not diverge at $T_c$ because a finite frequency provides a limit to the observation of the critical slowing down near $T_c$. The determination of $T_c$ from the peak in $\sigma_1$ is a reasonable choice [107]. It is also important to note that $\sigma_1$ and $\sigma_2$ have individually different temperature and frequency dependence, even though they result from the same underlying physics. Testing a given theoretical model becomes more stringent when two curves have to be fitted with the same set of parameters. Recently, the high-frequency

electromagnetic response of vortices has been investigated [112–115].

The expressions for the ac fluctuation conductivity in zero magnetic field in the Gaussian regime have been deduced within the TDGL theory of Schmidt [116]. Using general physical arguments, Fisher, Fisher, and Huse [117] provided a formulation for the scaling of the complex ac conductivity as

$$\sigma(\omega) \propto \xi^{z+2-d} S_{\pm}(\omega\xi^{z}), \tag{5.1}$$

where $\xi$ is the correlation length, $z$ is the dynamical critical exponent, $d$ is the dimensionality of the system, and $S_{\pm}(\omega\xi^{z})$ are some complex scaling functions above and below $T_c$, with the correlation length diverging at $T = T_c$ as $\xi \sim \epsilon^{-\nu}$ , where sufficiently close to $T_c$, $\epsilon = (T/T_c - 1)$. This form of fluctuation conductivity was claimed to hold in both the Gaussian and critical regimes. Dorsey [118] has deduced the scaling functions in the Gaussian regime above $T_c$ and verified the previous results of Schmidt [116]. More recently, Wickham and Dorsey [119] have shown that even in the critical regime, where the quartic term in the GL free energy plays a role, the scaling functions preserve the same form as in the Gaussian regime.

In high-$T_c$ cuprates at relatively high temperatures, vortices move and vibrate due to thermal fluctuations to the extent that the lattice can melt becoming a "vortex liquid" which was introduced in 2.5.1. Recently, Lin and Lipavsky [120] used the TDGL equation to calculate the far infrared conductivity in the Abrikosov vortex lattice state of a Type-II superconductor, and the results were in good agreement with experiment data. Thermal fluctuations neglected. This work is complementary.

Measurements of the complex conductivity as a function of frequency [108] analyzed in terms of the above-mentioned theory have revealed a somehow puzzling behavior: in fact, the complex conductivity $\sigma(\omega)$ does exhibit a scaling behavior close to the expected one, but the so-obtained critical exponents, $\nu \simeq 1.2$ and $z = 2.6$, are quite different with respect to the Gaussian values, $\nu = 0.5$ and $z = 2$; the critical exponent $\nu$ is

also in conflict with the prediction for the $3DXY$ uncharged fluid, $\nu = 2/3$ [121]. The determination of the critical exponents close to $T_c$ is uncertain: in fact, a different scaling analysis of measurements of the frequency-dependent conductivity up to 2 GHz in zero magnetic field gave large exponents, $\nu \simeq 1.7$ and $z = 5.6$ [109], in contrast with those previously obtained. The authors [110] extended the renormalized-fluctuations theory in zero magnetic field developed by Dorsey [118] by introducing an anisotropic mass tensor, and they compared the results to resistive transitions in zero field obtained in dc and at high frequency, above the critical temperature. The temperature dependence of the resistivity in zero magnetic field at all the frequencies investigated could be well described by the theory [110] from slightly above $T_c$, with values of the parameters in good agreement with common values. Far from above $T_c$ the theory did not apply, and more extensions are needed.

The electromagnetic response to microwaves in the mixed state of YBCO was measured [114] in order to investigate the electronic state inside and outside the vortex core. The magnetic-field dependence of the complex surface impedance at low temperatures was in good agreement with a general vortex dynamics description assuming that the field-independent viscous damping force and the linear restoring force were acting on the vortices. In other words, both real and imaginary parts of the complex resistivity, $\delta\rho_1$, and $\delta\rho_2$, were linear in $B$. However, at higher temperatures, there is a clear deviation from the B-linear behavior. This deviation became more prominent with increasing temperature. In the high temperature region, thermal effects on the vortices cannot be neglected, and the low temperature approximation will be no longer accurate. The microscopic calculation of the Larkin-Varlamov included lowest Landau level and high Landau levels (HLL) [8], but the result of HLL is cumbersome and cutoff dependence.

In this study we will calculate the complex conductivity and resistivity in linear response in a layered superconductor under magnetic field by using TDGL with thermal fluctuations conveniently modeled by the Langevin white noise. The interaction term in dynamics is treated in self-consistent Gaussian approximation. The results is compared

with experimental data [114] at high temperature where thermal effects on the vortices should be included.

## 5.2 Dissipative dynamics of vortices and electric fields in the mixed state

In order to calculate complex conductivity in linear response we also use TDGL Eq. (3.4) for layered superconductor. However, in this case the scalar potential is function of time.

$$\frac{\hbar^2\gamma'}{2m^*}D_t\Psi_n = -\frac{\delta}{\delta\Psi_n^*}\frac{F_{GL}}{s'} + \xi_n, \tag{5.2}$$

where the covariant time derivative is

$$D_t = \frac{\partial}{\partial t} - i\frac{e^*}{\hbar}\Phi_t, \tag{5.3}$$

with $\Phi_t = -E_t y$ being the scalar electric potential describing the driving force in a purely dissipative dynamics. The variance of the thermal noise was introduced in section 3.2.

We assume that the electric field is coordinate independent but is a monochromatic periodic function of time

$$E(t) = E\exp(-i\omega t). \tag{5.4}$$

Keeping the same notation as in previous section, the TDGL Eq. (5.2) in dimensionless units in the Gaussian approximation reads:

$$D_t\psi_n - \left(\frac{1}{2}D^2 + \frac{b}{2}\right)\psi_n + \frac{1}{2d^2}(2\psi_n - \psi_{n+1} - \psi_{n-1}) + \varepsilon\psi_n = \overline{\zeta}_n. \tag{5.5}$$

The Gaussian white-noise correlation in dimensionless units $\left\langle \overline{\zeta}_n^*(\mathbf{r},t)\overline{\zeta}_m(\mathbf{r}',t')\right\rangle$ was also introduced in section 3.2.

## 5.3 The gap equation

In linear response regime the electric field is supposed to be small enough, so let us first solve the TDGL Eq. (5.5) without electric field. The TDGL Eq. (5.5) then become

$$\frac{\partial}{\partial t}\psi_n - \left(\frac{1}{2}D^2 + \frac{b}{2}\right)\psi_n + \frac{1}{2d^2}(2\psi_n - \psi_{n+1} - \psi_{n-1}) + \varepsilon\psi_n = \overline{\zeta}_n, \tag{5.6}$$

The TDGL Eq. (5.6) is solved using the retarded ($G^0 = 0$ for $t < t'$) GF $G^0_{k_z}(\mathbf{r}, t; \mathbf{r}', t')$:

$$\psi_n(\mathbf{r}, t) = \int_0^{2\pi/d} \frac{dk_z}{2\pi} e^{-ink_z d} \int d\mathbf{r}' \int d\tau' G^0_{k_z}(\mathbf{r}, t; \mathbf{r}', t')\overline{\zeta}_{k_z}(\mathbf{r}', t'). \tag{5.7}$$

The GF satisfies

$$\left[\frac{\partial}{\partial t} - \frac{1}{2}D^2 - \frac{b}{2} + \frac{1}{d^2}[1 - \cos(k_z d)] + \varepsilon\right] G^0_{k_z}(\mathbf{r}, \mathbf{r}', t - t') = \delta(\mathbf{r} - \mathbf{r}')\delta(t - t'), \tag{5.8}$$

It is easy to get $G^0_{k_z}(\mathbf{r}, t; \mathbf{r}', t')$ from $G_{k_z}(\mathbf{r}, t; \mathbf{r}', t')$ in Appendix A by putting $v = 0$ corresponding to the linear case. So the GF $G^0_{k_z}(\mathbf{r}, t; \mathbf{r}', t')$ is written as

$$G^0_{k_z}(\mathbf{r}, t, \mathbf{r}', t') = \exp\left[\frac{ib}{2}X\,(y + y')\right] g^0_{k_z}\,(X, Y, \tau)\,, \tag{5.9}$$

where

$$g^0_{k_z}\,(X, Y, \tau) = C^0(k_z)\theta\,(\tau) \exp\left(-\frac{X^2 + Y^2}{2\beta}\right), \tag{5.10}$$

$$C^0(k_z, \tau) = \frac{b}{4\pi} \exp\left\{-\left(\varepsilon - \frac{b}{2} + \frac{1}{d^2}[1 - \cos(k_z d)]\right)\tau\right\} \sinh^{-1}\left(\frac{b\tau}{2}\right), \tag{5.11}$$

$$\beta = \frac{2}{b}\tanh\left(\frac{b\tau}{2}\right), \tag{5.12}$$

with $X = x - x', Y = y - y', \tau = t - t'$,

The superfluid density can be expressed via the GF $G^0_{k_z}(\mathbf{r},t;\mathbf{r}',t')$ as

$$\begin{aligned}\left\langle|\psi_n(\mathbf{r},\tau)|^2\right\rangle &= 2\eta_{mf}\bar{t}_{mf}\frac{d}{s}\int_0^{2\pi/d}\frac{dk_z}{2\pi}\int d\mathbf{r}'\int_{-\infty}^{\tau}dt'\left|G^0_{k_z}(\mathbf{r},t;\mathbf{r}',t')\right|^2 \\ &= 2\eta_{mf}\bar{t}_{mf}\frac{d}{s}\int_0^{2\pi/d}\frac{dk_z}{2\pi}\int d\mathbf{r}'\int_0^{\infty}d\tau\left|C^0\right|^2\exp\left(-\frac{X^2+Y^2}{\beta}-2vX\right) \\ &= 2\pi\eta_{mf}\bar{t}_{mf}\frac{d}{s}\int_0^{\infty}d\tau\beta\int_0^{2\pi/d}\frac{dk_z}{2\pi}\left|C^0\right|^2, \qquad (5.13)\end{aligned}$$

Note that

$$\begin{aligned}\int_0^{2\pi/d}\frac{dk_z}{2\pi}\left|C^0\right|^2 &= \left(\frac{b}{4\pi}\right)^2\int_0^{2\pi/d}\frac{dk_z}{2\pi}\exp\left\{-\left(2\varepsilon-b+\frac{2}{d^2}[1-\cos(k_zd)]\right)\tau\right\} \\ &= \frac{1}{d}\left(\frac{b}{4\pi}\right)^2\exp\left\{-\left(2\varepsilon-b+\frac{2}{d^2}\right)\tau\right\}I_0\left(2\tau/d^2\right). \qquad (5.14)\end{aligned}$$

where $I_0$ is the Gamma function introduced in section 3.3.1. Then the expression (5.13) takes form

$$\left\langle|\psi_n(\mathbf{r},t)|^2\right\rangle = \frac{\eta_{mf}\bar{t}_{mf}b}{2\pi s}\int_{\tau=\tau_{cut}}^{\infty}\frac{f^0(\varepsilon,\tau)}{\sinh(b\tau)}, \qquad (5.15)$$

where

$$f^0(\varepsilon,\tau) = e^{-(2\varepsilon-b)\tau}e^{-2\tau/d^2}I_0\left(2\tau/d^2\right). \qquad (5.16)$$

The gap equation in this case can be written as

$$\varepsilon = -a_h + \frac{\eta_{mf}\bar{t}_{mf}b}{\pi s}\int_{\tau=\tau_{cut}}^{\infty}\frac{f^0(\varepsilon,\tau)}{\sinh(b\tau)}. \qquad (5.17)$$

The equation (5.17) can be obtained easily from Eq. (3.29) by putting $v = 0$. The renormalization of the "mean field" critical temperature $T_c^{mf}$ should be treated the same as section 3.3.2. The gap equation (5.17) thus reads as

$$\varepsilon = -a_h^r - \frac{\eta\bar{t}}{\pi s}\left\{\int_0^{\infty}\ln[\sinh(b\tau)]\frac{d}{d\tau}\left[\frac{f^0(\varepsilon,\tau)}{\cosh(b\tau)}\right]-\gamma_E+\ln(bd^2)\right\}. \qquad (5.18)$$

## 5.4 Fluctuation ac conductivity

### 5.4.1 Linear response to electric field

The supercurrent density, defined by Eq. (3.9), was already expressed via the GF Eq. (3.47). In a similar manner one also has

$$j_y^s = i\eta\bar{t}\frac{d}{s}\int_0^{2\pi/d}\frac{dk_z}{2\pi}\int_{\mathbf{r}',t'} G^*_{k_z}(\mathbf{r},t;\mathbf{r}',t')\frac{\partial}{\partial y}G_{k_z}(\mathbf{r},t;\mathbf{r}',t') + c.c. \tag{5.19}$$

where $G_{k_z}(\mathbf{r},\mathbf{r}',\tau)$ as the GF of the linearized TDGL Eq. (5.5) in the presence of the scalar potential. One finds correction to the GF to linear order in the electric field

$$\begin{aligned} G_{k_z}(\mathbf{r},t,\mathbf{r}',t') &= G^0_{k_z}(\mathbf{r},t,\mathbf{r}',t') + i\int d\mathbf{r}_1\int dt_1 G^0_{k_z}(\mathbf{r},t,\mathbf{r}_1,t_1)\phi(\mathbf{r}_1,t_1)G^0_{k_z}(\mathbf{r}_1,t_1,\mathbf{r}',t') \\ &= G^0_{k_z}(\mathbf{r},\mathbf{r}',\tau) - i\int d\mathbf{r}_1\int dt_1 G^0_{k_z}(\mathbf{r},\mathbf{r}_1,\tau_1)\mathcal{E}(t_1)y_1 G^0_{k_z}(\mathbf{r}_1,\mathbf{r}',\tau_2), \end{aligned} \tag{5.20}$$

where $\phi(\mathbf{r}_1,t_1)$ and $\mathcal{E}(t_1)$ are the scalar electric potential and electric field in dimensionless units respectively, $\tau_1 = t - t_1$, and $\tau_2 = t_1 - t'$.

Substituting the full GF (5.20) into expression (5.19), the supercurrent density takes form:

$$j_y^s = j_{y0}^s + j_{y1}^s, \tag{5.21}$$

where

$$j_{y0}^s = \eta\bar{t}\frac{d}{s}\int_0^{2\pi/d}\frac{dk_z}{2\pi}\int d\mathbf{r}'\int dt'\left[\frac{ib}{2}(x-x') - \frac{y-y'}{\beta}\right]G^0_{k_z}(\mathbf{r},\mathbf{r}',\tau)G^0_{k_z}(\mathbf{r},\mathbf{r}',\tau), \tag{5.22}$$

and

$$
\begin{aligned}
j^s_{y1} &= \eta\bar{t}\frac{d}{s}\int_0^{2\pi/d}\frac{dk_z}{2\pi}\int d\mathbf{r}'\int dt'\int d\mathbf{r}_1\int dt_1\Bigg\{\left[\frac{ib}{2}(x-x_1)-\frac{y-y_1}{\beta_1}\right]G^0_{k_z}(\mathbf{r},\mathbf{r}_1,\tau_1)\\
&\times\mathcal{E}(t-\tau_1)y_1G^0_{k_z}(\mathbf{r}_1,\mathbf{r}',\tau_2)G^0_{k_z}(\mathbf{r}',\mathbf{r},\tau)-G^0_{k_z}(\mathbf{r}',\mathbf{r}_1,\tau_2)G^0_{k_z}(\mathbf{r}_1,\mathbf{r},\tau_1)\mathcal{E}(t-\tau_1)y_1\\
&\times\left[\frac{ib}{2}(x-x')-\frac{y-y'}{\beta}\right]G^0_{k_z}(\mathbf{r},\mathbf{r}',\tau)\Bigg\}. \qquad (5.23)
\end{aligned}
$$

Carrying out the integration (5.22) over $\mathbf{r}'$ one obtains

$$j^s_{y0}=0, \qquad (5.24)$$

while carrying out the integration (5.23) over $\mathbf{r}_1,\mathbf{r}'$ one can find

$$
\begin{aligned}
j^s_{y1} &= \frac{b}{4\pi s}\eta\bar{t}\int_0^\infty d\tau\exp\left\{-\left(2\varepsilon-b+\frac{2}{d^2}\right)\tau\right\}I_0\left(\frac{2\tau}{d^2}\right)\int_0^\tau d\tau_1\mathcal{E}(t-\tau_1)\\
&\times\frac{\tanh\left(\frac{b\tau}{2}\right)+\tanh\left(\frac{b(\tau-\tau_1)}{2}\right)-\tanh\left(\frac{b\tau_1}{2}\right)-\tanh\left(\frac{b\tau}{2}\right)\tanh\left(\frac{b\tau_1}{2}\right)\tanh\left(\frac{b(\tau-\tau_1)}{2}\right)}{\left\{\tanh\left(\frac{b\tau}{2}\right)+\tanh\left(\frac{b(\tau-\tau_1)}{2}\right)+\tanh\left(\frac{b\tau_1}{2}\right)+\tanh\left(\frac{b\tau}{2}\right)\tanh\left(\frac{b\tau_1}{2}\right)\tanh\left(\frac{b(\tau-\tau_1)}{2}\right)\right\}^2}\\
&\times\frac{1}{\cosh\left(\frac{b\tau}{2}\right)\cosh\left(\frac{b\tau_1}{2}\right)\cosh\left(\frac{b(\tau-\tau_1)}{2}\right)}. \qquad (5.25)
\end{aligned}
$$

Substituting $\mathcal{E}(t-\tau_1)=\mathcal{E}\exp[-i\omega(t-\tau_1)]$ into the expression (5.25) and carrying out the integral over $\tau_1$, one gets

$$
\begin{aligned}
j_s(t) &= \frac{b}{4\pi s}\frac{\eta\bar{t}}{b^2+\omega^2}\mathcal{E}\exp(-i\omega t)\int_0^\infty d\tau\exp\left\{-\left(2\varepsilon-b+\frac{2}{d^2}\right)\tau\right\}I_0\left(\frac{2\tau}{d^2}\right)\\
&\times\csc^2(b\tau)\left\{b\cosh(b\tau)-b\cos(\omega\tau)+i[\omega\sinh(by)-b\sin(\omega\tau)]\right\}. \qquad (5.26)
\end{aligned}
$$

By putting $\omega=0$ in the expression (5.26) one gets back to dc current as:

$$j^s_{y1}=\frac{\eta\bar{t}}{4\pi s}\mathcal{E}\int_0^\infty d\tau\frac{1}{\cosh^2(b\tau/2)}\exp\left\{-\left(2\varepsilon-b+\frac{2}{d^2}\right)\tau\right\}I_0\left(\frac{2\tau}{d^2}\right), \qquad (5.27)$$

which is consistent with the expression (3.49) in linear response case.

By doing the Fourier transform expression (5.26) with respect to frequency, then one

obtains complex conductivity as:

$$\begin{aligned}\sigma_s(\omega) &= \frac{j_s(\omega)}{\mathcal{E}(\omega)} = \frac{b}{4\pi s}\frac{\eta\bar{t}}{b^2+\omega^2}\int_0^\infty d\tau \exp\left\{-\left(2\varepsilon - b + \frac{2}{d^2}\right)\tau\right\} I_0\left(\frac{2\tau}{d^2}\right) \\ &\quad \times \csc^2(b\tau)\left\{b\cosh(b\tau) - b\cos(\omega\tau) + i[\omega\sinh(b\tau) - b\sin(\omega\tau)]\right\}. \end{aligned} \tag{5.28}$$

The complex conductivity (5.28) can be given in terms of the real part and the imaginary part

$$\sigma_s(\omega) = \sigma_1(\omega) + i\sigma_2(\omega), \tag{5.29}$$

with

$$\begin{aligned}\sigma_1(\omega) &= \frac{b^2}{4\pi s}\frac{\eta\bar{t}}{b^2+\omega^2}\int_0^\infty d\tau \exp\left\{-\left(2\varepsilon - b + \frac{2}{d^2}\right)\tau\right\} I_0\left(\frac{2\tau}{d^2}\right) \\ &\quad \times \csc^2(b\tau)[\cosh(b\tau) - \cos(\omega\tau)], \end{aligned} \tag{5.30}$$

$$\begin{aligned}\sigma_2(\omega) &= \frac{b}{4\pi s}\frac{\eta\bar{t}}{b^2+\omega^2}\int_0^\infty d\tau \exp\left\{-\left(2\varepsilon - b + \frac{2}{d^2}\right)\tau\right\} I_0\left(\frac{2\tau}{d^2}\right) \\ &\quad \times \csc^2(b\tau)[\omega\sinh(b\tau) - b\sin(\omega\tau)]. \end{aligned} \tag{5.31}$$

In limit $b \to 0$, one have

$$\sigma_1(\omega) = \frac{1}{4\pi s}\frac{\eta\bar{t}}{\omega^2}\int_0^\infty d\tau \exp\left\{-\left(2\varepsilon + \frac{2}{d^2}\right)\tau\right\} I_0\left(\frac{2\tau}{d^2}\right)\frac{1-\cos(\omega\tau)}{\tau^2}, \tag{5.32}$$

$$\sigma_2(\omega) = \frac{1}{4\pi s}\frac{\eta\bar{t}}{\omega^2}\int_0^\infty d\tau \exp\left\{-\left(2\varepsilon + \frac{2}{d^2}\right)\tau\right\} I_0\left(\frac{2\tau}{d^2}\right)\frac{\omega\tau - \sin(\omega\tau)}{\tau^2}. \tag{5.33}$$

In 2D case, the expression (5.32) and (5.33) become

$$\begin{aligned}\sigma_1(\omega) &= \frac{1}{4\pi s}\frac{\eta\bar{t}}{\omega^2}\int_0^\infty d\tau \exp\{-2\varepsilon\tau\}\frac{1-\cos(\omega\tau)}{\tau^2} \\ &= \frac{\eta\bar{t}}{8\pi s}\frac{1}{\varepsilon}\left\{\frac{\omega}{\varepsilon}\arctan\left(\frac{\omega}{2\varepsilon}\right) - \left(\frac{\varepsilon}{\omega}\right)^2 \ln\left[1+\left(\frac{\omega}{2\varepsilon}\right)^2\right]\right\}, \end{aligned} \tag{5.34}$$

$$\begin{aligned}\sigma_2(\omega) &= \frac{1}{4\pi s}\frac{\eta\bar{t}}{\omega^2}\int_0^\infty d\tau \exp\{-2\varepsilon\tau\}\frac{\omega\tau-\sin(\omega\tau)}{\tau^2} \\ &= \frac{\eta\bar{t}}{4\pi s}\frac{1}{\varepsilon}\left\{2\left(\frac{\varepsilon}{\omega}\right)^2\left(\arctan\frac{\omega}{2\varepsilon}-\frac{\omega}{2\varepsilon}\right)+\frac{\varepsilon}{2\omega}\ln\left[1+\left(\frac{\omega}{2\varepsilon}\right)^2\right]\right\},\end{aligned} \tag{5.35}$$

which agree with the results of A.T. Dorsey [118], and A. Larkin and A. Varlamov [8]. This results also agree with the results of Schmidt [116], which were derived by using the Kubo formula.

### 5.4.2 Comparison with experiment

Here we compare the results with the experimental results of Y. Tsuchiya *et al.* [114], obtained from the the microwave surface impedance measurements at $\omega/2\pi$=31.7 GHz on an overdoped YBCO slightly overdoped single crystal with $T_c$=91.2 K. The layer distance used the calculation is $d' = 11.68$ Å in Ref. [60]. The comparison is presented in Fig. 5.1. The complex resistivity is

$$\rho_s(\omega) = \frac{1}{\sigma_s(\omega)} = \frac{\sigma_1}{\sigma_1^2+\sigma_2^2} - i\frac{\sigma_2}{\sigma_1^2+\sigma_2^2} = \rho_1 - i\rho_2, \tag{5.36}$$

where

$$\rho_1 = \frac{\sigma_1}{\sigma_1^2+\sigma_2^2},\ \rho_2 = \frac{\sigma_2}{\sigma_1^2+\sigma_2^2}. \tag{5.37}$$

The change of resistivity from the zero-field is defined as

$$\delta\rho_1 = \rho_1(B) - \rho_1(0), \tag{5.38}$$

where returning to physical units

$$\rho_1 = \frac{k}{\sigma_n}\frac{\sigma_1}{\sigma_1^2+\sigma_2^2}, \tag{5.39}$$

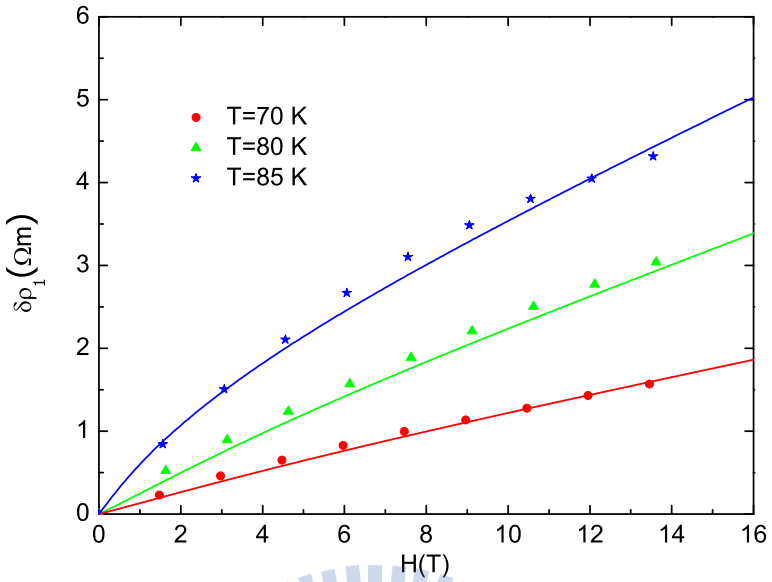


Figure 5.1: Points are resistivity for different temperatures of an overdoped YBCO in Ref. [114]. The solid line is the theoretical value of resistivity calculated from Eq. (5.38) with fitting parameters (see text).

The change of resistivity curves were fitted to Eq. (5.38) with the normal-state conductivity measured in Ref. [114] to be $\sigma_n = 3.3 \times 10^6\ (\Omega\ m)^{-1}$. The parameters we obtain from the fit are: $H_{c2}(0) = 180$ T (corresponding to $\xi = 13.5$ Å), $\kappa = 47.8$, $s' = 5.88$ Å, and $k = \sigma_n/\sigma_{GL} = 0.74$, where we take $\gamma = 7.8$ for optimally doped YBCO in Ref. [42]. Using those parameters, we obtain $Gi = 1.56 \times 10^{-3}$ (corresponding to $\eta = 0.176$). The order parameter effective thickness $s'$ can be taken to be equal to the layer thickness (see in Ref. [61]) of the superconducting $CuO_2$ plane plus the coherence length $2\xi_z = 2\frac{\xi}{\gamma}$ due to the proximity effect: 3.18 Å+$2\frac{13.6}{7.8}$ Å= 6.96 Å, roughly in agreement in magnitude with the fitting value of $s'$.

We also compare the change of resistivity Eq. (5.38) with the experimental results of T. Hanaguri *et al.* [115], obtained from the the microwave surface impedance measurements at 40.8 GHz on a Bi2212 single crystal with $T_c$=91 K. The layer distance and the normal-state conductivity used the calculation are $d' = 19.6$ Å in Ref. [61] and $\sigma_n = 1.42 \times 10^4$ $(\Omega\text{cm})^{-1}$ in Ref. [48], respectively. The comparison is presented in Fig. 5.2. The best fitting parameters are: $H_{c2}(0) = 178$ T (corresponding to $\xi = 13.6$ Å), $\kappa = 49.5$, $s' = 3.41$

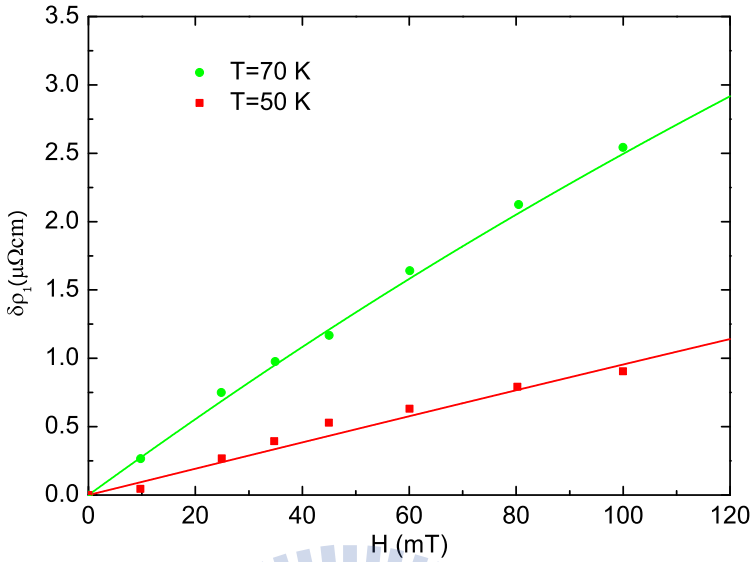


Figure 5.2: Points are resistivity for different temperatures of an overdoped Bi2212 in Ref. [115]. The solid line is the theoretical value of resistivity calculated from Eq. (5.38) with fitting parameters (see text).

Å, $k = 0.67$, and $\gamma = 34$ which give $Gi = 0.036$. The order parameter effective thickness $s'$ can be roughly estimated: 3.32 Å+$2\frac{13.6}{34}$ Å= 4.11 Å. The fitting parameters of ac resistivity are consistent with the fitting ones of dc resistivity in section 3.4.2.

## 5.5 Summary

We calculated the complex conductivity and resistivity in a layered Type-II superconductor under magnetic field in the presence of strong thermal fluctuations on the mesoscopic scale in linear response. Time dependent Ginzburg-Landau equations with thermal noise describing the thermal fluctuations is used to describe the vortex-liquid regime and arbitrary flux flow velocities. The nonlinear term in dynamics is treated using the renormalized Gaussian approximation. The renormalization of the critical temperature is calculated. We obtained explicit expressions for the complex conductivity $\sigma_s$ and resistivity $\rho_s$ including all Landau levels, so that the approach is valid for arbitrary values the magnetic field not too close to $H_{c1}(T)$.

The results were compared to the experimental data on HTSC. Our the resistivity results are in good qualitative and even quantitative agreement with experimental data on YBCO and Bi2212. We found that the change in the resistivity was linear in magnetic field at low temperature in YBCO and Bi2212. This linear behavior was was well described in terms of the Coffey-Clem unified theory [114, 122] of vortex motion with $B$-independent, and frequency-independent vortex dynamics parameters, and essentially not different from that in conventional superconductor. However, there is a clear derivation from the $B$-linear behavior due to thermal effect. The thermal fluctuation was included in the present approach, so that our results should be applicable for above and below $T_c$.

# Chapter 6

# Conclusion and future work

We quantitatively studied electrical transport and thermal transport phenomena in Type-II superconductor in magnetic field in the presence of strong thermal fluctuations on the mesoscopic scale in the linear response and also beyond the linear one. While in the normal state the dissipation involves unpaired electrons, in the mixed phase it takes a form of the flux flow. Time dependent Ginzburg-Landau equations with thermal noise describing the thermal fluctuations is used to describe strongly Type-II superconductor in the vortex-liquid regime in $2D$, $3D$, and layered superconductor. We avoid assuming the lowest Landau level approximation, so that the approach is valid for arbitrary values the magnetic field not too close to $H_{c1}(T)$.

Our main objective is to study layered high-$T_c$ materials for which the Ginzburg number characterizing the strength of thermal fluctuations is exceptionally high, in the moving vortex matter the crystalline order is lost and it becomes homogeneous on a scale above the average inter-vortex distances. This ceases to be the case at very low temperature at which two additional factors make the calculation invalid. One is the validity of the GL approach (strictly speaking not far from $T_c(H)$) and another is effect of quenched disorder. The later becomes insignificant at elevated temperature due to a very effective thermal depinning. Although sometimes motion tends to suppress fluctuations, they are still a dominant factor in flux dynamics. We also estimated the region in the parameter

space in which, on one hand vortex crystal is effectively destroyed by thermal fluctuations and, on the other hand disorder (significantly "weakened" by thermal fluctuations) is not strong enough to significantly affect the transport.

The nonlinear term in TDGL equation is treated using the self-consistent Gaussian approximation. In linear response we solve the linearized TDGL by expanding Green's function to linear order in the electric field. This allows us to obtain explicit expressions for the transverse thermoelectric conductivity $\alpha_{xy}$, the Nernst signal $e_N$ in $2D$ and $3D$, and the ac conductivity in layered superconductor including all Landau levels. In nonlinear response we also have an explicit form of the Green function incorporating all Landau levels. This allows to obtain explicit formulas for electrical conductivity and Hall conductivity beyond linear response without need to cutoff higher Landau levels. The results are presented using both the strength of the thermal fluctuation $\eta$ and more often used the Ginzburg number $Gi$ in $2D$ and $3D$.

We compared the transverse thermoelectric conductivity $\alpha_{xy}$ and the Nernst signal $e_N$ to the available $2D$ numerical simulation of the same model and the experiments on LaSCO and YBCO. Our the resistivity and Hall conductivity results were compared with experimental data on YBCO in strong electric fields as well as on Bi2212 in linear case. The renormalization of the critical temperature is calculated and is strong in layered high-$T_c$ materials. The change of ac resistivity was also compared to the experiment on YBCO and Bi2212. Our comparisons show a good agreement with several experiment and numerical simulation on HTSC.

Let us compare the present approach with a widely used Londons' approximation. Since we haven't neglected higher Landau levels, as very often is done in similar studies [11, 43], our results should be applicable even for relatively small fields in which the London approximation is valid and used. There is no contradiction since the two approximations have a very large overlap of applicability regions for strongly Type-II superconductors. The GL approach for the constant magnetic induction works for $H >> H_{c1}(T)$, while the Londons' approach works for $H << H_{c2}(T)$. Similar methods can be applied to other

electric transport phenomena like the Hall conductivity and thermal transport phenomena like the Nernst effect. The results, at least in $2D$, can be in principle compared to numerical simulations of Langevin dynamics. Efforts in this direction are under way.

In the future work, we will calculate ac conductivity beyond linear response and also consider pinning and crystalline correlation effects on the transport properties in Type-II superconductors.

# Appendix A

# Derivation of Green's function

In this appendix we outline the method for obtaining the Green's function in strong electric field for the linearized equation of TDGL (see Eq. (3.18))

$$\left\{\widehat{H}-\frac{b}{2}+\frac{1}{d^2}[1-\cos(k_z d)]+\varepsilon\right\}G_{k_z}(\mathbf{r},\mathbf{r}',t-t')=\delta(\mathbf{r}-\mathbf{r}')\delta(t-t'), \tag{A.1}$$

where $\widehat{H}=D_t-\frac{1}{2}D^2$, the covariant time derivative $D_t$ and the covariant derivatives $D$ in Landau gauge are as follows

$$D_t=\frac{\partial}{\partial t}+ivby; D_x=\frac{\partial}{\partial x}-iby; D_y=\frac{\partial}{\partial y}. \tag{A.2}$$

The Green's function is a Gaussian

$$G_{k_z}\left(\mathbf{r},\mathbf{r}',\tau\right)=\exp\left[\frac{ib}{2}X\left(y+y'\right)\right]g_{k_z}\left(X,Y,\tau\right), \tag{A.3}$$

where

$$g_{k_z}\left(X,Y,\tau\right)=C_{k_z}(\tau)\theta\left(\tau\right)\exp\left(-\frac{X^2+Y^2}{2\beta}-vX\right), \tag{A.4}$$

with $X=x-x'-v\tau, Y=y-y', \tau=t-t'$. $\theta\left(\tau\right)$ is the Heaviside step function, $C$ and $\beta$ are coefficients.

Substituting the Ansatz (A.3) into Eq. (A.1), one obtains coefficients

$$D_x G = \left(\frac{\partial}{\partial x} + iby\right) G = -\left(\frac{X}{\beta} - \frac{ibY}{2} - v\right) G, \tag{A.5}$$

$$D_x^2 G = \left[\left(\frac{X}{\beta} - \frac{ibY}{2} - v\right)^2 - \frac{1}{\beta}\right] G, \tag{A.6}$$

$$D_y G = \frac{\partial}{\partial y} G = -\left(\frac{Y}{\beta} + \frac{ibX}{2}\right) G, \tag{A.7}$$

$$D_y^2 G = \left[\left(\frac{Y}{\beta} + \frac{ibX}{2}\right)^2 - \frac{1}{\beta}\right] G, \tag{A.8}$$

$$D^2 G = \left\{-\frac{2}{\beta} + \left(\frac{X}{\beta} - \frac{ibY}{2} - v\right)^2 + \left(\frac{Y}{\beta} + \frac{ibX}{2}\right)^2\right\} G, \tag{A.9}$$

$$D_t G = \left\{\frac{\partial_t C}{C} + \frac{1}{2}\left(X^2 + Y^2\right)\frac{\partial_t \beta}{\beta^2} + v\left(v - \frac{X}{\beta}\right) + \frac{ivb}{2} Y\right\} G, \tag{A.10}$$

Substituting Eq. (A.9) and Eq. (A.10) into Eq. (A.1), one obtains pre-exponential factor which has only quadratic and constant parts

$$\frac{1}{2}\left(\frac{\partial_t \beta}{\beta^2} - \frac{1}{\beta^2} + \frac{b^2}{4}\right)\left(X^2 + Y^2\right) + \varepsilon - \frac{b}{2} + \frac{\nu^2}{2} + \frac{1}{d^2}[1 - \cos(k_z d)] + \frac{\partial_t C}{C} + \frac{1}{\beta},$$

Then one obtains following conditions condition:

$$\varepsilon - \frac{b}{2} + \frac{\nu^2}{2} + \frac{1}{d^2}[1 - \cos(k_z d)] + \frac{1}{\beta} + \frac{\partial_t C}{C} = 0, \tag{A.11}$$

$$\frac{\partial_t \beta}{\beta^2} - \frac{1}{\beta^2} + \frac{b^2}{4} = 0. \tag{A.12}$$

The Eq. (A.12) determines $\beta$, subject to an initial condition $\beta(0) = 0$,

$$\beta = \frac{2}{b}\tanh\left(b\tau/2\right), \tag{A.13}$$

while Eq. (A.11) determines $C$:

$$C = \frac{b}{4\pi} \exp\left\{ -\left( \varepsilon - \frac{b}{2} + \frac{v^2}{2} + \frac{1}{d^2}[1 - \cos(k_z d)] \right) \tau \right\} \sinh^{-1}\left( \frac{b\tau}{2} \right). \tag{A.14}$$

The normalization is dictated by the delta function term in definition of the Green's function Eq. (A.1).

It is easy to obtain the Green's function $G^0_{k_z}(\mathbf{r}, \mathbf{r}', \tau)$ for TDGL Eq. (A.1) in case without electric field by putting $v = 0$ in Eq. (A.3)

$$G^0_{k_z}(\mathbf{r}, \mathbf{r}', \tau) = \exp\left[ \frac{ib}{2} X (y + y') \right] g^0_{k_z}(X, Y, \tau), \tag{A.15}$$

where

$$g^0_{k_z}(X, Y, \tau) = C^0_{k_z}(\tau)\theta(\tau) \exp\left( -\frac{X_0^2 + Y^2}{2\beta} \right), \tag{A.16}$$

with $X_0 = x - x'$, and

$$C^0_{k_z} = \frac{b}{4\pi} \exp\left\{ -\left( \varepsilon - \frac{b}{2} + \frac{1}{d^2}[1 - \cos(k_z d)] \right) \tau \right\} \sinh^{-1}\left( \frac{b\tau}{2} \right). \tag{A.17}$$

# Appendix B

# Comparison with the Hartree approach

Here we explain the difference using an example of thermodynamics. The dynamics is not different since it always can be cast in the Martin-Siggia-Rose form (see [35]).

By using the Hartree approximation, one subsitube $|\psi|^4$ by $2\left\langle|\psi|^2\right\rangle|\psi|^2$ in the GL free energy Eq. (3.6) leading the "renormalized" value of the coefficient of the linear term in the TDGL Eq. (3.10)

$$\varepsilon = -a_h + \left\langle|\psi_n|^2\right\rangle. \tag{B.1}$$

In the framework of the variational Gaussian approximation, the GL free energy Eq. (3.6) is divided into an optimized quadratic part $K$, and a "small" part $V$. Then $K$ is chosen in such a way that the energy of a Gaussian state is minimal [43]. In liquid phase with an arbitrary homogeneous $U(1)$ symmetric state, just one variational parameter $\varepsilon$ is sufficient. Thus

$$K = \frac{s}{\eta_{mf}\bar{t}_{mf}} \sum_n \int d\mathbf{r} \left[\psi_n^* \left(-\frac{1}{2}D^2 - \frac{b}{2} + \varepsilon\right)\psi_n\right], \tag{B.2}$$

and the small perturbation becomes

$$V = \frac{s}{\eta_{mf}\bar{t}_{mf}} \sum_n \int d\mathbf{r} \left[ (-a_h - \varepsilon) |\psi_n|^2 + \frac{1}{2}|\psi_n|^4 \right]. \tag{B.3}$$

The eigenvalue of $N^{th}$ Landau level is

$$-\frac{1}{2}D^2\varphi_n = (N + \frac{1}{2})b\varphi_n. \tag{B.4}$$

The Gaussian energy which will be minimized therefore is

$$g_{gauss} \equiv -\log \left[ \int \mathfrak{D}\psi_n \mathfrak{D}\psi_n^* \exp(-K) \right] + \langle V \rangle_K , \tag{B.5}$$

where

$$\langle V \rangle_K = \sum_n \left[ (-a_h - \varepsilon) \left\langle |\psi_n|^2 \right\rangle + \left\langle |\psi_n|^2 \right\rangle \left\langle |\psi_n|^2 \right\rangle \right]. \tag{B.6}$$

Minimizing the Gaussian energy with respect to $\varepsilon$

$$\frac{\partial g_{gauss}}{\partial \varepsilon} = -\frac{\partial}{\partial \varepsilon} \log \left[ \int \mathfrak{D}\psi_n \mathfrak{D}\psi_n^* \exp(-K) \right] + \frac{\partial \langle V \rangle_K}{\partial \varepsilon} = 0. \tag{B.7}$$

The derivative of the first term in Eq (B.7) gives

$$\begin{aligned}
&\frac{\partial}{\partial \varepsilon} \log \left[ \int \mathfrak{D}\psi_n \mathfrak{D}\psi_n^* \exp(-K) \right] \\
&= \frac{\partial}{\partial \varepsilon} \log \left\{ \int \mathfrak{D}\psi_n \mathfrak{D}\psi_n^* \exp \left[ -\frac{s}{\eta_{mf}\bar{t}_{mf}} \sum_n \int d\mathbf{r} \, (Nb + \varepsilon) |\psi_n|^2 \right] \right\} \\
&= \frac{\int \mathfrak{D}\psi_n \mathfrak{D}\psi_n^* |\psi_n|^2 \exp \left[ -\frac{s}{\eta_{mf}\bar{t}_{mf}} \sum_n \int d\mathbf{r} \, (Nb + \varepsilon) |\psi_n|^2 \right]}{\int \mathfrak{D}\psi_n \mathfrak{D}\psi_n^* \exp \left[ -\frac{s}{\eta_{mf}\bar{t}_{mf}} \sum_n \int d\mathbf{r} \, (Nb + \varepsilon) |\psi_n|^2 \right]} \\
&= \left\langle |\psi_n|^2 \right\rangle .
\end{aligned} \tag{B.8}$$

while the second term gives

$$\frac{\partial \langle V \rangle_K}{\partial \varepsilon} = -\left\langle |\psi_n|^2 \right\rangle + (-a_h - \varepsilon) \frac{\partial}{\partial \varepsilon} \left\langle |\psi_n|^2 \right\rangle + 2 \left\langle |\psi_n|^2 \right\rangle \frac{\partial}{\partial \varepsilon} \left\langle |\psi_n|^2 \right\rangle . \tag{B.9}$$

Substituting Eq. (B.8) and Eq. (B.9) into Eq. (B.7) one obtains gap equation

$$\varepsilon = -a_h + 2 \left\langle |\psi_n|^2 \right\rangle . \tag{B.10}$$

While the Hartree method is generally simpler, the Gaussian method applied in it's consistent form conserves Ward identities (electric current) and its effective energy is positive definite. In addition it has the correct "large number of components" limit, unlike Hartree method.

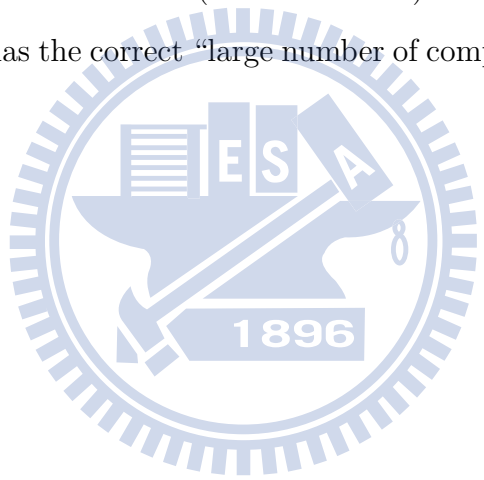

# Appendix C

# Comparison with thermodynamics

From TDGL, we obtained the superfluid density Eq. (3.36) in the case $b = 0$, $v = 0$ :

$$\left\langle |\psi_n(\mathbf{r},\tau)|^2 \right\rangle \simeq -\frac{\eta_{mf}\bar{t}_{mf}}{2\pi s}\{\ln\left(\tau_{cut}/d^2\right) + \gamma_E\} + O\left(\tau_{cut}\right). \tag{C.1}$$

In the case without external electric field (or $v = 0$), the equation obtained from TDGL shall approach the thermodynamics result. In thermodynamics method, we shall evaluate the partition function $Z = \int \mathfrak{D}\psi_n \mathfrak{D}\psi_n^* e^{-F_{GL}/T}$ where $F_{GL}/T$ is defined in Eq. (3.6).

The superfluid density in the thermodynamic approach at the phase transition point

$$\begin{aligned} \left\langle |\psi_n(\mathbf{r},\tau)|^2 \right\rangle &= \frac{\eta_{mf}\bar{t}_{mf} d}{(2\pi)^3 s} \int_0^{k_{\max}} d\mathbf{k} \int_0^{2\pi/d} dk_z \frac{1}{\frac{\mathbf{k}^2}{2} + \frac{1-\cos(k_z d)}{d^2}} \\ &\simeq \frac{\eta_{mf}\bar{t}_{mf}}{2\pi s}\{\ln\Lambda + \ln\left(2d^2\right)\} + O\left(\Lambda^{-1}\right), \end{aligned} \tag{C.2}$$

where $\Lambda = k_{max}^2/2$.

The relation between the cutoff "time" $\tau_{cut}$ and energy UV cutoff $\Lambda$ is obtained by comparing Eq. (C.1) with Eq. (C.2)

$$\tau_{cut} \simeq \frac{1}{2\Lambda e^{\gamma_E}}. \tag{C.3}$$

We also remark that in thermodynamic approach, if we use the self-consistent Gaussian approximation, we will get the exact same equation derived in Eq. (3.44) without electric field derived from TDGL after using Eq. (C.3).

# Appendix D

# Derivation of Green's function of TDGL for Hall effect

In the same way we outline the method for obtaining the Green's function in strong electric field for the linearized equation of TDGL (see Eq. (4.8))

$$\left\{(1+i\vartheta)D_t - \frac{1}{2}D^2 - \frac{b}{2} + \frac{1}{d^2}[1-\cos(k_z d)] + \varepsilon\right\} G'_{k_z}(\mathbf{r},\mathbf{r}',t-t') = \delta(\mathbf{r}-\mathbf{r}')\delta(t-t'), \quad \text{(D.1)}$$

In Landau gauge the covariant time derivative $D_t$ and the covariant derivatives $D$ are as follows

$$D_t = \frac{\partial}{\partial t} + ivby; D_x = \frac{\partial}{\partial x} - iby; D_y = \frac{\partial}{\partial y}. \quad \text{(D.2)}$$

The Green's function is a Gaussian

$$G'_{k_z}(\mathbf{r},\mathbf{r}',\tau) = \exp\left[\frac{ib}{2}X(y+y')\right] g'_{k_z}(X,Y,\tau), \quad \text{(D.3)}$$

where

$$g'(X,Y,\tau) = C'(k_z)\theta(\tau)\exp\left[-\frac{X^2+Y^2}{2\beta'} - v(1+i\vartheta)X\right], \quad \text{(D.4)}$$

with $X = x - x' - v\tau, Y = y - y', \tau = t - t'$. $\theta(\tau)$ is the Heaviside step function, $C'$ and $\beta'$ are coefficients.

Substituting the Ansatz (D.3) into Eq. (D.1), one obtains coefficients

$$D_x G' = \left(\frac{\partial}{\partial x} - iby\right) G' = -\left[\frac{X}{\beta'} + \frac{ibY}{2} + v(1+i\vartheta)\right] G', \tag{D.5}$$

$$D_x^2 G' = \left\{\left[\frac{X}{\beta'} + \frac{ibY}{2} + v(1+i\vartheta)\right]^2 - \frac{1}{\beta'}\right\} G', \tag{D.6}$$

$$D_y G' = \frac{\partial}{\partial y} G' = \left(\frac{ibX}{2} - \frac{Y}{\beta'}\right) G', \tag{D.7}$$

$$D_y^2 G' = \left[\left(\frac{ibX}{2} - \frac{Y}{\beta'}\right)^2 - \frac{1}{\beta'}\right] G', \tag{D.8}$$

$$D_r^2 G' = \left\{-\frac{2}{\beta'} + \left[\frac{X}{\beta'} + \frac{ibY}{2} + v(1+i\vartheta)\right]^2 + \left(\frac{ibX}{2} - \frac{Y}{\beta'}\right)^2\right\} G', \tag{D.9}$$

$$D_t G' = \left[\frac{\partial_t C'}{C'} + \frac{1}{2}\left(X^2 + Y^2\right)\frac{\partial_t \beta'}{\beta'^2} + v^2(1+i\vartheta) + v\frac{X}{\beta'} + \frac{ivb}{2}Y\right] G', \tag{D.10}$$

Substituting Eq. (D.9) and Eq. (D.10) into Eq. (D.1), one obtains pre-exponential factor which has only quadratic and constant parts

$$\frac{1}{2}\left[(1+i\vartheta)\frac{\partial_t \beta'}{\beta'^2} - \frac{1}{\beta'^2} + \frac{b^2}{4}\right](X^2+Y^2) + \varepsilon - \frac{b}{2} + \frac{v^2(1+i\vartheta)^2}{2} + \frac{1}{d^2}[1-\cos(k_z d)] + (1+i\vartheta)\frac{\partial_t C'}{C'} + \frac{1}{\beta'},$$

Then one obtains following conditions condition:

$$\varepsilon - \frac{b}{2} + \frac{v^2(1+i\vartheta)^2}{2} + \frac{1}{d^2}[1-\cos(k_z d)] + \frac{1}{\beta} + (1+i\vartheta)\frac{\partial_t C'}{C'} = 0, \tag{D.11}$$

$$(1+i\vartheta)\frac{\partial_t \beta'}{\beta'^2} - \frac{1}{\beta'^2} + \frac{b^2}{4} = 0. \tag{D.12}$$

The Eq. (D.12) determines $\beta'$, subject to an initial condition $\beta'(0) = 0$,

$$\beta' = \frac{2}{b}\tanh\left[\frac{b}{2}\frac{\tau}{(1+i\vartheta)}\right], \tag{D.13}$$

while Eq. (D.11) determines $C'$:

$$C' = \frac{b}{4\pi} \exp\left\{ -\left( \varepsilon - \frac{b}{2} + \frac{v^2(1+i\vartheta)^2}{2} + \frac{1}{d^2}[1-\cos(k_z d)] \right) \tau \right\} \sinh^{-1}\left( \frac{b\tau}{2} \right). \quad \text{(D.14)}$$

The normalization is dictated by the delta function term in definition of the Green's function Eq. (D.1).

# Bibliography


[1] M. Tinhkham, *Introduction to superconductivity*, McGraw-Hill, 1996.

[2] V. L. Ginzburg, L. Landau, Zh. Eksperim. i Teor. Fiz. **20**, 1064 (1950).

[3] A. A. Abrikosov, Soviet Physics JETP **5**, 1174 (1957).

[4] J. Bardeen, L. N. Cooper, J. R. Schrieffer, Phys. Rev. **106**, 162; ibid. **108**, 1175 (1957).

[5] V.L.Ginzburg, Soviet Solid State Physics **2**, 61 (1960).

[6] L. G. Aslamazov and A. I. Larkin, Phys. Lett. **26A**, 238 (1968).

[7] R.E. Glover, Phys. Rev. Lett. **A25**, 542 (1967).

[8] A. Larkin and A. Varlamov, *Theory of fluctuations in superconductors*, (Clarendon Press, Oxford, 2005).

[9] K. Maki, Prog. Theor. Phys. **39**, 897; ibid. **40**, 193 (1968).

[10] R.S. Thompson, Phys. Rev. B **1**, 327 (1970).

[11] S. Ullah and A.T. Dorsey, Phys. Rev. Lett. **65**, 2066 (1990); S. Ullah and A.T. Dorsey, Phys. Rev. B **44**, 262 (1991).

[12] I. Ussishkin, S.L. Sondhi, and D.A. Huse , Phys. Rev. Lett. **89**, 287001 (2002).

[13] I. Ussishkin, Phys. Rev. B **68**, 024517 (2003).

[14] S. Mukerjee and D.A. Huse, Phys. Rev. B **70**, 014506 (2004).

[15] S. Tan and K. Levin, Phys. Rev. B **69**, 064510 (2004).

[16] T.T.M. Palstra, B. Batlogg, L.F. Schneemeyer, and J.V. Waszczak, Phys. Rev. Lett. **64**, 3090 (1990).

[17] J.A. Clayhold, A.W. Linnen, Jr., F. Chen, and C.W. Chu, Phys. Rev. B **50**, 4252 (1994).

[18] C. Hohn, M. Galffy and A. Freimuth, Phys. Rev. B **50**, 15875 (1994).

[19] Z.A. Xu, N.P. Ong, Y. Wang, T. Kakeshita, and S. Uchida, Nature (London) **406**, 486 (2000).

[20] Y. Wang, Z.A. Xu, T. Kakeshita, S. Uchida, S. Ono, Y. Ando, and N.P. Ong, Phys. Rev. B **64**, 224519 (2001).

[21] Y. Wang, N.P. Ong, Z.A. Xu, T. Kakeshita, S. Uchida, D.A. Bonn , R. Liang, and W.N. Hardy, Phys. Rev. Lett. **88**, 257003 (2002).

[22] C. Capan, K. Behnia, Z.Z Li, H. Raffy, and C. Marin, Phys. Rev. B **67**, 100507(R) (2003).

[23] Y. Wang, L. Li and N.P Ong, Phys. Rev. B **73**, 024510 (2006).

[24] R. Bel and K. Behnia, Phys. Rev. Lett. **91**, 066602 (2003); A. Pourret, H. Aubin, J. Lesueur, C. A. Marrache-Kikuchi, L. Berge, L. Dumoulin and K. Behnia, Nature Physics, **2**, 683 (2006); A. Pourret, H. Aubin, J. Lesueur, C. A. Marrache-Kikuchi, L. Berge, L. Dumoulin and K. Behnia, Phys. Rev. B **76**, 214504 (2007).

[25] F. A. Otter and P. R. Solomon, Phys. Rev. Lett. **16**, 681 (1966); A. T. Fiory and B. Serin, *ibid.* **19**, 227 (1967).

[26] R. P. Huebener and A. Seher, Phys. Rev. **181**, 701 (1969); **181**, 710 (1969); V. A. Rowe and R. P. Huebener, *ibid.* **185**, 666 (1969).

[27] P. W. Anderson, Rev. Mod. Phys. **38**, 298 (1966).

[28] D.J. Thouless, Phys. Rev. Lett. **34**, 946 (1975); G.J. Ruggeri and D.J. Thouless, J. Phys. F: Met. Phys. **6**, 2063 (1976); A.J. Bray, Phys. Rev. B **9**, 4752 (1974).

[29] D. Li and B. Rosenstein, Phys. Rev. B **60**, 9704 (1999); *idib.* **65**, 024513 (2001); **65**, 220504(2002); **70**, 144521 (2004); D. Li and B. Rosenstein, Phys. Rev. Lett. **90**, 167004 (2003); B. Rosenstein and D. Li, Rev. Mod. Phys. **82**, 109 (2010).

[30] N. Kokubo, K. Kadowaki, and K. Takita, Phys. Rev. Lett. **95**, 177005 (2005); N. Kokubo, T. Asada, K. Kadowaki, K. Takita, T.G. Sorop, and P.H. Kes, Phys. Rev. B **75**, 184512 (2007).

[31] K. Maki, Phys. Rev. B **43**, 1252 (1991); *idib.* **43**, 13685 (1991).

[32] C. Uher, J. Supercond. Novel Magn. **3**, 337 (1990).

[33] H. Beidenkopf, N. Avraham, Y. Myasoedov, H. Shtrikman, E. Zeldov, B. Rosenstein, E.H. Brandt, and T. Tamegai, Phys. Rev. Lett. **95**, 257004 (2005); D.P. Li, B. Rosenstein, and V. Vinokur, J. of Superconductivity and Novel Magnetism **19**, 369 (2006); H. Beidenkopf, T. Verdene, Y. Myasoedov, H. Shtrikman, E. Zeldov, B. Rosenstein, D. Li, and T. Tamegai, Phys. Rev. Lett. **98**, 167004 (2007).

[34] J. B. Ketterson and S. N. Song, *Superconductivity* (Cambridge University Press, Cambridge, 1999); M. Tinkham, *Introduction to Superconductivity* (McGraw-Hill, New York, 1996).

[35] B. Rosenstein and V. Zhuravlev, Phys. Rev. B **76**, 014507 (2007).

[36] R. J. Troy and A. T. Dorsey, Phys. Rev. B **47**, 2715 (1993).

[37] C. Caroli and K. Maki, Phys. Rev. **164**, 591 (1967).

[38] N. Kopnin, *Vortices in Type-II Superconductors: Structure and Dynamics* (Oxford University Press, Oxford, 2001).

[39] N. R. Cooper, B. I. Halperin, and I. M. Ruzin, Phys. Rev. B **55**, 2344 (1997).

[40] A. Kovner and B. Rosenstein, Phys. Rev. D **39**, 2332 (1989); H. Kleinert, *Path Integrals in Quantum Mechanics, Statistics, and Polymer Physics* (World Scientific, Singapore, 1995).

[41] J.Y. Juang, M.C. Hsieh, C.W. Luo, T.M. Uen, K.H. Wu, and Y.S. Gou, Physica C **329**, 45 (2000).

[42] D. Li and B. Rosenstein, Phys. Rev. B **65**, 220504(R) (2002).

[43] G. Blatter, M. V. Feigel'man, V. B. Geshkenbein, A. I. Larkin, and V. M. Vinokur, Rev. Mod. Phys. **66**, 1125 (1994).

[44] K. Kajimura, N. Mikoshiba, and K. Yamaji, Phys. Rev. B **4**, 209 (1971).

[45] C. Villard, C. Peroz, and A. Sulpice, J. Low Temp. Phys. **131**, 516 (2003); C. Peroz et al., Physica C **369**, 222 (2002).

[46] A. Schmid, Phys. Rev. **180**, 527 (1969).

[47] D. Li, A. M. Malkin and B. Rosenstein, Phys. Rev. B **70**, 214529 (2004).

[48] D. V. Livanov, E. Milani, G. Balestrino and C. Aruta, Phys. Rev. B **55**, R8701 (1997); G. Balestrino, E. Milani, C. Aruta, and A. A. Varlamov, Phys. Rev. B **54**, 3628 (1996).

[49] I. Puica, W. Lang, K. Siraj, J. D. Pedarnig and D. Bauerle, Phys. Rev. B **79**, 094522 (2009).

[50] L. G. Aslamazov and A. I. Larkin, Phys. Lett. **26A**, 238 (1968).

[51] B. D. Tinh and B. Rosenstein, Phys. Rev. B **79**, 024518 (2009); B. D. Tinh and B. Rosenstein, J. Supercond. Novel. Magn. **23**, 815 (2010); B. D. Tinh and B. Rosenstein, J. Phys: Conf. Ser. **153**, 012030 (2009); *idib.* **150**, 052028 (2009).

[52] J. P. Hurault, Phys. Rev. **179**, 494 (1969).

[53] A. A. Varlamov and L. Reggiani, Phys. Rev. B **45**, 1060 (1992).

[54] T. Mishonov, A. Posazhennikova, and J. Indekeu, Phys. Rev. B **65**, 064519 (2002).

[55] J. C. Soret, L. Ammor, B. Martinie, J. Lecomte, P. Odier, and J. Bok, Europhys. Lett. **21**, 617 (1993).

[56] L. Fruchter, I. Sfar, F. Bouquet, Z. Z. Li, and H. Raffy, Phys. Rev. B **69**, 144511 (2004).

[57] W. Lang, I. Puica, M. Peruzzi, L. Lemmermann, J. D. Pedarnig, and D. Bäuerle, Phys. Status Solidi C **2**, 1615 (2005).

[58] I. Puica and W. Lang, Phys. Rev. B **68**, 212503 (2003); I. Puica and W. Lang, Phys. Rev. B **70**, 092507 (2004).

[59] W. E. Masker, S. Marcelja, and R. D. Parks, Phys. Rew. **188** 745 (1969); T. Mishonov and E. Penev, Int. J. Mod. Phys. B **14**, 3831 (2000).

[60] Y. Yan and M. G. Blanchin, Phys. Rev. B **43**, 13717 (1991).

[61] C. P. Poole Jr., H. A. Farach, R. J. Creswick and R. Prozorov, *Superconductivity* (Academic Press, Amsterdam, 2007).

[62] Nicolas Doiron-Leyraud, Cyril Proust, David LeBoeuf, Julien Levallois, Jean-Baptiste Bonnemaison, Ruixing Liang, D. A. Bonn, W. N. Hardy and Louis Taillefer, Nature (London) **447**, 565 (2007).

[63] S. J. Hagen, C. J. Lobb, R. L. Greene, M. G. Forrester, and J. H. Kang, Phys. Rev. B **41**, 11630 (1990).

[64] J. P. Rice, N. Rigakis, D. M. Ginsberg, and J. M. Mochel, Phys. Rev. B **46**, 11050 (1992).

[65] I. Puica, W. Lang, W. Göb, and R. Sobolewski, Phys. Rev. B **69**, 104513, (2004).

[66] Z.D. Wang, J.M. Dong, and C.S. Ting, Phys. Rev. Lett. **72**, 3875 (1994).

[67] V.M. Vinokur, V.B. Geshkenbein, M.V. Feigelman, and G. Blatter, Phys. Rev. Lett. **71**, 1242 (1993).

[68] A.V. Samoilov, A. Legris, F. Rullier-Albenque, P. Lejay, S. Bouffard, Z.G. Ivanov, and L.-G. Johansson, Phys. Rev. Lett. **74**, 2351 (1995).

[69] W. Liu, T.W. Clinton, A.W. Smith, and C.J. Lobb, Phys. Rev. B **55**, 11 802 (1997).

[70] J. Roa-Rojas, P. Prieto, and P. Pureur, Mod. Phys. Lett. B **15**, 1117 (2001).

[71] N. Kokubo, J. Aarts, and P.H. Kes, Phys. Rev. B **64**, 014507 (2001).

[72] J.M. Graybeal, J. Luo, and W.R. White, Phys. Rev. B **49**, 12 923 (1994).

[73] W.N. Kang, D.H. Kim, S.Y. Shim, J.H. Park, T.S. Hahn, S.S. Choi, W.C. Lee, J.D. Hettinger, K.E. Gray, and B. Glagola, Phys. Rev. Lett. **76**, 2993 (1996).

[74] W. Lang, G. Heine, P. Schwab, and X.Z. Wang, Phys. Rev. B **49**, 4209 (1994); W. Lang, I. Puica, W. Göb, and R. Sobolewski, Int. J. Mod. Phys. B **17**, 3496 (2003).

[75] W. Lang, G. Heine, W. Kula, and R. Sobolewski, Phys. Rev. B **51**, 9180, (1995).

[76] W. Lang, Physica C **233,** 282-287, (1997).

[77] G. Heine, W. Lang, X.L. Wang, and X.Z. Wang, Journal of Low Temperature Physics **105**, 945, (1996).

[78] L.M. Wang, H. Yang, and H.E. Horn, Phys. Rev. B **59**, 14031, (1999).

[79] J.P. Rice, N. Rigakis, D.M. Ginsberg, and J.M. Mochel, Phys. Rev. B **46**, 11 050 (1992).

[80] T.W. Clinton, A.W. Smith, Q. Li, J.L. Peng, R.L. Greene, C.J. Lobb, M. Eddy, and C.C. Tsuei, Phys. Rev. B **52**, R7046 (1995).

[81] A.V. Samoilov, Phys. Rev. Lett. **71**, 617 (1993).

[82] N.V. Zavaritsky, A.V. Samoilov, and A.A. Yurgens, Physica C **180**, 417 (1991).

[83] S.J. Hagen, C.J. Lobb, and R.L. Greene, Phys. Rev. B **43**, 6246 (1991).

[84] W.N. Kang, S.H. Yun, J.Z. Wu, and D.H. Kim, Phys. Rev. B **55**, 621 (1997).

[85] K. Nakao, K. Hayashi, T. Utagawa, Y. Enomoto, and N. Koshizuka, Phys. Rev. B **57**, 8662 (1998).

[86] W. Gob, W. Liebich, W. Lang, I. Puica, R. Sobolewski, R. Rossler, J.D. Pedarning, and D. Bauerle, Phys. Rev. B **62**, 9780 (2000).

[87] W.N. Kang, B.W. Kang, Q.Y. Chen, J.Z. Wu, Y. Bai, W.K. Chu, and S.-I. Lee, Phys. Rev. B **61**, 722 (2000).

[88] A. van Otterlo, M.V. Feigelman, V.B. Geshkenbein, and G. Blatter, Phys. Rev. Lett. **75**, 3736 (1995).

[89] Y. Kato, J. Phys. Soc. Jpn. **68**, 3798 (1999).

[90] R.J. Troy and A.T. Dorsey, Phys. Rev. B **47**, 2715 (1993).

[91] N.B. Kopnin, B.I. Ivlev, and V.A. Kalatski, J. Low Temp. Phys. **90**, 1 (1993).

[92] N.B. Kopnin, Phys. Rev. B **54**, 9475 (1996).

[93] J. Kolacek and P. Vasek, Physica C **336**, 199 (2000).

[94] T. Nishio and H. Ebisawa, Physica C **290**, 43 (1997).

[95] M.V. Feigelman, V.B. Geshkenbein, A.I. Larkin, and V.M. Vinokur, Pisma Zh. Eksp. Teor. Fiz. **62** (10), 811 (1995) [JETP Lett. **62**, 834 (1995)].

[96] A.W. Smith, T.W. Clinton, W. Liu, C.C. Tsuei, A. Pique, Q. Li, and C.J. Lobb, Phys. Rev. B **56**, R2944 (1997).

[97] D.A. Beam, N.C. Yeh, and F. Holtzberg, J. Phys.: Condens. Matter 10, 5955 (1998).

[98] R. Ikeda, Physica C **316**, 189 (1999).

[99] N.B. Kopnin and A.V. Lopatin, Phys. Rev. B **51**, 15291 (1995).

[100] T. Nagaoka, Y. Matsuda, H. Obara, A. Sawa, T. Terashima, I. Chong, M. Takano, and M. Suzuki, Phys. Rev. Lett. **80**, 3594 (1998).

[101] H. Fukuyama, H. Ebisawa, and T. Tsuzuki, Prog. Theor. Phys. **46**, 1028 (1971); A. G. Aronov and S. Hikami, Phys. Rev. B **41**, 9548 (1990).

[102] R. Ikeda, T. Ohmi, and T. Tsuneto, J. Phys. Soc. Jpn. **60**, 1051 (1991).

[103] C. De Dominicis and L. Peliti, Phys. Rev. B **18**, 353 (1978).

[104] G. Rietveld, N. Y. Chen, and D. van der Marel, Phys. Rev. Lett. **69**, 2578 (1992).

[105] N.B. Kopnin and V.M. Vinokur, Phys. Rev. Lett. **83**, 4864 (1999).

[106] G.G.N. Angilella, R. Pucci, A.A. Varlamov, and F. Onufrieva, Phys. Rev. B **67**, 134525 (2003).

[107] S. M. Anlage, J. Mao, J. C. Booth, D. H. Wu, and J. L. Peng, Phys. Rev. B **53**, 2792 (1996).

[108] J. C. Booth, D. H. Wu, S. B. Qadri, E. F. Skelton, M. S. Osofsky, A. Piqué, and S. M. Anlage, Phys. Rev. Lett. **77**, 4438 (1996).

[109] G. Nakielski, D. Görlitz, Chr. Stodte, M. Welters, A. Krämer, and J. Kötzler, Phys. Rev. B **55**, 6077 (1997).

[110] D. Neri, E. Silva, S. Sarti, R. Marcon, M. Giura, R. Fastampa, and N. Saprvieri, Phys. Rev. B **58**, 14 581 (1998).

[111] O. Klein, E. J. Nicol, K. Holczer, and G. Grüner, Phys. Rev. B **50**, 6307 (1994).

[112] Y. Ikebe, R. Shimano, M. Ikeda, T. Fukumura, and M. Kawasaki, Phys. Rev. B **79**, 174525 (2009).

[113] A. Maeda, H. Kitano, K. Kinoshita, T. Nishizaki, K. Shibata, and N. Kobayashi, J. Phys. Soc. Jpn. **76**, 094708 (2007).

[114] Y. Tsuchiya, K. Iwaya, K. Kinoshita, T. Hanaguri, H. Kitano, A. Maeda, K. Shibata, T. Nishizaki, and N. Kobayashi, Phys. Rev. B **63**, 184517 (2001).

[115] T. Hanaguri, T. Tsuboi, Y. Tsuchiya, K. Sasaki, and A. Maeda, Phys. Rev. Lett. **82**, 1273 (1999).

[116] H. Schmidt, Z. Phys. **216**, 336 (1968); *ibid.* **232**, 443 (1970).

[117] D. S. Fisher, M. P. A. Fisher, and D. A. Huse, Phys. Rev. B **43**, 130 (1991).

[118] Alan T. Dorsey, Phys. Rev. B **43**, 7575 (1991).

[119] R. A. Wickham and A. T. Dorsey, Phys. Rev. B **61**, 6945 (2000).

[120] Pei-Jen Lin and P. Lipavsky, Phys. Rev. B **80**, 212506 (2009).

[121] C. J. Lobb, Phys. Rev. B **36**, 3930 (1987).

[122] M. W. Coffey and J. R. Clem, Phys. Rev. Lett. **67**, 386 (1991).